DTU Library

Geodetic measurements of present-day climate changes in Greenland

Dahl-Jensen, Trine S.

Publication date:
2022

Document Version
Publisher's PDF, also known as Version of record

Citation (APA):
Dahl-Jensen, T. S. (2022). *Geodetic measurements of present-day climate changes in Greenland*. Technical University of Denmark.

DTU Space
Department of Geodesy and Earth Observation

Geodetic measurements of present-day climate changes in Greenland

PhD Thesis

Trine S. Dahl-Jensen

Geodetic measurements of present-day climate changes in Greenland

PhD Thesis
August 24th, 2022

By
Trine S. Dahl-Jensen

Supervision:
Prof. Shfaqat Abbas Khan, DTU Space
Prof. Ole Baltazar Andersen, DTU Space (co-supervisor)
Prof. Per Knudsen, DTU Space (co-supervisor)

Published by: DTU, Department of Geodesy and Earth Observation,
Elektrovej, Building 328, 2800 Kgs. Lyngby, Denmark
www.space.dtu.dk

Abstract

Global mean sea level has been rising about 3 mm/yr since 1993 due to global warming. Today, Greenland is the largest mass contributor to global mean sea level rise and has been so since the early 2000s. In order to study the movement of the bedrock in response to ice mass loss a network of permanent GNSS stations was developed along the coast of Greenland in 2007-2009. The network (GNET) gives valuable insights into the dynamics and mass loss of nearby glaciers as the uplift decreases rapidly with the distance to the station.

During the last decade or so a method called GNSS interferometric reflectometry (GNSS-IR) has been developed using GNSS data to study the surrounding environment. It utilizes the interference between the direct signals and the signals reaching the antenna after being reflected off a surface. In the first study of this thesis we test the use of GNSS-IR for studies of inter annual sea level variations in Thule, Greenland, using the existing THU2 GNSS station from 2008 - 2019. We find that the two methods show much of the same sea level variations but also that there are differences significantly larger than the estimated errors. We suggest that the difference are likely a result of a combination of factors; sea ice will affect the two measurements differently and induce an error which is not accounted for, the tide gauge is not datum controlled and the tide gauge was moved to a new location in 2015.

For the second study we use a GNSS station which was installed at the PROMICE automatic weather station, NUK-K, in March-August 2020. The aim of the installation was to test if the setup could be used for high precision positioning with the goal of tracking glacier flow. We use the GNSS data from the station to extract snow heights using GNSS-IR and compare the results to a sonic ranger mounted on the weather station. Though the data is limited, we find a good correspondence between the GNSS-IR results and the sonic ranger. We suggest that the deviations during some of the melt period is due to the much larger footprint of GNSS-IR and an uneven snow and melt distribution.

In the third paper we study the draining cycles of the ice dammed Lake Tininnilik. We use a combined set of observations of lake water level since 1940. The lake has been known to drain periodically about every 10 years at approximately the same water level up until 2003. At this point it starts to drain at continuously lower water levels and at shorter time intervals. The decreasing water level at drainage coincides with a thinning of the damming glacier. Measurements from a nearby GNSS station show an uplift in 2020 of about half of the uplift during the 2010 event, confirming the reduction in drained water volume. Using the trend in maximum lake level and an infill rate based on the last three cycles we suggest that the lake will drain again in 2024. If no continuous spillways are formed and the trend in maximum water level continues, we estimate that the quasi periodic drainage events will cease in 2053 where the water level at drainage reaches the level of the drained lake.

Resume

Det globale havniveau er steget med ca. 3 mm om året siden 1993 som et resultat af den globale opvarmning. Siden omkring år 2000 har Grønland stået for det største masse bidrag til havniveaustigningerne. For at studere undergrundens reaktion på masseændringer af indlandsisen blev der i 2007-2009 etableret et netværk af permanente GNSS stationer langs Grønlands kyst. Netværket (GNET) giver værdifuld indsigt i dynamikken og massetabet af de nærliggende gletsjere da landhævningen er stærkt afhængning af afstanden til GNSS stationen.

GNSS Interferometrisk Reflektometri (GNSS-IR) er en metode til at bruge GNSS data til at undersøge det omkringliggende område. Metoden udnytter de signaler der når GNSS antennen efter at være blevet reflekteret fra en overflade til at bestemme fx. havniveau, snehøjder eller vandindholdet i jorden. I den første artikel inkluderet i afhandlingen tester vi brugen af GNSS data fra GNET stationen THU2 til at måle årlige variationer af havniveaut i Thule fra 2008-2019. Vi ser at de to metoder groft set observerer det samme havniveau, men også at forskellene er større end usikkerhederne angiver. Vi vurdere at forskellene har flere mulige årsager, heriblandt: forskellig påvirkning af havisen om vinteren, manglende datum kontrol på tidevandsstationen og at tidevandsstationen flyttes til en ny position i 2015.

I den anden artikel bruger vi en GNSS station som var installeret på vejrstationen NUK-K i marts-april 2020. Målet med installationen var at test evnen til at måle positioner med høj nøjagtighed for at kunne følge gletsjerflydningen på PROMICE stationerne i fremtiden. Vi bruger GNSS-IR til at måle snehøjden og sammenligner med data fra en sonic ranger på vejrstationen. Til trods for en begrænset datamængde giver de to metoder omtrent samme afsmeltning henover sæsonen. Der er dog også perioder hvor forskellen er større end usikkerhederne angiver. Vi konkluderer at dette sansynligvis skyldes at både sneen og afsmeltningen er ujævnt fordelt og at GNSS-IR måler over et langt større område end sonic rangeren.

I den tredje artikel undersøger vi dræningsmønsteret af den isdæmmede sø Tininnilik. Vi bruger et kombineret datasæt over vandhøjden startende i 1940. Søen har været kendt for at dræne ca. hvert tiende år frem til 2003 hvor den begynder at dræne oftere og ved kontinuerligt aftagende vandstand. Den faldende vandstand når søen dræner falder sammen med en aftagende tykkelse på den gletsjer der dæmmer søen ind. Den nærliggende GNSS station måler en landhævning ved dræningen i 2020 der er omtrent halvt så stor som i 2010 hvilket bekræfter at det drænede volumen er faldende. Ved at kombinere den omtrent lineært aftagende vandstand ved dræning med et estimat af opfyldningsraten forventer vi at søen drænes igen i løbet af 2024. Hvis den nuværende tendens fortsætter, og der ikke dannes nogle permanente afløb, vil den maximale vandstand nå vandstanden efter dræning omkring 2053 og de quasi-cykliske dræninger vil stoppe.

Preface

This thesis is submitted to the PhD school at the National Space Institute, DTU Space, Technical University of Denmark for the completion of my PhD studies. The study was supervised by prof. Shfaqat Abbas Khan and co-supervisors prof. Ole Baltazar Andersen and prof. Per Knudsen.

The PhD project was funded by the EC Horizon 2020-project, Integrated Arctic Observation System (INTAROS), Grant Agreement no. 727890.

During my study I participated in two international summer schools; The SCAR summer school on Polar Geodesy held outside Saint Petersburg and the Karthaus Summer School on Ice Sheets and Glaciers in the Climate System held in northern Italy, both in 2018. As for conferences I presented a poster on measuring sea levels using GNSS-IR in Thule at the online EGU general assembly in 2020 and gave a talk on snow measurements at the automatic weather station NUK-K at the EGU general assembly in 2022.

For my external stay I was supposed to visit the Geological Survey of Denmark and Greenland (GEUS) but, since the office was closed down during the period of my stay due to the COVID pandemic, in the end the collaboration was mostly remote. The work done in collaboration with the department at GEUS is published and included as the second paper in this thesis.

As part of my PhD work I have prepared three papers (two published and one submitted):

Dahl-Jensen, T. S., Andersen, O. B., Williams, S. D. P., Helm, V and Khan, S. A. 2021. GNSS-IR Measurements of Inter Annual Sea Level Variations in Thule, Greenland from 2008–2019. *Remote Sensing*, 13(24).

Dahl-Jensen, T. S., Citterio, M, Jakobsen, J., Ahlstrøm, A. P., Larson, K. M. and Khan, S. A. 2022. Snow depth measurements by GNSS-IR at automatic weather station, NUK-K. *Remote Sensing*, 14(11).

Dahl-Jensen, T. S., Kjeldsen, K. K., Colgan, W., Bevis, M. and Khan, S. A. The evolution of the drainage cycles of Lake Tininnilik. (Submitted to Journal of Geodesy)

Acknowledgements

First of all I want to thank my supervisor Abbas Khan for his guidance throughout my PhD. He has always been available for discussions and questions when I was unsure where my work was going and ever optimistic that we would make it work. Also a great thank you to my co-supervisors Ole B. Andersen and Per Knudsen for good discussions during my time at DTU and to Ole for invaluable assistance with the work on sea level measurements in Thule.

A thank you to Michele Citterio, Andreas Ahlstrøm, Jakob Jakobsen and the rest of the PROMICE team at GEUS for good collaboration on the snow study at NUK-K. Though unfortunately the COVID-19 pandemic resulted in my external stay being more of an online collaboration, we made the best of it.

Thank you to my colleagues at the GEO department at DTU Space for discussions, encouragement and good company throughout the years. A special thanks to my office body Karina - it has been great sharing an office with you these last years and working towards the end of our PhD studies together.

Last but definitely not least, thank you to my friends and family who have supported me so much along the way. The greatest thank you to my husband Svend. Thank you for listening to my ramblings, good and bad, and for always supporting me to do what I believe in. Thank you for believing in me and to you and the kids for reminding me that although this thesis is an important piece of work to me, there is also a world outside. You are the best and I could not have done this without you.

List of Figures

Acronyms

AIS	Antarctic Ice Sheet
AWS	Automatic Weather Station
ENSO	El Niño-Southern Oscillation
Envisat	Environmental Satellite
ERS	European Remote Sensing
GC-Net	Greenland Climate Network
GEUS	Geological Survey of Denmark and Greenland
GIA	Glacial Isostatic Adjustment
GIS	Greenland Ice Sheet
GLOF	Glacial Lake Outburst Flood
GMSL	Global Mean Sea Level
GNET	Greenland GPS Network
GNSS	Global Navigation Satellite System
GNSS-IR	Global Navigation Satellite System Interferometric Reflectometry
GPS	Global Positioning System
GRACE	Gravity Recovery and Climate Experiment
ICESat	Ice, Cloud and Land Elevation Satellite
LRM	Low Resolution Mode
LSP	Lomb Scargle Periodogram
NASA	National Aeronautics and Space Administration
NOAA	National Oceanic and Atmospheric Administration
NSIDC	National Snow and Ice Data Center
PROMICE	Programme for Monitoring of the Greenland Ice Sheet
PSMSL	Permanent Service for Mean Sea Level
RMSD	Root Mean Square Deviation
RSL	Relative Sea Level
SAR	Synthetic Aperture Radar
SARin	Synthetic Aperture Radar interferometric mode
SNOTEL	Snow Telemetry
SNR	Signal to Noise ratio
SMB	Surface Mass Balance
SST	Sea Surface Temperatures
SWE	Snow Water Equivalent
TEOS-10	Thermodynamic Equation of Sea Water 2010
TOPEX	The Ocean Topography Experiment
VLM	Vertical Land Motion

Contents

1 Introduction

During recent years global warming and the consequences thereof has become a topic of increasing attention. Global air and ocean temperatures are rising, and as a result so is the sea level. Since 2000 annual surface air temperatures in the Arctic has, on average, increased at twice the rate of the global mean (e.g. Meredith *et al.*, 2019; Moon *et al.*, 2021). The main reasons for this Arctic amplification is still discussed. However, there is a general agreement that the mechanisms includes an albedo feedback from decreasing sea ice and snow cover, Planck feedback related to the nonlinear dependence of outgoing radiation on temperatures, an atmospheric lapse-rate feedback and a northward transport of heat and moisture (e.g. Stuecker *et al.*, 2018; Meredith *et al.*, 2019; Previdi *et al.*, 2021). The enhanced temperature rise at the poles leads to increased ice melt and thereby contributions to sea level rise.

1.1 Sea level rise

Global Mean Sea Level (GMSL) has been rising since the early 1900s (e.g. Spada & Galassi, 2012; Palmer *et al.*, 2021). Rising sea level as a consequence of global warming is affecting coastal civilisations all around the world. Currently, just over 1 % of the global population is exposed to a 100 year flood (meaning a flood of a size happening on average every 100 years). Continuing the current sea level rise this number may increase to up to 10 % at the end of this century (Oppenheimer *et al.*, 2019).
GMSL has increased at a rate of about 3 mm/yr during the altimetry era since 1993 (WCRP, 2018; Oppenheimer *et al.*, 2019; Palmer *et al.*, 2021) and has accelerated since the 1960s (Dangendorf *et al.*, 2019). Previously the rate was thought to be more or less constant during the altimetry era but after correcting for an instrument drift in TOPEX A it has been found to accelerate (Chen *et al.*, 2017; Dieng *et al.*, 2017; Oppenheimer *et al.*, 2019). Dieng *et al.* (2017) use an ensemble of sea level records and find a GMSL rise of 2.67 $\pm$ 0.19 from 1993 to 2004 and a rate of 3.49 $\pm$ 0.14 from 2005 to 2015 similar to other studies (e.g. Chen *et al.*, 2017; Oppenheimer *et al.*, 2019). The recent acceleration in GMSL rise is mainly due to increased mass loss from the Greenland Ice Sheet (GIS) (Dieng *et al.*, 2017; Oppenheimer *et al.*, 2019).
GMSL rise can be divided into two main contributions: mass changes and steric sea level change. Steric sea level change is a change in the volume of the ocean without changing its mass. The main contribution to this is thermal expansion as a result of increasing ocean temperatures. Locally and on shorter timescales salinity can also influence sea level significantly (Forget & Ponte, 2015; Meyssignac *et al.*, 2017). Mass changes cover all processes that add or remove water to/from the ocean. GMSL rise from mass changes is mostly a result of melting ice masses on land including the GIS, Antarctic Ice Sheet (AIS), and glaciers and ice caps (WCRP, 2018; Oppenheimer *et al.*, 2019; Wouters *et al.*, 2019). While steric sea level rise accounted for 50 % of total GMSL rise in 1993 it was reduced to 30 % in 2014 as a result of increased ice mass loss (Chen *et al.*, 2017). In the 20th century glaciers and ice caps was the largest mass contributor to GMSL rise but since 2000 the mass loss from the GIS has increased and it is now the main mass contributor (Vaughan *et al.*, 2013; Bamber *et al.*, 2018). Other contributions are terrestrial water storage, atmospheric water vapor and changes in snow masses.
While GMSL illustrates the general effect of global warming on sea level it is the local Relative Sea Level (RSL) referenced to the ground that affects people and ecosystems. Super-

imposed on the GMSL are several mechanisms resulting in both spatial and temporal variability. Wind stress, uneven warming and climate patterns such as the El Niño-Southern Oscillation (ENSO) creates patterns of high variability in regional sea level (Church *et al.*, 2004; Forget & Ponte, 2015; Meyssignac *et al.*, 2017). When ice melts at the ice sheets and glaciers it affects not only the GMSL by adding mass but also changes the gravity field of the Earth. This effect results in a lowering of the sea level close to the mass loss while sea level rise is above average further from the source. This pattern is often called the *sea level fingerprint* and can be seen in figure 1.1 where sea level from ice mass loss is negative close to the ice sheets where large ice masses are lost while being enhanced at low latitudes (Bamber & Riva, 2010; Hsu & Velicogna, 2017; Adhikari *et al.*, 2019).
Relative sea level is affected, not only by changes in eustatic sea level, but also by uplift or subsidence of the ground caused by e.g. present and previous ice mass changes, tectonic movements and groundwater depletion (Wöppelmann & Marcos, 2016; Oppenheimer *et al.*, 2019). In Greenland and other glaciated areas the effect of previous and present day ice mass changes is the main contributor to trends in Vertical Land Motion (VLM) and a limitation in the use of tide gauge data for estimates of GMSL rise (Spada & Galassi, 2012; King *et al.*, 2012; Wöppelmann & Marcos, 2016).

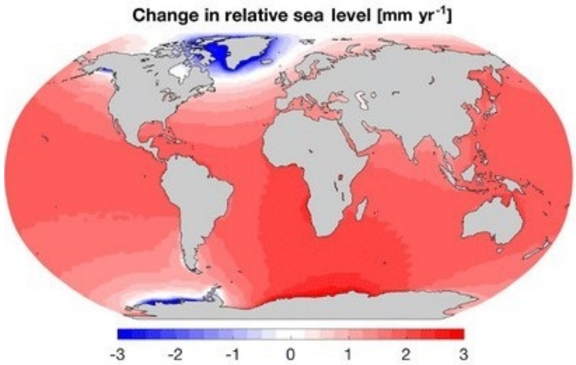

Figure 1.1: Trend in sea level fingerprints estimated from GRACE data. Published by Adhikari *et al.* (2019).

1.2 Mass balance of the Greenland ice sheet

As a result of the ongoing warming the GIS has been loosing mass at an average rate above 200 Gt/year during the last two decades (Luthcke *et al.*, 2013; Meredith *et al.*, 2019; The IMBIE Team, 2020). The shift towards a consistently negative mass balance happened during the 1990s. Before this the total mass balance was within the measurement uncertainties (van den Broeke *et al.*, 2017; Sørensen *et al.*, 2018; Meredith *et al.*, 2019).
The mass loss from the GIS can be divided into two main parts; changes in the Surface Mass Balance (SMB) and dynamic mass loss from calving of marine terminating glaciers. The relative contribution from the two has changed over time and lately SMB processes have been dominating the mass loss from the Greenland ice sheet (van den Broeke *et al.*, 2017; Mouginot *et al.*, 2019; The IMBIE Team, 2020). The SMB contribution to mass loss reached a maximum level around year 2012 where the ice sheet experienced an extreme melt event during the summer (Mouginot *et al.*, 2019; The IMBIE Team, 2020). Since then the rate of mass loss from SMB decreased for some years, likely due to a shift in the pattern of the North Atlantic circulation but has now returned to a rapid mass loss (The IMBIE Team, 2020; Sasgen *et al.*, 2020). The ice discharge from Jakobshavn, Hel-

heim and Kangerdlussuaq glaciers increased drastically in the early 2000s resulting in a strong increase in dynamic mass loss and a dominance of dynamic mass loss around this time (Mouginot *et al.*, 2019; King *et al.*, 2018). While SMB is strongly related to air temperatures through melt rates, predicting dynamic mass loss in a warming climate is complicated by local factors at the individual glaciers, such as the topography of the bed and the water circulation in the fjord, strongly affecting the influence of increasing air- and ocean temperatures (Benn *et al.*, 2007; Nick *et al.*, 2013; Meredith *et al.*, 2019).
A large number of mass balance estimates have been published through the years and they can generally be divided into three main groups. The first group of estimates are based on measuring changes in the elevation of the ice sheet typically using altimetry (see section 2.1). This method has the advantage of a relatively high spatial resolution but it relies on modelling firn compaction and densities in order to convert elevation change to mass loss (Sørensen *et al.*, 2011; Smith *et al.*, 2020; Simonsen *et al.*, 2021). The second method is often called the input/output method. It is based on estimating the SMB and ice discharge and combining the two to calculate the total mass balance. SMB relies on regional climate models tuned by observations and ice discharge relies on glacier speeds as well as widths and thicknesses. Uncertainties in all these add to the uncertainty of the method, but it is the only method partitioning the mass loss into physical processes and thereby improving our understanding of the ice sheets response to climate changes. (Mouginot *et al.*, 2019; Mankoff *et al.*, 2020; Hofer *et al.*, 2020). The last general category of mass loss estimates is the direct gravitational measurement of mass loss. It is the most recent method and generally relies on data from the Gravity Recovery and Climate Experiment (GRACE, 2002-2017) and GRACE-Follow On (GRACE-FO, launched 2018) missions. The GRACE satellites directly measures the gravity field of the earth by accurately measuring the distance between two satellites. The method has the advantage of directly measuring mass changes but it is not available until the launch of the GRACE satellites in 2002 and has a spatial resolution of about 300 km (Chen *et al.*, 2006; Luthcke *et al.*, 2013; Sasgen *et al.*, 2020).

1.3 Elastic and isostatic adjustment to ice mass changes.

When the mass load on the earth changes, e.g. by melting glaciers and ice sheets, the crust reacts by two processes: Elastic- and isostatic adjustment. The elastic adjustment is an instantaneous reaction to changes in the load. It is responsible for annual cycles in VLM as a result of seasonal changes in ice masses, snow cover and atmospheric pressure as well as the instantaneous reaction to other changes in mass load (Khan *et al.*, 2007; Bevis *et al.*, 2012; Nielsen *et al.*, 2012; Liu *et al.*, 2017). The isostatic adjustment is a slow process taking thousands of years to reach equilibrium. The process is related to the slow moving mantle flowing in under the crust when a load is removed or away when a load is added (figure 1.2). The Glacial Isostatic Adjustment (GIA) from the huge ice mass loss at the end of the last ice age can be assumed to be constant on the timescales we are typically looking at (a few decades to one century) (Wake *et al.*, 2016; Schumacher *et al.*, 2018). Since the GIA can be assumed constant any acceleration in the uplift rate indicates present day changes in the load such as a current ice mass loss (Jiang *et al.*, 2010; Khan *et al.*, 2010b; Bevis *et al.*, 2019).

1.4 Objectives

The work of this thesis aims at using geodetic measurements, and Global Navigation Satellite System (GNSS) data in particular, to study the effects of climate change in Greenland. In order to study the displacement of the bedrock, the Greenland GPS Network

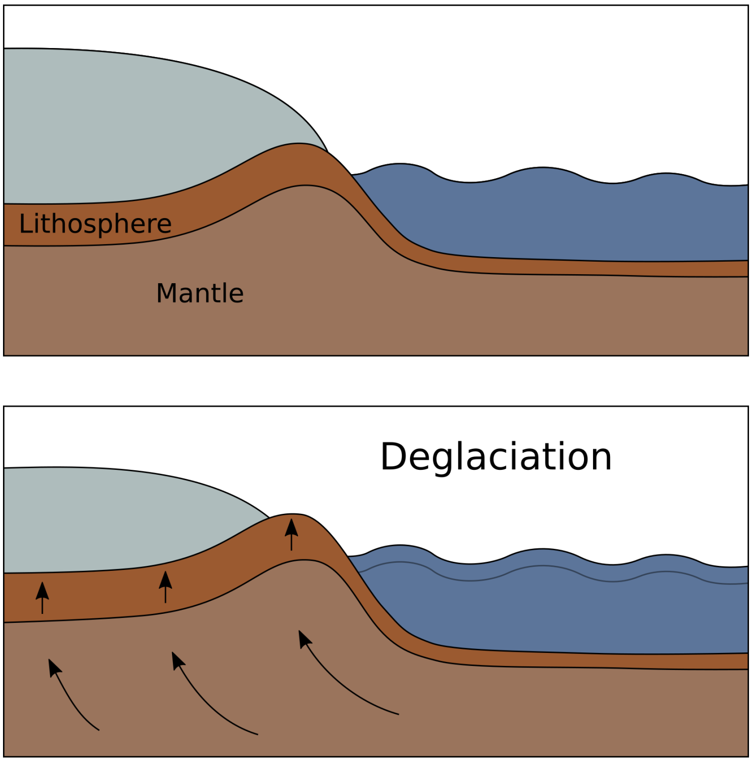

Figure 1.2: The figure illustrates the uplift of the bedrock as a result of deglaciation. During deglaciation the extend of the ice sheet is reduced resulting in an uplift of the previously ice covered area. As a result the relative sea level seen from the hill in front of the ice sheet is decreasing though the eustatic sea level is rising. Two main processes are involved in the uplift; the instantaneous elastic uplift and the glacial isostatic adjustment taking thousands of years to reach equilibrium after large ice mass changes.

(GNET) was established in 2007-2009. It currently counts 59 GNSS stations on bedrock along the coast of Greenland (figure 1.3). The data has been used to study ongoing mass loss of the GIS (Khan *et al.*, 2010a; Bevis *et al.*, 2012, 2019) as well as verifying GIA models (Khan *et al.*, 2008, 2016). The vertical movement is directly related to the mass loss and depends strongly on the distance to the loading change and thus gives valuable information on where mass loss is located (Khan *et al.*, 2010b; Bevis *et al.*, 2019).
Recently, several studies have shown that GNSS stations can also be used to study the surroundings using reflected signals. The first paper included in this thesis aims at testing GNSS Interferometric Reflectometry (GNSS-IR) for sea level measurements using data from the GNET station in Thule (THU2) where the measurement is complicated by sea ice and ice bergs. The resulting sea levels are compared to measurements from a nearby tide gauge and radar altimetry. The second study also focus on GNSS-IR but in this case we tested a new GNSS setup at the Programme for Monitoring of the Greenland Ice Sheet (PROMICE) Automatic Weather Station (AWS), NUK-K, for measurements of snow height by comparing results to a sonic ranger on the weather station. The third paper studies the changes in the drainage cycles of the ice dammed lake Tininnilik using satellite altimetry and uplift data from the GNET stations TIN1 and ILUL. All mentioned stations can be found on figure 1.3.

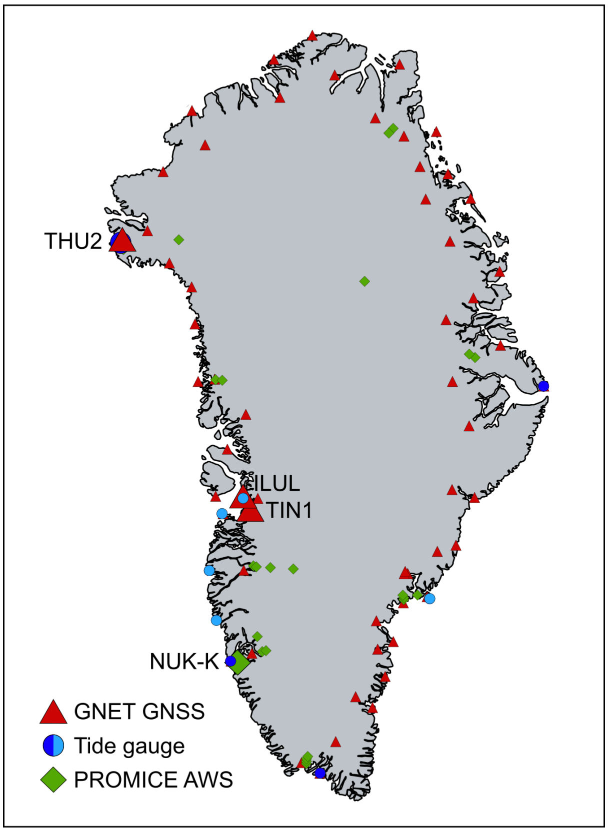

Figure 1.3: Map of Greenland with GNET GNSS stations, PROMICE AWSs and tide gauges. Dark blue tide gauges are operating while light blue are decommissioned. Stations used in this work are marked with large symbols and GNET stations and PROMICE stations are named. The used tide gauge station in Thule is right next to THU2 on the map.

1.5 Thesis outline

In section 2 I describe the observations used in the work of this thesis. Section 3 gives an introduction to GNSS and in particular GNSS-IR measurements of sea level and snow heights. In section 4 I give a short summary of each of the three papers included in the thesis. In section 5 I discuss the results and options of improving or continuing the work. Section 6 summarizes the main conclusions of of the thesis, including the three papers.
The three papers as well as the supplementary material for paper one is attached in the appendix.

2 Observations of ice, snow and water levels in the Greenland

2.1 Altimetry

Since the 1960s satellite remote sensing has made observations of the otherwise hardly accessible arctic region increasingly available. Satellite radar altimetry is one such method, observing the height of the surface beneath the satellite, and is widely used to study both sea level (Idzanovic *et al.*, 2017; Quartly *et al.*, 2019; Rose *et al.*, 2019) and the height of ice sheets and glaciers (Sørensen *et al.*, 2018; Simonsen *et al.*, 2021; The IMBIE Team, 2020). The continuous coverage of the arctic region by satellite altimetry started with the launch of ERS-1 in 1991. Unfortunately, there are some issues with the data quality and thus the altimetry era is often said to start in 1993 after the launch of TOPEX/Poseidon (Rose *et al.*, 2019). However, TOPEX/Poseidon as well as the Jason satellites only observe the Earth up to 66° north and are thus not useful for studies in the arctic regions. Figure 2.1 summarizes the satellite altimetry missions covering a significant part of the arctic regions.
The basic principle of satellite radar altimetry is that a radar pulse is emitted from the satellite and the time it takes it to return is used to calculate the distance to the reflecting surface using the speed of light. The nadir reflection point on the returned waveform is estimated using a retracker. Several different retrackers are available and the choice depend on the reflecting surface as well as the demands of the results. From this distance, called the range, the height of the surface above the ellipsoid is calculated using the known position of the satellite. To this result several correction are typically applied including atmospheric delays and solid earth tides (Sørensen *et al.*, 2015; Rose *et al.*, 2019).

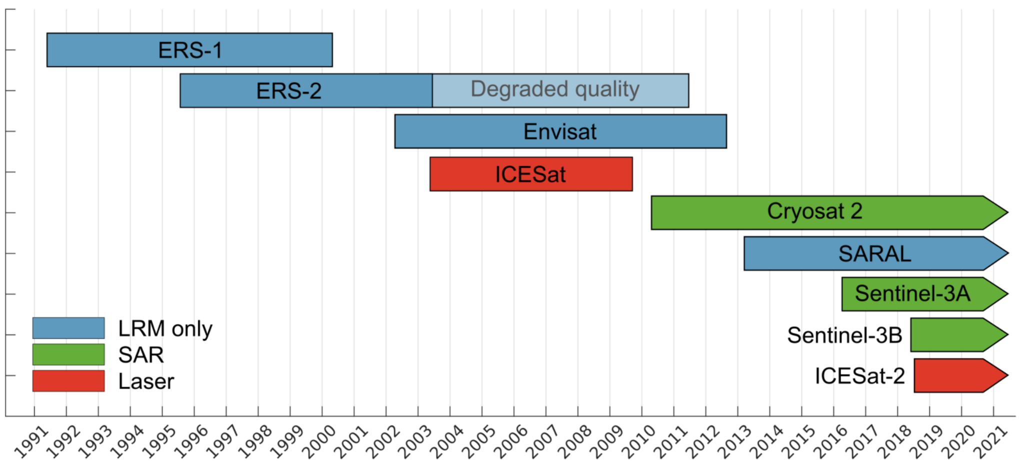

Figure 2.1: Timeline of satellite altimetry covering the arctic regions.

Satellite radar altimetry has a large pulse limited footprint of several km in diameter. This results in complications in regions of highly varying topography such as studies of coastal sea level or glacier margins (Sørensen *et al.*, 2018; Idzanovic *et al.*, 2018). Some modern radar altimeters are capable of working in Synthetic Aperture Radar (SAR) and SAR interferometric (SARin) mode (SARin is currently CryoSat-2 only) as well as the conventional

Low Resolution Mode (LRM). In SAR mode the doppler modulation of the signal is utilized to increase the spatial resolution in the along-track direction. In SARin mode a second antenna is activated and used to determine the angle of arrival reducing issues with off-nadir reflections. The improved resolution is particularly useful in challenging topographic areas such as sea level in coastal regions and marginal ice heights and when using leads in the sea ice to estimate sea level over ice covered water (Armitage & Davidson, 2014; Idzanovic *et al.*, 2017; Sørensen *et al.*, 2018). CryoSat-2 is operating in all three modes based on a geographical mask. It operates in SARin along the coast of Greenland and in SAR mode over most of the Arctic ocean while it operates in LRM over the interior of the Greenland ice sheet (Quartly *et al.*, 2019).

Over glaciers and ice caps, penetration of the radar signal into the snow and firn is a known error source. The amount of penetration depends on the state of the snow/firn layer, particularly whether it is wet or dry and thus varies over time introducing errors in the estimated elevation changes (Nilsson *et al.*, 2015; Sørensen *et al.*, 2015, 2018). Nilsson *et al.* (2015) find elevation biases of up to 89 cm in CryoSat-2 data of the GIS after the melt event in 2012 due to newly developed ice lenses. Laser altimetry solves the issue with penetration of the snow as the short wavelength of laser signals reflect directly off the air-snow interface. It also has a much smaller footprint ($\sim$60 m for ICESat and $\sim$14.5 m for ICESat-2) meaning that observations are possible in areas with a complex topography (Sørensen *et al.*, 2015; Smith *et al.*, 2020). However, a drawback from the short wavelength is that laser altimetry is unable to observe through cloud cover. The differences between laser and radar altimetry are illustrated on figure 2.2. In order to bridge the gap between the two laser altimetry missions; ICESat (2003-2009) and ICESat-2 (launched in 2018), NASA has been carrying out annual campaigns over the arctic regions called Operation IceBridge. These flights carry multiple instruments including radar- and laser altimeters. The results have been widely used to estimate elevation changes of the GIS as well as the AIS and glaciers in Alaska (MacGregor *et al.*, 2021).

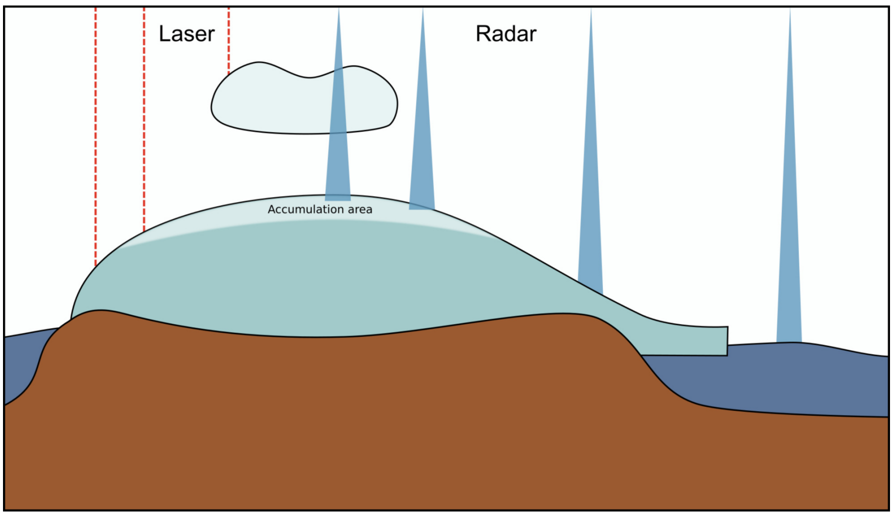

Figure 2.2: Illustration of laser and radar altimetry. Radar altimetry has a much larger footprint than the laser altimetry and penetrates into the dry snow in the interior of the ice sheet. It does not penetrate bare ice and penetration is decreasing as the snow gets increasingly wet towards the ablation zone. Radar altimetry has the advantage of being able to observe through clouds while laser altimetry is not.

2.2 Tide gauges

Tide gauges are used for in situ measurements of sea level. As they are fixed to a reference e.g. a pier they measure RSL variations between the reference and the water level. In studies of GMSL, tide gauge data needs to be corrected for movement of the reference point. Due to VLM from both ongoing ice mass loss and GIA, data from tide gauges in glaciated regions are often omitted from studies of GMSL if there is no co-located GNSS station (Woeppelmann *et al.*, 2009; Spada & Galassi, 2012).

The Permanent Service for Mean Sea Level (PSMSL, psmsl.org) collects long term tide gauge data from all over the world (Holgate *et al.*, 2013). There are generally a low density of tide gauges towards the arctic ocean and many have been discontinued. Particularly, a large number of Russian tide gauge stations were discontinued in the early 1990s. In Greenland there are data from a total of nine tide gauges. However, only four of these are in operation today, the rest were discontinued in 1997 - 1999 (figure 1.3). Only the recent re-installation of the tide gauge in Nuuk is properly datum controlled and therefore the data from the other stations should be used with caution as there may be unknown changes to the reference point.

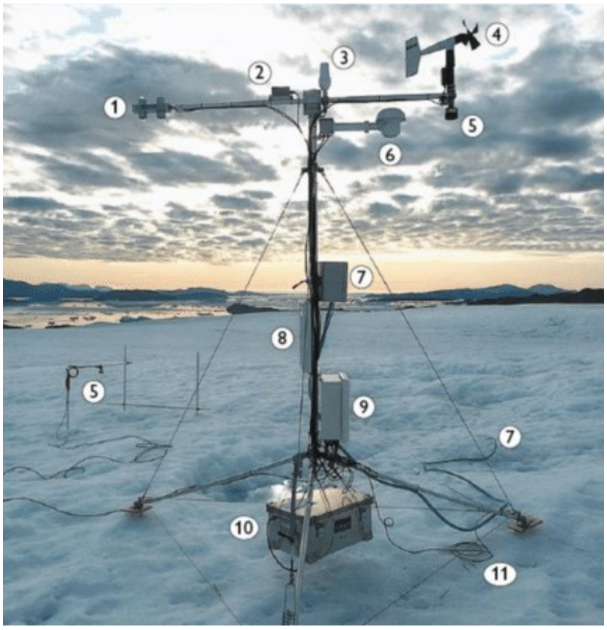

Figure 2.3: PROMICE weather station, MIT. From: van As *et al.* (2011). 1: Radiometer, 2: Inclinometer, 3: Satellite antenna, 4: Wind speed and -direction, 5: Sonic rangers (snow/ice height), 6: air temperature and humidity, 7: Pressure transducer (ice ablation), 8: Solar panel, 9: Data logger, barometer and GPS, 10: Battery, 11: Thermistor string (ice temperatures).

2.3 Automatic weather stations

Traditionally in situ measurements of SMB have been done using stakes and snowpits. Another way to obtain in situ measurements of SMB is using AWSs, which have the advantage of high temporal resolution while only requiring visits for maintenance (typically no more than once a year). These generally measure several climate parameters and can thus give a wide level of information on the local climate. PROMICE is a network of such AWS stations in Greenland maintained by the Geological Survey of Denmark and Greenland (GEUS). Another large network of weather stations in Greenland is the Green-

land Climate Network (GC-Net) which was originally operated by NASA's climate research program but is now run by GEUS as well (promice.org). The first GC-Net station was installed in 1990 at Swizz Camp and the first PROMICE station in 2007. While most of the PROMICE stations are placed in the ablation zone of the Greenland ice sheet (figure 1.3) the GC-Net stations are mainly spread over the interior of the ice sheet.
The PROMICE stations measure classic weather parameters such as wind speed and -direction, air temperature, air pressure and humidity as well as upward and downward radiation, surface height (using sonic rangers and a pressure transducer drilled into the ice) and subsurface temperatures (thermistor string drilled down to 10 m) (see figure 2.3). The stations are equipped with a simple GPS unit logging only position. They transmit data every hour during summer when there is plenty of sunlight and daily in winter (Fausto *et al.*, 2021).

3 GNSS measurements

Today four GNSSs systems are operational: The well known American Global Positioning System (GPS), the Russian GLONASS, the European Galileo and Chinese BeiDou. They are all used to estimate the position of a GNSS antenna by estimating the distance from a number of satellites to the antenna at a given time (figure 3.1a). In order to calculate the position, at least fours satellites need to be in view. In theory three could be enough if the time was known very precisely at both the time of transmission from the satellite and when the signal is received at the antenna. However, the receiver clock is too inaccurate and a fourth satellite is needed to account for this. If more satellites are observed at once, the position measurement will be more precise.
There are several error sources in GNSS positioning including satellite clock inaccuracies, orbit errors, tropospheric- and ionospheric delay, and multipaths. Satellite orbit errors are reduced by taking into account the phase center offsets. Tropospheric- and ionospheric delays are modelled (Boehm *et al.*, 2006). Ocean- and solid earth tides are modelled and accounted for. Multipaths are GNSS signals reaching the antenna after reflecting off a surface. In order to reduce these, some antennas are equipped with choke rings to minimize signals from below and the antenna gain pattern is constructed to enhance signals from high elevation angles. This reduces the amount of reflected signals reaching the antenna but it does not remove all multipaths. The remaining multipath error is unmoddeled in positioning as it depends on the environment around each individual station.

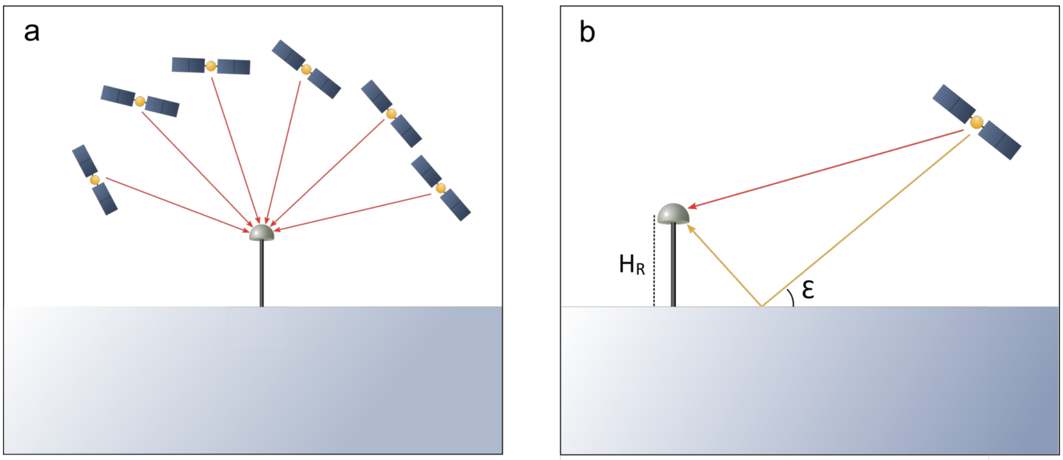

Figure 3.1: a: In order to calculate the position of a GNSS station a minimum of four satellites are observed at once and the distance to the GNSS antenna is calculated. From these distances the position of the GNSS station is estimated. b: In GNSS-IR we study each satellite passing individually and use the interference between the direct and reflected signal (red and yellow arrow, respectively) to the estimate reflector height, H_R.

3.1 GNSS Interferometric Reflectometry

Reflected GNSS signals, also called multipaths, are an unmodelled source of error in GNSS positioning. In GNSS reflectometry the reflected signal is utilized to study the reflecting surface. For the first two studies included in this thesis we used GNSS-IR using one antenna and the calculations were done using the code developed by Larson (2021). It is available on github and is described by Roesler & Larson (2018). Other types of GNSS reflectometry exist. One such method consist of a two antenna system with one antenna looking up and one down, and has been tested for measurements of sea level and compared to GNSS-IR based on one antenna (Löfgren *et al.*, 2011; Larson *et al.*, 2013a). Another example is airborne reflectometry that can e.g. be used for studies of soil moisture (Katzberg *et al.*, 2006).

GNSS-IR is based on studying the interference pattern created by the direct and reflected signal. We use the Signal to Noise Ratio (SNR) data but multipaths are registered in the carrier phase as well. However, it is difficult to isolate it in the carrier phase data due to the influence of atmospheric delays, clocks, orbits and position (Larson *et al.*, 2008). The method has bees developed as a way to study the environment around a GNSS station during the last decade or so. It can be used to study soil moisture (Larson *et al.*, 2008, 2010), vegetation water content (Wan *et al.*, 2015; Larson, 2016a), sea ice detection (Strandberg *et al.*, 2017), permafrost processes (Liu & Larson, 2018), snow depths (Larson *et al.*, 2009; Gutmann *et al.*, 2012; Siegfried *et al.*, 2017) and sea level variations on different time scales (Larson *et al.*, 2013b, 2017; Tabibi *et al.*, 2020). While the first three of these applications focus on studying the properties of the reflecting surface the others try to extract the vertical position of the reflecting surface relative to the GNSS antenna. Most GNSS-IR studies take advantage of geodetic GNSS stations already installed for other reasons but there are also studies specifically installing a GNSS station with reflectometry in mind (e.g. Williams *et al.*, 2020). This section will describe how the vertical distance between the antenna and a horizontal reflecting surface, called the reflector height, is determined.

While we need to observe several satellites at once to estimate positions, in GNSS-IR we study the satellite tracks individually. The reflected signal, also called the multipath, reaches the GNSS antenna after reflecting off a surface. The additional travel distance causes a delay compared to the direct signal dependent on the position of the reflector and the satellite elevation angle (figure 3.1b). For a planar horizontal reflector the delay can be expressed as (Georgiadou & Kleusberg, 1988):

$$d = 2H_R sin(\epsilon) \tag{3.1}$$

Where H_R is the reflector height and ϵ is the satellite elevation angle. For a stationary, horizontal reflector this results in a phase difference of (Georgiadou & Kleusberg, 1988):

$$\theta = \frac{4\pi H_R}{\lambda} sin(\epsilon) \tag{3.2}$$

Where λ is the wavelength of the transmitted signal. As the phase difference depends on the elevation angle it creates a varying interference between the direct and reflected signal where the two signals will oscillate between positive and negative interference. The frequency of this interference pattern can be found using that:

$$f = \frac{1}{2\pi} \frac{d\theta}{dt} \tag{3.3}$$

If we assume a constant horizontal reflector the resulting frequency is:

$$f = \frac{2H_R}{\lambda} cos(\epsilon) \frac{d\epsilon}{dt} \tag{3.4}$$

In order to simplify this we follow the strategy from Axelrad *et al.* (2005) changing the variable from t to $sin(\epsilon)$ as this will eliminate the derivative and result in a constant frequency:

$$f_{sin(\epsilon)} = \frac{1}{2\pi}\frac{d\theta}{dsin(\epsilon)} \Rightarrow \tag{3.5}$$

$$f_{sin(\epsilon)} = \frac{2H_R}{\lambda} \tag{3.6}$$

Thus, if we can extract this frequency from the SNR data we can also estimate the reflector height. The SNR data from the GNSS station consists of contributions from both the direct and the reflected signal. Two examples of what this data may look like in the case of a horizontal reflector can be seen on figure 3.2. Figure 3.2a shows the SNR data from a satellite track at THU2. The direct signal contribution is the slowly varying part which is a result of SNR increasing with increasing elevation angle (and vice versa). The fluctuations are a result of the interference with between the direct signal and the multipath and the frequency of this is what we can use to estimate reflector height. Figure 3.2b shows the SNR data for a satellite track at the GNSS station at NUK-K. Here we see only the descending part of the satellite track as the logging time is limited to 3 hours each day which have resulted in an incomplete logging of the satellite track. The frequency of the oscillation at the two sites are clearly different which is a result of the different reflector heights of approximately 20 m at THU2 and less than one meter at NUK-K. The red line at both plots indicate the part of the SNR data below 25 degrees which is typically used for GNSS-IR as the interference pattern is strongest at low elevation angles due to the less effective multipath reduction at the antenna.

In order to estimate the frequency of the interference pattern, the direct signal contribution to the SNR data is first removed. This can be done by fitting and subtracting a low order polynomial to the data. When this is done the remaining dSNR data can be described by a sinusoid:

$$dSNR(\epsilon) = A(\epsilon)sin\left(\frac{4\pi H_R}{\lambda}sin(\epsilon) + \phi\right) \tag{3.7}$$

where $A(\epsilon)$ is the amplitude and ϕ is the phase shift. The amplitude, $A(\epsilon)$, depends on the properties of the reflecting surface and the antenna gain pattern as well as the elevation angle of the satellite. While GNSS-IR studies of vegetation water content are based on changes in the amplitude (Wan *et al.*, 2015; Larson, 2016a), changes in soil moisture affect both the amplitude, A, and the phase shift, ϕ, and both methods have been tested for estimating soil moisture in the top 5 cm (e.g. Larson *et al.*, 2008, 2010). The height of the reflector can now be found by estimating the dominant frequency of the dSNR data with respect to $sin(\epsilon)$ using spectral analysis.

GNSS stations typically record data, including SNR, at a constant rate in time but not as a function of the sine of the satellite elevation angle and thus we have to use a method for spectral analysis that performs well for unevenly spaced data. For this purpose we use the Lomb Scargle Periodogram (LSP) (Lomb, 1976). Figure 3.3 shows the LSPs from the GNSS station at NUK-K from the 19th of May for the GPS L1 signal. Red lines are accepted tracks and grey lines are tracks that are not accepted. The rejection of tracks is done by choosing a set of QC parameters, namely the peak amplitude and the signal to noise ratio of the LSPs. The QC parameters should be set for each site individually after studying the LSPs. The amplitude will vary from site to site but also depends on e.g. what satellite elevation range the SNR data is extracted for. The signal to noise ratio of the LSPs also depend strongly on the range used to calculate it which should be decided on a site to site basis as it should include the expected peak position. The QC process

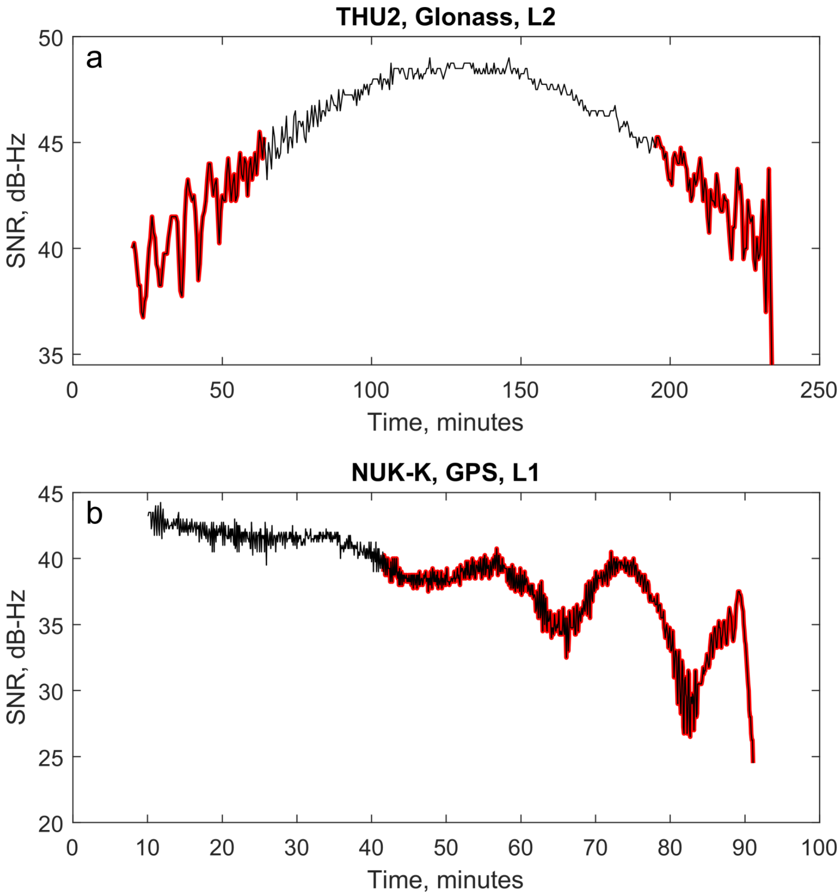

Figure 3.2: a: SNR data from the THU2 GNSS station in Thule for the L2 signal from the passing of a GLONASS satellite on the 19th of May 2020. Red lines show data from below 25° elevation angle which is the part typically used for GNSS-IR. b: SNR data from the GNSS station on the NUK-K weather station for the L1 signal from the passing of a GPS satellite on the 19th of May 2020. The red line show data from below 25° elevation angle. Only the descending part is measured due the limited logging time (see publication 2).

also ought to reject arcs that are too short and the code used here requires that the track covers the satellite elevation arc investigated plus/minus some elevation difference which can be set by the user. The median which is also shown in the plot is the median of the peak reflector height from all accepted arcs, and is used to eliminate outliers when calculating daily average reflector heights.

3.1.1 Sensing zone and limitations

The footprint of GNSS-IR can be approximated by the first Fresnel zone. These zones take the form of ellipses around the specular point and the size depends on the satellite elevation angle, signal wavelength and height of the reflector (Löfgren *et al.*, 2011; Katzberg *et al.*, 2006). The dependence on reflector height is of particular interest as it will change over time and thus so will the sensing area. Figure 3.4 shows the first Fresnel zones for the GPS L1 signal at NUK-K (figure 3.4a) and THU2 (figure 3.4b). The illustrated Fresnel zones at NUK-K are calculated using a reflector height of 3 m, corresponding to the

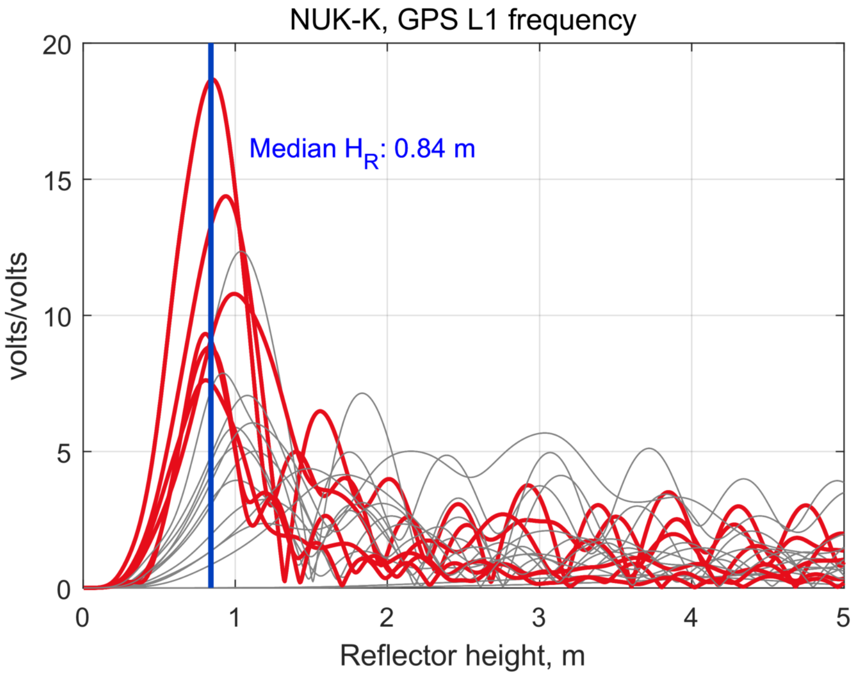

Figure 3.3: Periodogram from GNSS station at NUK-K the 19th of May 2020 for the GPS L1 signal. Red lines are accepted satellite tracks and grey lines are rejected. The median is used to remove outliers for calculation of daily average reflector heights

distance to the ice surface resulting in a diameter of the sensing zone of approximately 80 m. For THU2 the Fresnel zones are calculated using a reflector height of 20 m which approximates the distance to the sea surface and the result is a radius of about 320 m. In reality there was an obstruction between 85 and 215 degrees at NUK-K so these angles could not be used but here all azimuths are shown for completeness. Similarly, at Thule only azimuths over the ocean are used in the sea level study.

In order to estimate the reflector heights, the surface must act as a specular reflector. For

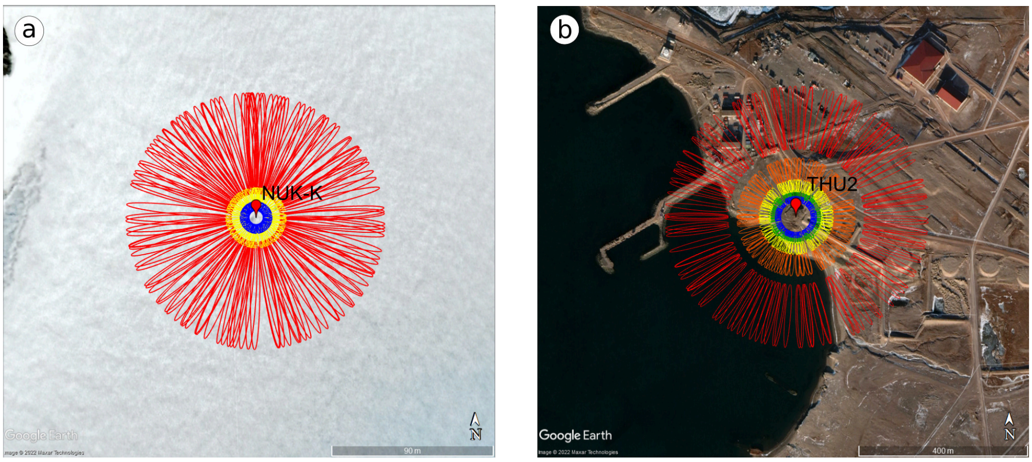

Figure 3.4: Fresnel zones at a: NUK-K and b: THU2 including all azimuths. Elevation angles are: 5° (red), 10° (orange) 15° (yellow), 20° (green), 25° (blue).

this to be true, the surface has to be nearly planar and sufficiently smooth in the vicinity of the first Fresnel zone for all relevant satellite elevations. For sea level studies this can

cause trouble at times of strong wind (Larson *et al.*, 2021a) and a lot of wave action. In snow studies fractures in the ice surface or substantial vegetation can make extractions impossible (Larson & Nievinski, 2013; Larson *et al.*, 2015).
As for other spectral methods there is a minimum required logging rate in order for the extraction of the reflector height to be possible. In spectral analysis the Nyquist limit determines the maximum frequency that can be extracted from a data set based on the distance between measurements. For evenly spaced data the limit is half the sampling rate. For unevenly spaced data it is not well defined and several different definitions of a pseudo-Nyquist limit exists (VanderPlas, 2018). A simple an commonly used estimate of the pseudo-Nyquist limit is defined from the average spacing between two observations (VanderPlas, 2018; Roesler & Larson, 2018):

$$f_{Ny} = \frac{1}{2}\frac{N}{W} \tag{3.8}$$

where N is the number of observations and W is the window length. This is a conservative estimate as the uneven sampling can generally extract larger frequencies than evenly sampled data. It can, however, be used as a rough estimate on how high your sample rate should be in order to extract a given reflector height. For most snow studies 30 s sampling would be sufficient as the reflector height is rarely above 3-5 m. For some sea level studies the reflector height is very large (100s of meters) and in these cases one should be careful to set the sampling rate high enough. As an example a sampling interval of 1s results in a max reflector height of about 400 m based on the average observation spacing (Roesler & Larson, 2018). Similarly any reflector height below 2λ, equivalent to about 40-50 cm, will be poorly resolved (Larson *et al.*, 2009; Roesler & Larson, 2018).

3.1.2 Snow studies

In GNSS-IR snow studies the GNSS signal will reflect off layers in the snow pack as well as the air-snow interface, however, the air-snow interface is the dominating reflector (Gutmann *et al.*, 2012; Larson *et al.*, 2015). The first paper using GNSS-IR to study snow depth was Larson *et al.* (2009) who tested the method on a GNSS site in a field near Boulder, Colorado, during two snow storms in spring 2009 and compared the results to nearby sonic rangers. Since then, multiple studies have been conducted using GNSS-IR for measurements of snow depth; both on ground (e.g. Hefty & Gerhatova, 2014; McCreight *et al.*, 2014; Larson & Small, 2016b) and on glaciers and ice sheets (e.g. Siegfried *et al.*, 2017; Larson *et al.*, 2020; Pinat *et al.*, 2021). Some studies compare results to other measurements from e.g. stakes or sonic rangers. They generally find that GNSS-IR slightly overestimates reflector heights possibly due to penetration of the upper few cm of snow (Ozeki & Heki, 2012; McCreight *et al.*, 2014; Siegfried *et al.*, 2017). In the studies were the other snow data is obtained locally and close to the GNSS station, results show that we can estimate daily snow height with an accuracy of at about 10 cm or better (Hefty & Gerhatova, 2014; McCreight *et al.*, 2014; Larson *et al.*, 2020). GNSS-IR has also been used for different modelling studies, e.g. Larson *et al.* (2015) compares GNSS-IR reflector height to results from a firn compaction model and Shean *et al.* (2017) use it for a model of SMB and basal melt at Pine Island glacier in Antarctica.
McCreight *et al.* (2014) use GNSS-IR at 18 GNSS stations in western U.S. to study Snow Water Equivalent (SWE). The density is modelled and compared to measurements from a single snow pit at each site. Using the modelled density SWE is calculated at compared to measurements from nearby Snow Telemetry (SNOTEL) sites. They find that the bias and RMSD is as would be expected by scaling the depth error with density (below 2 cm SWE at most sites) and conclude that GNSS-IR could be used for measurements of SWE for water resource management.

An advantage of GNSS-IR as compared to more traditional snow depth measurements such as a sonic ranger is that the position of the antenna is measured in a geocentric reference frame at high precision. Combining the position of the antenna with the reflector height one can estimate the height of the snow surface in the geocentric reference frame (e.g. Shean *et al.*, 2017; Pinat *et al.*, 2021). These geocentric surface heights can be used to calibrate satellite altimetry products. However, as glaciers and ice sheets are flowing, it is necessary to correct for the downflow motion in order to compare variations in the height of the surface with satellite altimetry or other stationary products (Larson *et al.*, 2015; Pinat *et al.*, 2021).
Most GNSS-IR studies of snow were done using SNR data as described here but since SNR data is not always included in the data files some studies also tested the method on the geometry free linear combination of L1 and L2 carrier phases called L4 (Ozeki & Heki, 2012; Hefty & Gerhatova, 2014). Ozeki & Heki (2012) find that the method works for L4 as well but the oscillations from the interference between the multipath and the direct signal are less pronounced and the results more noisy. Furthermore, L4 is affected by ionospheric variability and therefore they recommend using SNR data when it is available.

3.1.3 Sea level measurements and $\dot{H}$ correction

Measuring sea level using GNSS-IR has the immediate benefit that the vertical motion of the bedrock is measured at high precision. Thus, it is possible to correct for any motion related to elastic or isostatic rebound or tectonic plate motion. These movements are otherwise a considerable source of error as they can be difficult to model in order to use tide gauges for measurements of absolute sea level and for verification of altimetry products. Another advantage is that there is no need for in-water infrastructure such as stilling wells, resulting in a generally more simple and less maintenance demanding installation (Larson *et al.*, 2013a).
While the assumption that the reflector height is constant over the time of a satellite passage is reasonable for studies of snow height, it is not generally the case for sea level studies as tides can cause relatively large sea level variations over short timescales (Larson *et al.*, 2013b; Löfgren *et al.*, 2014). When studying sea levels it is therefore often necessary to take into account the changing reflector height. If we assume that the reflector height is varying in time, the derivative of the phase will then become (equation 3.2 and 3.5) (Löfgren *et al.*, 2014):

$$f_{sin(\epsilon)} = \frac{1}{2\pi}\frac{d\theta}{dsine\epsilon} = \frac{1}{2\pi}\frac{d\theta}{dt}\frac{dt}{dsine\epsilon} \Rightarrow \tag{3.9}$$

$$f_{sin(\epsilon)} = \frac{2\dot{H}_R}{\lambda}\frac{tan(\epsilon)}{\dot{\epsilon}} + \frac{2H_R}{\lambda} \tag{3.10}$$

where the dot denotes the time derivative. Rearranging to isolate H_R we have that:

$$H_R = \frac{f_{sin(\epsilon)}\lambda}{2} - \dot{H}_R\frac{tan(\epsilon)}{\dot{\epsilon}} \tag{3.11}$$

The first term is equivalent to the reflector height estimated assuming a constant reflector and the second term we will call the $\dot{\text{H}}$ correction. The reflector height for a time varying reflector can then be calculated from the result of the standard method as:

$$H_R = \tilde{H}_R - \dot{H}_R\frac{tan(\epsilon)}{\dot{\epsilon}} \tag{3.12}$$

Where $\tilde{H}_R$ is the reflector height calculated assuming a constant reflector height. Calculating the correction term requires an estimate of the time derivative of the reflector height.

For this one could use either a model of the tides or, if it is expected to be sufficiently accurate, the standard solution as done in Larson *et al.* (2013b).

Löfgren *et al.* (2014) studies sea level using GNSS-IR at five different sites and find that it is absolutely necessary to use the extended method at the station in Brest, France (BRST), where the tidal range is 7.72 m. At this site the RMSD with a local tide gauge halves after applying the extended method, taking into account the time dependent reflector height. The results also improve slightly at SCO2 at Friday Harbor, USA, where the tidal range is 4.02 m. For the rest of the stations the tidal range is up to 3.64 m and the result does not improve significantly.

GNSS-IR using the spectral method with the $\dot{H}$ correction applied has been tested for both short- and long term sea level monitoring as well as tidal analysis and compared to results from nearby tide gauges (e.g. Löfgren *et al.*, 2014; Larson *et al.*, 2017; Tabibi *et al.*, 2020; Williams *et al.*, 2020). They generally find that the uncertainty is much larger for GNSS-IR than for tide gauges when looking at the individual measurements while the two agree within a few cm when comparing daily average sea levels (Larson *et al.*, 2013b, 2017). Löfgren *et al.* (2014) find large variations in the RMSD from nearby tide gauge at five GNSS-IR stations with the largest being BRST with a RMSD of 43 mm after applying the $\dot{H}$ correction.

The need to have an estimate of the time derivative of the reflector height, in order to take into account the varying reflector heights using the spectral method, has motivated using inverse modelling to extract reflector height for sea level studies (Strandberg *et al.*, 2016; Tabibi *et al.*, 2020). Strandberg *et al.* (2016) used an inverse model based on a B-spline to extract reflector heights at two stations (GTGU in Onsala, Sweden and SPBY in Spring Bay, Tasmania) directly accounting for a varying reflector height. They find significant improvement in the comparison with tide gauge measurements compared to the $\dot{H}$ corrected spectral method on individual measurements.

In regions where sea ice covers the ocean during winter it will affect the GNSS-IR measurements. The reflector will now be the top of the ice which is higher than what would be measured by a tide gauge station by the freeboard of the sea ice. If a considerable snow layer is established on the sea ice it will further enhance this difference. Strandberg *et al.* (2017) studies the effect of sea ice on GNSS-IR and finds that the change in the reflecting surface results in changes to the attenuation of the amplitude of the interference pattern with elevation that are significantly different from the variations from open sea and that this can be used to indicate when the water is ice covered. All in all GNSS-IR is a useful tool in sea level extractions but at the moment it cannot replace tide gauges. There are two main reasons for this. First, the accuracy on the individual measurements are considerably worse than for traditional tide gauges (e.g. Larson *et al.*, 2013b, 2017). Second, the sampling of GNSS-IR is limited by the number of satellite passes and unevenly spread over the day, though for high reflector heights it is possible to divide one track into multiple parts due to the high frequency as done for BRST in Löfgren *et al.* (2014) resulting in a higher temporal resolution. The limited sampling rate can be further reduced due to the often quite narrow azimuth range covering the ocean compared to snow studies where a larger azimuth range can often be used.

4 Summary of papers

4.1 Publication 1: Sea level in Thule

The first publication (Dahl-Jensen *et al.*, 2021) was published in MDPI - Remote Sensing in December 2021. It can be found in appendix A. The aim of the study was to test the ability of GNSS-IR to measure inter annual sea level variations in arctic conditions. GNSS-IR is particularly useful in arctic regions since changes in ice masses result in vertical movement of the bedrock. This results in large uncertainties when using tide gauges for studies of absolute sea level rise as these vertical movements cannot be modeled with the accuracy needed in order to study long term sea level change. Furthermore, GNSS stations require considerably less maintenance than tide gauge stations which is an advantage in areas where regular maintenance is difficult and expensive.

We use the GNET GNSS station THU2 located in Thule in northern Greenland. This station was chosen because it is the only GNET station with a view of the ocean which is co-located with a tide gauge station. We calculate inter annual sea level variations from GNSS-IR, tide gauge and satellite altimetry from 2008-2019 and compare the results after correcting tide gauge and GNSS-IR sea levels for uplift using the position data from the GNSS station.

All three methods show a negative sea level trend in Thule with large inter annual variability. However, from the comparison we find larger differences between the results than would be expected from the estimated uncertainties for all three methods. This is not totally unexpected for the comparison with altimetry as it is not a local measurement as both GNSS-IR and tide gauge are. Potential explanations for the difference between the results from GNSS-IR and tide gauge are investigated. First, we look into the deviations of individual GNSS-IR measurements from tide gauge as well as the daily averages. We find that the RMSD of individual measurements of variation when calculated for one month at a time is 13 cm which is comparable to what other studies find. However, if we calculate the RMSD of the daily estimates for the whole period the result is 65 mm which is about 3 times what other studies find. The RMSD for the daily measurements is smaller than the estimated uncertainty on both GNSS-IR and tide gauge and we therefore suggest that the cause for the unexpectedly large deviations are non-random differences between the two measurements not captured by the uncertainty estimate.

We investigate sea ice cover as a potential cause by comparing annual sea level variations limiting the data to August and September, where the ocean is assumed to be ice free. The results do not improve and we conclude that it cannot fully explain the differences. A possible explanation is that the tide gauge is not datum controlled and therefore there could potentially be small shifts or drift in the tide gauge data not accounted for.

We also model the effect of reduced gravitational attraction as a result of ice mass loss on sea level and find a trend of -3 mm/year. This can at least to some extend explain the negative sea level trend. The inter annual variability in modelled gravitational sea level is small and thus cannot explain the large inter annual variations in observed sea level.

4.2 Publication 2: Snow measurements at NUK-K

The second publication (Dahl-Jensen *et al.*, 2022) was published in the MDPI remote sensing special issue *Satellite Earth Observation of Climate Change Effects on Glaciers and Ice Sheets* in May 2022. It can be found in appendix C. The aim of the study was to investigate if a new GNSS installation at the PROMICE AWS, NUK-K, could be used for GNSS-IR studies of snow height. The GNSS installation was designed to be able to communicate with the weather station and minimize the power consumption. The main purpose of the installation was to develop a GNSS setup for high precision positioning with the goal of measuring glacier flow with high precision. The GNSS system was installed in March 2020 and removed again almost six months later in August.

Due to the need to reduce the power consumption, the GNSS station was set up to log for only three hours a day, and on many days the time is further reduced due to limited power. This greatly reduces the amount of GNSS-IR extractions since a satellite elevation arc of at least 15 degrees (in this case) is needed to extract the reflector heights. Furthermore, a hill to the south-east of the weather station is blocking the view of the satellites at the low elevation angles needed for GNSS-IR between 85° and 215° azimuth, further reducing the available satellite tracks.

We successfully extract GNSS-IR reflector heights from GPS, Galileo and GLONASS signals and compare daily reflector heights with results from a sonic ranger installed on the weather station (part of the standard PROMICE setup). The results are promising as the GNSS-IR results show largely the same snow melt and onset of the main melt period as well as small fluctuations of melt and snowfall in spring. However, there are also considerable differences between the two methods. Looking into the azimuthal distribution of the GNSS reflections we don't find any relationship between this and the deviation from the sonic ranger results. We conclude that the deviation is most likely due to the much larger footprint of GNSS-IR (2,500-13,000 m^2) compared to the sonic ranger ($\sim$ 1 m^2) and an uneven snow distribution and melt.
After the snow has melted completely, towards the end of the data collection, the estimated uncertainty on the daily GNSS-IR results start to increase due to a larger spread on the individual extractions. Looking at these we find that the individual peaks are also less pronounced than previously. We conclude that it is likely due to a change in the surface towards more roughness which disturbs the measurement.

If similar installations are done at other PROMICE weather stations, with reflectometry in mind, it should be considered to expand the power supply in order to get a longer and more stable logging time. This is especially important if the height of the ice surface in the ablation zone is of interest, as the roughness of this greatly increases the uncertainty on the measurement. At some PROMICE stations it may only be possible to extract reflector heights when the surface is completely snow covered due to a fractured or otherwise too rough surface. In the end, the feasibility of the technique will have to be assessed on a case by case basis.

4.3 Publication 3: Ice-dammed Lake Tininnilik

The third paper was submitted to Journal of Geodesy in August. It can be found in appendix D. We studied the drainage cycles of the ice dammed Lake Tininnilik located in the Disko Bay area in West Greenland. From 1940 up until 2003 the lake drained approximately every ten years at about the same water level. Since 2003 it has been draining at shorter time intervals and at continuously lower water levels. The most recent drainage event happened in 2020, 5 years after the last event, at a record low water level of 224 m. The decreasing maximum water level coincides with a thinning of the damming glacier observed by altimetry. This supports the theory that drainage events occur when the hydrostatic pressure at the bottom of Lake Tininnilik exceeds the ice overburden pressure. Both in 2015 and 2020 we observe a period of approximately constant water level after the drainage event. However, since both events occur in the autumn, where we might expect that there is not much melt water present, we cannot conclude when the drainage system closed.

The GNET station TIN1 is located a few kilometers from the lake. There is position data from the station for the events in 2010 and 2020. The event in 2010 is clearly visible from the vertical position data from the station. In 2020 it is also seen but less pronounced and the uplift is of similar size as other variations. To enhance the uplift from lake drainage, we subtract the vertical position of GNET station ILUL 55 km away, assuming that the variations from atmosphere and ice mass changes are approximately the same for the two stations. The resulting differential uplift shows a clear uplift signal of the lake drainage both in 2010 and 2020. In both years the uplift is quite sudden and thus we conclude that at least most of the water volume exits the lake over just a few days. The total uplift in 2010 is 19 mm while it is 9 mm in 2020, supporting the decreasing drained volume observed from the water level time series. If TIN1 could have been used to measure the water level using GNSS-IR we would have had a water level time series at high temporal resolution covering the two events in 2010 and 2020. Unfortunately, that is not possible with the current setup. The station is placed a bit too far in on a plateau and the vertical distance to the lake is about 300 m which is far beyond the limit for the available 15 s sampling rate.

We estimate the infill rate using the last three drainage cycles and combine it with the trend in decreasing water level at drainage to estimate when the lake will drain again. This simple model suggests that the next drainage event will happen during 2024. The lake level at drainage has been decreasing at a rate of 1.5 m/year while the drained water level is constant, at least since 1993. If the current trend in the maximum water level continues and no continuous spillways are formed, the lake will drain at continuously lower water levels until the maximum water level will reach the level of the drained lake around 2053 and the quasi-cyclic drainage events will cease.

5 Discussion

5.1 GNSS-IR measurements of snow at PROMICE weather stations

The GNSS station used for the study of snow at the PROMICE weather station NUK-K was a test setup, removed at the visit in the end of August 2020 (paper 2). The main goal of the setup was to test the suitability for high precision positioning in order to track glacier flow at the PROMICE stations. We tested the usefulness of this setup for GNSS-IR measurements of snow height and though the station was far from optimal for reflectometry purposes we got reasonable result from a comparison with the sonic ranger on the weather station. Last summer (2021) a GNSS station was installed at a tripod next to another PROMICE station, QAS-M in south Greenland (figure 5.2). Unfortunately, the station is not transmitting and the data has not been collected yet, and thus we don't yet know if it is useful for reflectometry.

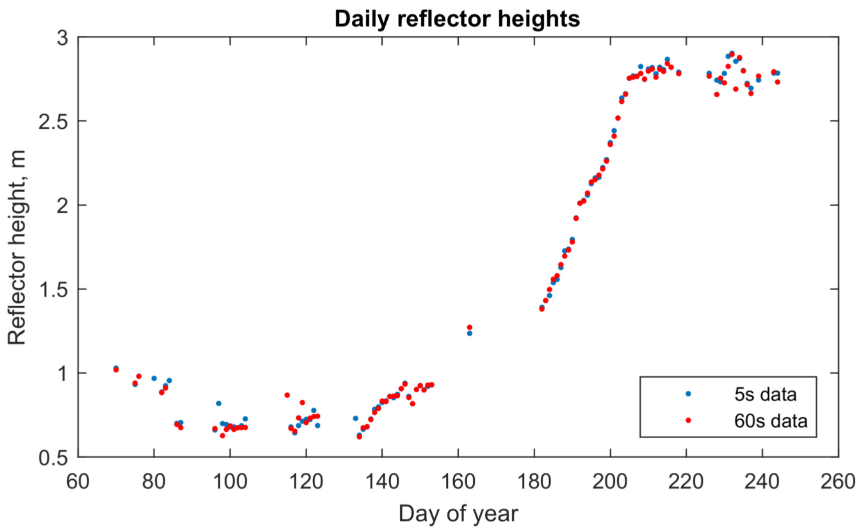

Figure 5.1: Reflector heights at NUK-K using 5 s data compared to reflector heights estimated using data reduced to a 60 s sampling rate.

It is the plan to install GNSS stations at all PROMICE stations to monitor glacier flow starting next year. There is a wish to be able to get relatively high precision positions in real time which results in a need to transmit the raw GNSS data. Transmitting requires a lot of power, and to fulfill this the logging time and rate has been reduced. The transmitted data will be about one hour daily at a 60 s sampling rate and GPS only. Running tests at NUK-K gives results at 60 s sampling rate very similar to the 5 s sampling (figure 5.1). It is unusual to use such low sampling rates but due to the low reflector height it is just within the pseudo Nyquist limit. However, even with 3 hours of daily data we rarely have more than 3-4 extractions a day using GPS only. Reducing the logging time to 1 hour will further reduce this and thus it is unlikely that the standard settings for the new GNSS setup will be useful for GNSS-IR. However, the setup comes with an option to remotely change the logging rate and time, allowing for campaigns at interesting locations and times where the logging can be improved for reflectometry purposes. The additional campaign data may

be stored locally to reduce the additional power consumption from transmission. Similarly, GLONASS and Galileo data could be logged and stored at a local drive for pickup at maintenance.
It is important to keep in mind that reflectometry might not be suitable at all locations. Some PROMICE stations are located where the surface is quite rough and fractured. Here, it may only be possible to do reflectometry when the snow cover is thick, smoothing much of the roughness. Another issue is that the snow cover at some stations during winter may be thick enough to make reflectometry impossible. Though the snow may not physically cover the instrument, a reflector height of at least 2 time GNSS signal wavelength ($\sim$ 0.4 - 0.5 m) is required for the measurement (Larson *et al.*, 2009; Roesler & Larson, 2018). The option to do short campaigns allow for testing reflectometry at different sites without additional installations. At sites where reflectometry appears particularly useful and interesting it could be an option to install a simple consumer grade GNSS station which logs to a local drive. Such a setup is both cheap and requires little power compared to the geodetic GNSS station. Studies show that reflectometry results are at least as good as for a geodetic station (Williams *et al.*, 2020). Some studies have even been done using smartphones and tablets with good results though these may not be suitable for the Arctic climate (Strandberg & Haas, 2020; Altuntas & Tunalioglu, 2021; Liu *et al.*, 2022). However, the position results of the consumer grade GPS/GNSS equipment is an order of magnitude worse than for a geodetic station, partly due to less multipath suppression (Williams *et al.*, 2020). As the main goal of installing GNSS stations at the PROMICE stations is to track glacier flow, a consumer grade GNSS station for reflectometry would be an addition to the geodetic station and not a replacement.

5.2 Water monitoring in Greenland

In the first paper included in this thesis we tested GNSS-IR at Thule for sea level monitoring by comparing reflectometry results to data from a nearby tide gauge and satellite altimetry. Currently, five GNSS stations in Greenland are included in the PSMSL GNSS-IR portal of sea level retrievals (www.psmsl.org/data/gnssir/). Four of these show good results with regards to GNSS-IR sea level retrievals (THU3, KULL, QAAR and PLPK, marked with green triangles on figure 5.2), while one gives questionable results (KULU, marked with a yellow triangle on figure 5.2). Extending the network of stations used for GNSS-IR measurements of sea level requires that the stations are suitable for this purpose. Several GNET stations are located with an open view of the ocean. However, stations at remote locations with a local power supply are only logging every 15 s which result in a maximum measurable reflector height of about 25 m. Many of the GNET stations have a vertical distance to the sea surface far larger than this. Stations with this sampling rate issue, which could otherwise be potential GNSS-IR sea level sites, include: KAGZ, KMOR, JWLF, KMJP, KBUG, LYNS. It could be considered to test the possibility of increasing the power supply and the sampling rate to test if the stations could then be useful for GNSS-IR measurements of sea level. One way to do this could be to transmit data from every 15 s but log every 1 s and store it on a local drive to be picked up at maintenance and thereby reducing the additional power consumption.

The Fresnel zones of four of the stations at possible test sites for an increased logging rate can be seen on figure 5.3. The plotted Fresnel zones do not take into account obstacles blocking the view of the ocean and thus it is unlikely that all reflection zones that seems to be over ocean are also available.
The KMOR station is located on a small island and has a reflector height of about 200

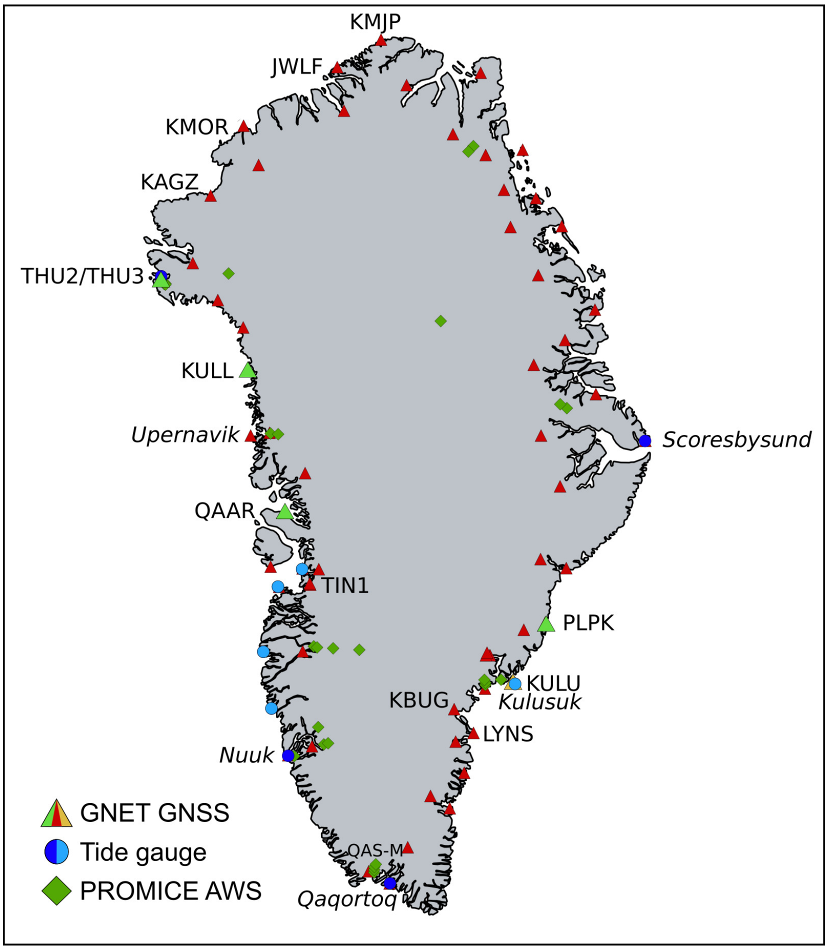

Figure 5.2: Map of Greenland including GNET stations, tide gauges and PROMICE weather stations. Green triangles mark GNET stations successfully included in the PSMSL GNSS-IR portal. Light blue tide gauges are decommissioned and dark blue are in operation. GNET stations mentioned in the discussion is labelled using capital letters. Other mentioned locations are labeled in italic.

m which has previously been shown to be measurable at a 1 s sampling rate (Williams & Nievinski, 2017). The Fresnel zones cover the ocean at all azimuths and though it is unlikely that there is free view of the ocean in all directions it is like likely that there is sufficient view over a reasonable azimuth range.

LYNS has a reflector height of about 130 m and also has a wide range of azimuths with reflection zones over the ocean, adding to the chance that there is sufficient view.

KBUG is located close to the front of Køge Bugt glacier and has some view of the ocean which may be sufficient. It has an approximate reflector height of 245 m which should be within the limit for 1 s sampling. It could be an interesting site to study influences of local water level on glacier dynamics but the potential azimuths are more limited than at LYNS and KMOR.

KAGZ has the advantage that the reflector height is somewhat smaller than for the other four stations at about 72 m which should be within the limit for a 5 s sampling rate and thus it requires less power than the other three sites.

In order to decide which locations are be most suitable for GNSS-IR the Fresnel zone plots should be combined with a visual inspection of the ocean view at the sites.

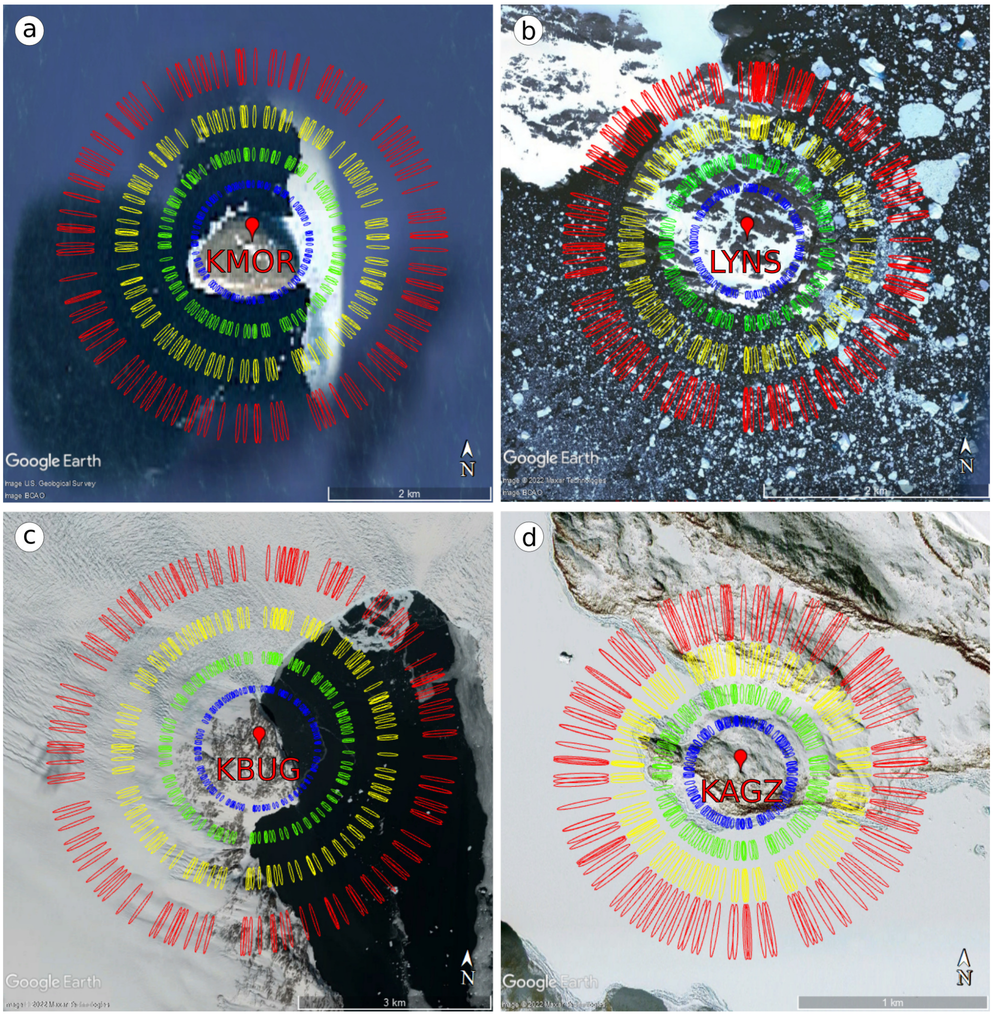

Figure 5.3: Fresnel zones for four GNET stations; KMOR, LYNS, KBUG and KAGZ. Elevation angles are 5° (red), 7° (yellow), 10° (green) and 15° (blue). The location of the stations can be seen on figure 5.2.

In the coming years, the current tide gauge stations in Greenland will be updated with new Valeport MIDAS water level recorders and additionally two stations will be installed at new locations; one in Upernavik and one in Kulusuk (figure 5.2). When the tide gauges are replaced a GNSS station will be placed at the site allowing for direct measurement of bedrock motion and potentially also GNSS-IR measurements of sea level. This would allow for a high quality comparison between tide gauge data and GNSS-IR in Greenland. The new tide gauge station in Nuuk is planned to be installed this year in order to run parallel with the current station for a year before it is decommissioned. The installation of the remaining new tide gauge stations are planned to start next year (2023).
Along the north-east coast of Greenland it is difficult to find a good location for a tide gauge station as these require a steep drop for the in water installation. Currently, no tide gauges are planned for this area and it could therefore be a particularly interesting area for a GNSS station with the ability of measuring sea level.

Ice dammed lakes

Unfortunately, it is not possible to observe the water level of lake Tininnilik using GNSS-IR from the GNET station TIN1. Such a data set would have resulted in a water level measurement of high temporal resolution allowing us to study the details of the water level during the drainage events. As a further development, it could be considered to install a GNET station suitable for GNSS-IR next to Lake Tininnilik or another regularly draining lake in Greenland to further study the lake dynamics. If possible the GNSS station could be placed at a location overlooking both the lake and the glacier and thereby also allowing measurements of changes in the surface height of the damming glacier.

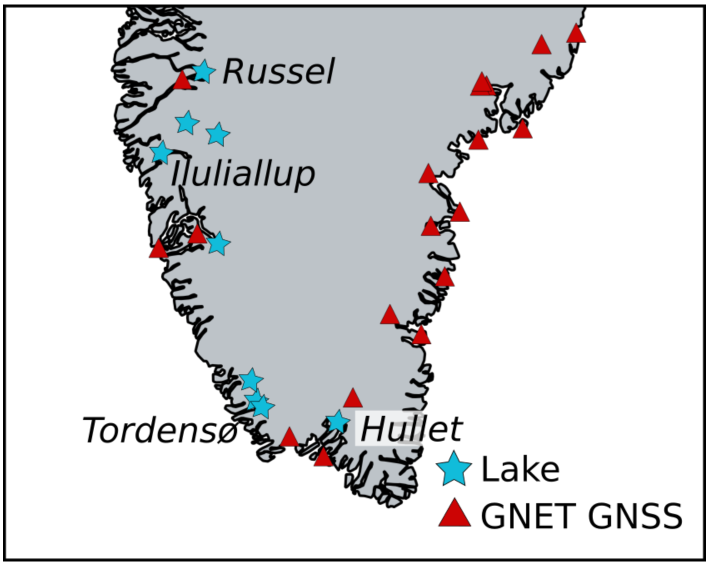

Figure 5.4: Map of South Greenland with GNET stations and ice dammed lakes known to drain in sudden events. Lakes mentioned in the text are named on the figure.

Carrivick & Tweed (2019) gives an overview of lakes in Greenland which have been shown to produce Glacial Lake Outburst Floods (GLOFs). Apart from Tininnilik, none of these lakes are located close enough to a GNET station to give strong uplift signals at drainage. The regularly draining lakes of considerable size are all but one located in south/southwest Greenland (figure 5.4). It may seem like some of them are quite close to nearby GNET stations but at distances of about 40 km a huge change in loading would be required for it to be distinguishable from other variations. However, some of the mentioned lakes, besides Tininnilik, could be interesting sites for a GNSS station studying drainage events of ice dammed lakes.

The draining lake at Russel Glacier is widely studied (Russell *et al.*, 2011; Carrivick *et al.*, 2017). After 20 years of stability it started a new cycle of draining events in 2007. Russell *et al.* (2011) estimates that the drained volume is 39 $\cdot 10^6$ m^3 which is about two orders of magnitude less than what Kjeldsen *et al.* (2017) estimates for Lake Tininnilik (1.48-2.28 $\cdot 10^9$ m^3). Thus, we don't expect to be able to distinguish uplift from draining of the lake from other loading effects even if a GNSS station was placed closer to the lake. Another lake that could be an interesting site for a GNSS station is Iluliallup Tasersua. Helk (1966) find that the volume lost at drainage events is about 6.2 $\cdot 10^9$ m^3. Though this value may be smaller today, Carrivick & Tweed (2019) note that the lake gained $\tilde{2}$ $\cdot 10^9$ m^3 of water between 2016 and 2018. Therefore, a GNSS station close to this lake would likely be able to measure a distinct uplift at drainage and therefore it could be an interesting site to further study drainage of ice dammed lakes in Greenland using GNSS positions and reflectometry. The last drainage event of the lake can be observed from Landsat 8 images to happen some time in August-September 2019 where the lake almost completely empties (figure 5.5). The two lakes Tordensø and Hullet both have relatively large drainage volumes, though still an order of magnitude smaller than Tininnilik.

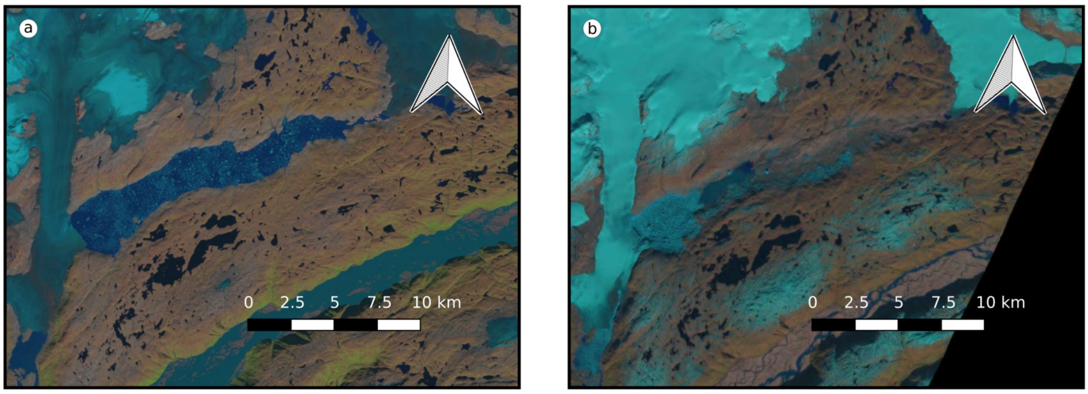

Figure 5.5: Map of Iluliallup Tasia before and after draining in 2019. a: Landsat 8 image from the 4th of August 2019, b: Landsat 8 image from the 19th of September 2019. Both are courtesy of the U.S. Geological Survey. The drainage of the lake between the two dates is clearly visible.

5.3 Sea level variations in Thule

5.3.1 Vertical Land Motion

The sea level measured by GNSS-IR and tide gauge in Thule is affected not only by changes in eustatic sea level but also vertical movement of the bedrock (section 2.2). The elastic uplift as a result of recent ice mass changes in Greenland and North America is modelled in order to see how it varies on inter-annual scales, and how well the model describes the measured uplift. This is done by convolving ice mass changes with the Green's function derived by Wang *et al.* (2012) for elastic Earth model iasp91 with refined crustal structure from Crust 2.0. The mass loss data is the same as was used in paper 1 for the gravimetric sea level.

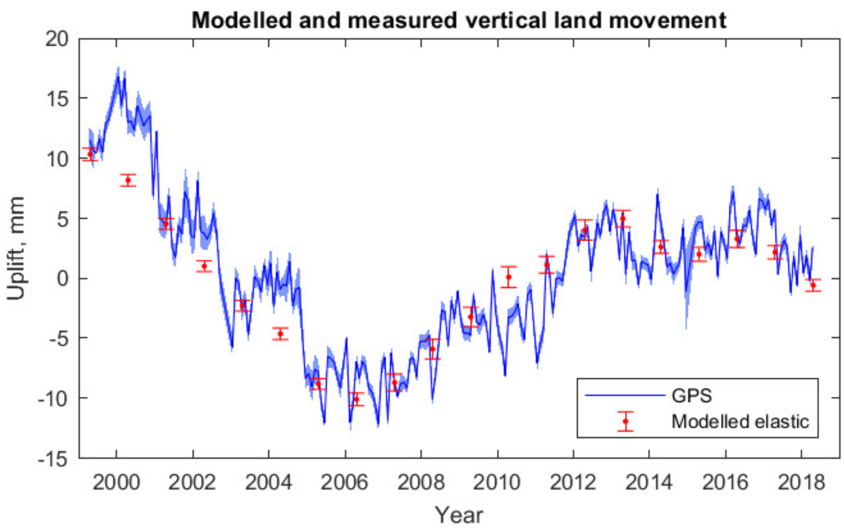

Figure 5.6: Monthly de-trended uplift measured by the THU2 GNSS station together with de-trended modeled elastic uplift.

Comparing the measured VLM in Thule with the modeled elastic uplift from 1998 to 2018, the trend in measured VLM is 6.6 mm/yr while it is 4.1 mm/yr for the modeled elastic uplift. The difference in trend may in part be due to GIA from the last ice age. However, though models show somewhat different results in this area, the modelled GIA is typically too small to explain this difference and in some cases even negative (Khan *et al.*, 2008, 2016; Schumacher *et al.*, 2018; Ludwigsen *et al.*, 2020). In order to compare measured and modeled uplift without needing to consider the GIA we compare de-trended variations in uplift. Since the GIA can be assumed constant over timescales of a few decades it is effectively removed from the comparison. The de-trended time series of measured uplift and modeled elastic uplift can be seen on figure 5.6. The modeled elastic uplift captures much of the inter-annual variation, suggesting that much of the elastic uplift in the area can be modeled using the mass changes of the GIS and glaciers in North America.

5.3.2 Temperature and salinity

In the paper we modelled the gravimetric sea level in Thule and found that it could, at least partly, explain the observed negative eustatic sea level trend in Thule (Dahl-Jensen *et al.*, 2021). However, the inter-annual variability in observed sea level is much larger than in the modelled gravimetric sea level. These inter annual variations could be caused by variations in temperature and/or salinity.

Monthly Sea Surface Temperature (SST) extracted from HadISST1 (Rayner *et al.*, 2003) are used to test this theory. Figure 5.7a,b show the measured sea level anomalies and SSTs. The trend in SST is negligible compared to the inter-annual variations. Comparing de-trended SST the de-trended sea level we find a significant linear correlation with SST of -0.9 and -0.8 for GNSS-IR and tide gauge, respectively. Though it is unlikely that SSTs are representative of the full water column, the thermosteric contribution to sea level is calculated using a 50 m water column and salinities of 28-32, as suggested by measurements from the tide gauge station. The correlation between the thermosteric sea level and the measured sea level is still negative (-0.8 for both tide gauge and GNSS-IR) and the annual variations are at least an order of magnitude smaller than in the measured sea levels (figure is included in appendix E). Therefore, a direct thermosteric sea level contribution of a water column with the same temperature as the surface cannot explain the sea level variations seen in the observations. Forget & Ponte (2015) and Meyssignac *et al.* (2017) studied regional variability in sea level and both find that barotropic flow forced by wind stresses has a strong influence on sea level variability on inter annual time scales in the arctic regions. Thus, the correlation between sea level anomaly and SST could be a result of a relation between the SST and variations in atmospheric pressure or ocean circulation patterns.

The steric sea level change in Thule is calculated using temperature and salinity measured by the tide gauge station. We expect this temperature data to be more representative of the water column than the SSTs as it is measured in water. The halosteric and thermosteric sea level change can be calculated as (Stammer, 1997; Calafat *et al.*, 2012):

$$S_T = \frac{1}{\rho_0}\int_{-h}^{0} \alpha\delta T dz \tag{5.1}$$

$$S_H = -\frac{1}{\rho_0}\int_{-h}^{0} \beta\delta S dz \tag{5.2}$$

Where ρ_0 is a reference density, h is the local ocean depth, δT is the conservative temperature anomaly and δS is the absolute salinity anomaly. α and β are the thermal expansion and saline contraction coefficients, respectively. These are calculated using the Thermodynamic Equation of Sea Water 2010 (TEOS-10) software (Roquet *et al.*, 2015) from the conservative temperature, absolute salinity and pressure.

Figure 5.7c,d shows the steric sea level variations. These results are calculated assuming a constant temperature and salinity with depth, and a total water depth of 50 m. For both steric contributions there are no significant trend and the thermosteric contributions are much too small to explain the large inter annual variations we see. For the halosteric contribution the order of magnitude is large enough that changes in salinity could explain the inter annual variability but the correlation is poor (0.3 for tide gauge sea level and 0.07 for GNSS-IR sea level when the linear trend is removed). Thus, variation in salinity could potentially explain the inter annual sea level but in that case the salinities measured by the tide gauge are not representative of the water column or area in general.

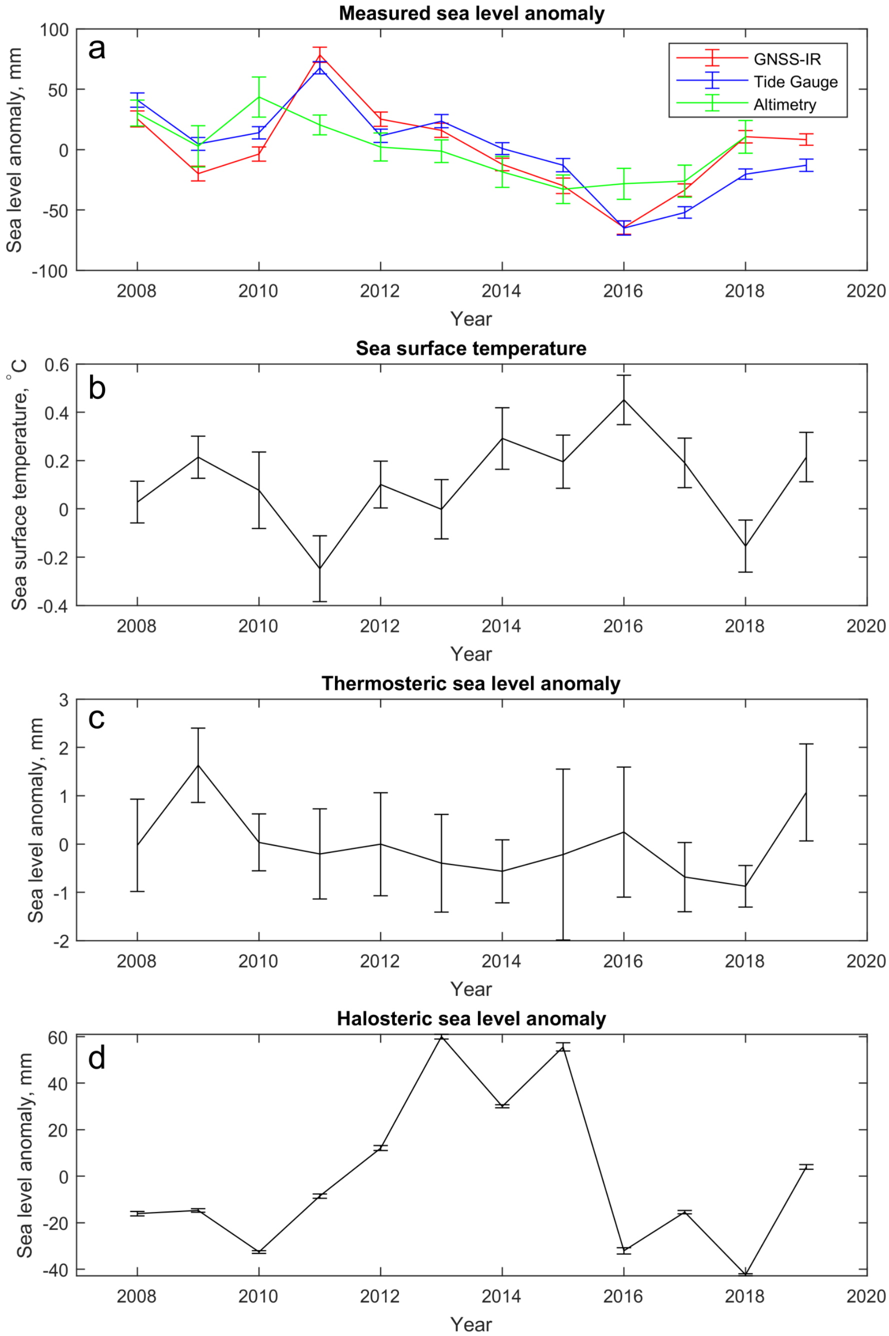

Figure 5.7: a: Annual average sea level change from GNSS-IR, tide gauge and altimetry. b: Annual average SSTs. c: Thermosteric sea level contribution calculated using tide gauge temperatures. d: Halosteric sea level contribution calculated using tide gauge salinity. The inter annual variations in both SST, thermosteric and halosteric sea level are large compared to the trend.

5.3.3 Ice free sea level variations

Sea ice cover affects the sea level measurements by GNSS-IR and tide gauge differently. The tide gauge measurements are based on the pressure in the water at the depth of the pressure transducer and therefore the measured tide gauge sea level when the ocean is ice covered is largely as it would be if the ice melted. GNSS-IR measures the top of the sea ice and thus there will be a positive bias in sea levels from GNSS-IR compared to the tide gauge. In the paper we note that limiting the measurement period to August and September, where the ocean around Thule is assumed ice free, does not improve the RMSD between the two measurements.

The time series of August-September sea level anomalies can be seen on figure 5.8a. The RMSD between the two is 37 mm and the correlation is 0.69. As mentioned in the paper this is worse than the results from the full year averages. Figure 5.8b shows the difference between annual sea level change from tide gauge and GNSS-IR for both annual and ice free (August-September) sea level. From 2015 the ice free sea level has similar variations for the two methods and the differences are within the estimated errors. The differences before 2015 are much larger for the ice free period than for the annual average. Thus, post 2015 sea ice could explain at least some of the difference between the two methods. However, there must be other factors causing the large deviations in previous years. The GNSS stations tracks only GPS signals until 2012 where it is updated and GLONASS data is included in the reflectometry estimates. However, since this change happens in 2012 it cannot explain why the results seem to be better for the ice free months after 2015. The tide gauge was moved to a new location in 2015. This could be part of the explanation as there could be some datum shifts or drift at the old location which is not accounted for.

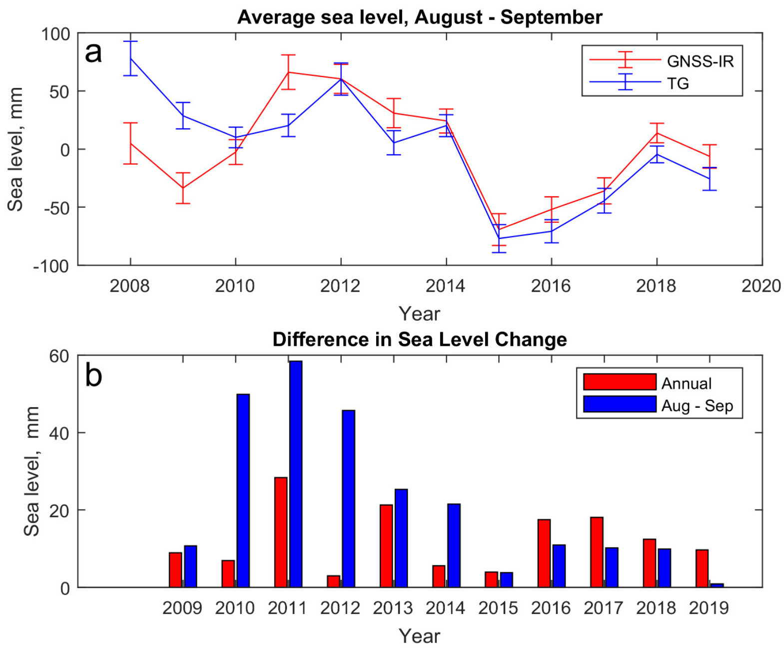

Figure 5.8: a: Annual sea level variations from GNSS-IR and tide gauge calculated for August - September where the ocean is assumed to be ice free. b: Bar plot of difference between change in sea level from GNSS-IR and tide gauge for annual and ice free averages.

5.4 GNSS-IR for measurements of extreme water

Studies of GNSS-IR for sea level monitoring generally agree that it is a very useful method but that it cannot replace tide gauges. There are several reasons for this; e.g. the measurement frequency is fundamentally limited by the number of satellite overflights and the uncertainty on individual measurement are not as good. Furthermore, the tide gauges are used for real time monitoring and warning systems in case of extreme water levels where GNSS-IR is challenged. The issues affecting the potential use of GNSS-IR in warning systems and to detect extreme water levels include:

- Temporal resolution is limited by satellite overflights
- Estimated water level is an average over the time period of the used part of the satellite arc
- Latency from the fact that a sufficient section of a satellite track is needed for an extraction
- Correcting for the moving reflector cannot be done using tidal modelling as it is not representative of the large changes in water level.
- Water surface gets rough during high wind introducing uncertainties and at some point making extractions impossible.

During the last couple of years a few studies have been done testing the use of GNSS-IR for measurements of extreme water levels and trying to overcome some of these obstacles (Peng *et al.*, 2019; Tabibi & Francis, 2020; Larson *et al.*, 2021a). The temporal resolution, average water level and latency can all partly be mitigated by using a sliding window. Here, the satellite arc is divided into sliding windows and the reflector height calculated for each of these. The sliding interval can be anything down to the data sampling interval while the window has to be long enough to extract the multipath frequencies in the SNR data (Kim *et al.*, 2021; Kim & Park, 2021). This length will depend on the minimum reflector height as a small reflector height results in lower frequency (equation 3.6) which will in turn require a longer window to be resolved. The issue of the $\dot{\mathrm{H}}$ correction can be solved by using an inverse model in stead of the LSP or using an enhanced spectral method to simultaneously determine H_R and the $\dot{\mathrm{H}}$ correction (Tabibi & Francis, 2020; Kim *et al.*, 2021). Larson *et al.* (2021a) suggest another method where the issue of the $\dot{\mathrm{H}}$ correction is avoided by combining a raising and setting satellite at the same time, as the $\dot{\mathrm{H}}$ correction will have opposite signs for the two. The resulting height retrievals are promising but the temporal resolution is further limited by the requirement of having a rising and setting satellite arc at the same time. Generally, the studies show near real time results at best, with a time lag of at least half the measurement windows and temporal resolution limited by satellite overflights and window length. The sampling can be greatly improved using multiple constellations but it is still a limitation.
However, GNSS-IR also has advantages compared to traditional tide gauges. Namely, traditional tide gauges require in-water logistics and are thus vulnerable in case of extreme water levels. In contrast, GNSS stations are often installed at high locations which make them useful for studying large tsunamis and storm floods where tide gauges are damaged. As of now GNSS stations can be valuable in the post-event studies of tsunamis, storm floods etc. but work remains before they can be used as a trusted part of the warning systems where reducing the latency is particularly important.

6 Conclusion

This thesis have focused on the use of geodetic measurements, and in particular GNSS data, for studies of the effects of climate changes in Greenland. We use GNSS reflectometry to study both sea level variations and snow heights with promising results using geodetic GNSS stations. Unfortunately, it is not possible to study the water level of Lake Tininnilik by GNSS-IR using existing GNSS stations and thus at this site the GNSS data is only used for uplift measurements.

The first study compares annual average sea level variations measured by GNSS-IR, tide gauge and altimetry. We find that though GNSS-IR and tide gauge observe largely the same sea level variations there are differences which are larger than the estimated errors. One possible error source is the sea ice cover in winter, but calculating the annual average using only data from August and September, where the water is assumed ice free, generally result in worse correlation and RMSD between the two. However, if we look only at data after 2015 where the tide gauge is moved, results from August-September are significantly better than before. This indicates that there may be some issues with the datum at the original tide gauge site.
Currently, four GNET stations with successful extractions are included in the PSMSL GNSS-IR portal. The issue for some of the existing GNET stations, when it comes to GNSS-IR extractions of sea level, is the height above sea level combined with the current 15 s sampling rate. Some of the stations may be useful for estimating sea level if the logging is increased to a 1 s sampling rate. Choosing stations where this could be tested should be based on a combination of visual inspection of the ocean view and the Fresnel zone plots. Possible candidates include KMOR, LYNS, KBUG and KAGZ (see figure 5.2). An area of particular interest for a potential new GNET station with GNSS-IR in mind could be the north-east coast where it is difficult to find a suitable place for a tide gauge station due to the topography. Sea level measurements by GNSS-IR could be a way to close this gap in in-situ measurements of sea level.

In the second paper we study snow heights at the AWS, NUK-K. We compare snow height measured using GNSS-IR with results from a sonic ranger on the weather station. A hill is obstructing the view at the low elevation angles needed for GNSS-IR over a 130° azimuth range, and due to limited power the GNSS station is logging at most 3 hours a day. Nevertheless, the two measurement show largely the same total snow melt during the melt season. However, there is a period towards the end of the melt season where the difference between the two is well beyond the error estimates. We suggest that the difference is due to the much larger footprint of GNSS-IR than for the sonic ranger and (at least partly) a result of actual differences in snow melt in the area.
It is the plan to install geodetic quality GNSS stations at all PROMICE stations to track the ice flow. The standard settings will be that the stations are logging (and transmitting) 1 hour pr. day at a 60 s sampling rate of GPS signals only. This is not likely to be useful for GNSS-IR. However, it will be possible to remotely adjust these settings at individual stations and thereby do specific reflectometry campaigns.

In the third paper we study the drainage cycles of the ice dammed Lake Tininnilik. The lake has drained about every 10 years from the 1940s up until 2003, where it starts to drain more often and at a continuously lower water level. In 2020 the lake drains 5 years

after the last event at a water level of 224 m, continuing the decreasing trend in water level at drainage. We combine the trend in maximum water level with an infill rate based on the last three cycles and estimate that the lake will drain again during 2024. If the current trend in maximum lake level continues it will reach the level of the drained lake around year 2053 and the draining cycles will cease, assuming that no continuous spillways are formed before then.
As mentioned it is not possible to observe the water level of the lake using the existing GNET station next to the lake, TIN1. However, GNSS-IR could be a highly suitable method for investigating water level as it does not require any in-water instruments which are at risk of being damaged when the lake freezes. Also permanent GNSS stations tend to be robust and, if placed right, could also be used to observe the height changes of the damming glacier as well as VLM.

Generally, GNSS-IR can be a robust way to measure water level without requiring any in-water installation. It is also useful for snow studies and in both cases the ability of measuring position at high accuracy allows for measurement of snow or water height in a geocentric reference frame. Though existing sites were not installed with GNSS-IR in mind, they may still be used for reflectometry as it is done in the two first papers included in this thesis.

Bibliography

Adhikari, Surendra, Ivins, Erik R., Frederikse, Thomas, Landerer, Felix W., & Caron, Lambert. 2019. Sea-level fingerprints emergent from GRACE mission data. *EARTH SYSTEM SCIENCE DATA*, **11**(2), 629–646.

Altuntas, Cemali, & Tunalioglu, Nursu. 2021. Feasibility of retrieving effective reflector height using GNSS-IR from a single-frequency android smartphone SNR data. *DIGITAL SIGNAL PROCESSING*, **112**(MAY).

Armitage, Thomas W. K., & Davidson, Malcolm W. J. 2014. Using the Interferometric Capabilities of the ESA CryoSat-2 Mission to Improve the Accuracy of Sea Ice Freeboard Retrievals. *IEEE TRANSACTIONS ON GEOSCIENCE AND REMOTE SENSING*, **52**(1, 2), 529–536.

Axelrad, Penina, Larson, Kristine, & Jones, Brandon. 2005. Use of the Correct Satellite Repeat Period to Characterize and Reduce Site-Specific Multipath Errors. *ION GNSS 18th International Technical Meeting of the Satellite Division, 13-16 September 2005, Long Beach, CA*, 01.

Bamber, J., & Riva, R. 2010. The sea level fingerprint of recent ice mass fluxes. *CRYOSPHERE*, **4**(4), 621–627.

Bamber, Jonathan L., Westaway, Richard M., Marzeion, Ben, & Wouters, Bert. 2018. The land ice contribution to sea level during the satellite era. *ENVIRONMENTAL RESEARCH LETTERS*, **13**(6).

Benn, Douglas I., Warren, Charles R., & Mottram, Ruth H. 2007. Calving processes and the dynamics of calving glaciers. *EARTH-SCIENCE REVIEWS*, **82**(3-4), 143–179.

Bevis, Michael, Wahr, John, Khan, Shfaqat A., Madsen, Finn Bo, Brown, Abel, Willis, Michael, Kendrick, Eric, Knudsen, Per, Box, Jason E., van Dam, Tonie, Caccamise, II, Dana J., Johns, Bjorn, Nylen, Thomas, Abbott, Robin, White, Seth, Miner, Jeremy, Forsberg, Rene, Zhou, Hao, Wang, Jian, Wilson, Terry, Bromwich, David, & Francis, Olivier. 2012. Bedrock displacements in Greenland manifest ice mass variations, climate cycles and climate change. *PROCEEDINGS OF THE NATIONAL ACADEMY OF SCIENCES OF THE UNITED STATES OF AMERICA*, **109**(30), 11944–11948.

Bevis, Michael, Harig, Christopher, Khan, Shfaqat A., Brown, Abel, Simons, Frederik J., Willis, Michael, Fettweis, Xavier, van den Broeke, Michiel R., Madsen, Finn Bo, Kendrick, Eric, Caccamise, II, Dana J., van Dam, Tonie, Knudsen, Per, & Nylen, Thomas. 2019. Accelerating changes in ice mass within Greenland, and the ice sheet's sensitivity to atmospheric forcing. *PROCEEDINGS OF THE NATIONAL ACADEMY OF SCIENCES OF THE UNITED STATES OF AMERICA*, **116**(6), 1934–1939.

Boehm, Johannes, Werl, Birgit, & Schuh, Harald. 2006. Troposphere mapping functions for GPS and very long baseline interferometry from European Centre for Medium-Range Weather Forecasts operational analysis data. *JOURNAL OF GEOPHYSICAL RESEARCH-SOLID EARTH*, **111**(B2).

Calafat, F. M., Chambers, D. P., & Tsimplis, M. N. 2012. Mechanisms of decadal sea level variability in the eastern North Atlantic and the Mediterranean Sea. *JOURNAL OF GEOPHYSICAL RESEARCH-OCEANS*, **117**(SEP 18).

Carrivick, Jonathan L., & Tweed, Fiona S. 2019. A review of glacier outburst floods in Iceland and Greenland with a megafloods perspective. *EARTH-SCIENCE REVIEWS*, **196**(SEP).

Carrivick, Jonathan L., Tweed, Fiona S., Ng, Felix, Quincey, Duncan J., Mallalieu, Joseph, Ingeman-Nielsen, Thomas, Mikkelsen, Andreas B., Palmer, Steven J., Yde, Jacob C., Homer, Rachel, Russell, Andrew J., & Hubbard, Alun. 2017. Ice-Dammed Lake Drainage Evolution at Russell Glacier, West Greenland. *FRONTIERS IN EARTH SCIENCE*, **5**(NOV 28).

Chen, J. L., Wilson, C. R., & Tapley, B. D. 2006. Satellite gravity measurements confirm accelerated melting of Greenland ice sheet. *SCIENCE*, **313**(5795), 1958–1960.

Chen, Xianyao, Zhang, Xuebin, Church, John A., Watson, Christopher S., King, Matt A., Monselesan, Didier, Legresy, Benoit, & Harig, Christopher. 2017. The increasing rate of global mean sea-level rise during 1993-2014. *NATURE CLIMATE CHANGE*, **7**(7), 492+.

Church, JA, White, NJ, Coleman, R, Lambeck, K, & Mitrovica, JX. 2004. Estimates of the regional distribution of sea level rise over the 1950-2000 period. *JOURNAL OF CLIMATE*, **17**(13), 2609–2625.

Dahl-Jensen, Trine S., Andersen, Ole B., Williams, Simon D. P., Helm, Veit, & Khan, Shfaqat A. 2021. GNSS-IR Measurements of Inter Annual Sea Level Variations in Thule, Greenland from 2008-2019. *REMOTE SENSING*, **13**(24).

Dahl-Jensen, Trine S., Citterio, Michele, Jakobsen, Jakob, Ahlstrom, Andreas P., Larson, Kristine M., & Khan, Shfaqat A. 2022. Snow Depth Measurements by GNSS-IR at an Automatic Weather Station, NUK-K. *REMOTE SENSING*, **14**(11).

Dangendorf, Soenke, Hay, Carling, Calafat, Francisco M., Marcos, Marta, Piecuch, Christopher G., Berk, Kevin, & Jensen, Juergen. 2019. Persistent acceleration in global sea-level rise since the 1960s. *NATURE CLIMATE CHANGE*, **9**(9), 705+.

Dieng, H. B., Cazenave, A., Meyssignac, B., & Ablain, M. 2017. New estimate of the current rate of sea level rise from a sea level budget approach. *GEOPHYSICAL RESEARCH LETTERS*, **44**(8), 3744–3751.

Fausto, Robert S., van As, Dirk, Mankoff, Kenneth D., Vandecrux, Baptiste, Citterio, Michele, Ahlstrom, Andreas P., Andersen, Signe B., Colgan, William, Karlsson, Nanna B., Kjeldsen, Kristian K., Korsgaard, Niels J., Larsen, Signe H., Nielsen, Soren, Pedersen, Allan M., Shields, Christopher L., Solgaard, Anne M., & Box, Jason E. 2021. Programme for Monitoring of the Greenland Ice Sheet (PROMICE) automatic weather station data. *EARTH SYSTEM SCIENCE DATA*, **13**(8), 3819–3845.

Forget, Gael, & Ponte, Rui M. 2015. The partition of regional sea level variability. *PROGRESS IN OCEANOGRAPHY*, **137**(A), 173–195.

Georgiadou, P.Y (Yola), & Kleusberg, A. 1988. On Carrier Signal Multipath Effects in Relative GPS Positioning. *Map Collector*, **13**(01), 172–179.

Gutmann, Ethan D., Larson, Kristine M., Williams, Mark W., Nievinski, Felipe G., & Zavorotny, Valery. 2012. Snow measurement by GPS interferometric reflectometry: an evaluation at Niwot Ridge, Colorado. *HYDROLOGICAL PROCESSES*, **26**(19), 2951–2961.

Hefty, Jan, & Gerhatova, L'ubomira. 2014. USING GPS MULTIPATH FOR SNOW DEPTH SENSING - FIRST EXPERIENCE WITH DATA FROM PERMANENT STATIONS IN SLOVAKIA. *ACTA GEODYNAMICA ET GEOMATERIALIA*, **11**(1), 53–62.

Helk, J.V. 1966. Glacier mapping in Greenland. *Canadian Journal of Earth Science*, **3**(6), 771–774.

Hofer, Stefan, Lang, Charlotte, Amory, Charles, Kittel, Christoph, Delhasse, Alison, Tedstone, Andrew, & Fettweis, Xavier. 2020. Greater Greenland Ice Sheet contribution to global sea level rise in CMIP6. *NATURE COMMUNICATIONS*, **11**(1).

Holgate, Simon J., Matthews, Andrew, Woodworth, Philip L., Rickards, Lesley J., Tamisiea, Mark E., Bradshaw, Elizabeth, Foden, Peter R., Gordon, Kathleen M., Jevrejeva, Svetlana, & Pugh, Jeff. 2013. New Data Systems and Products at the Permanent Service for Mean Sea Level. *JOURNAL OF COASTAL RESEARCH*, **29**(3), 493–504.

Hsu, Chia-Wei, & Velicogna, Isabella. 2017. Detection of sea level fingerprints derived from GRACE gravity data. *GEOPHYSICAL RESEARCH LETTERS*, **44**(17), 8953–8961.

Idzanovic, Martina, Ophaug, Vegard, & Andersen, Ole Baltazar. 2017. The coastal mean dynamic topography in Norway observed by CryoSat-2 and GOCE. *GEOPHYSICAL RESEARCH LETTERS*, **44**(11), 5609–5617.

Idzanovic, Martina, Ophaug, Vegard, & Andersen, Ole Baltazar. 2018. Coastal sea level from CryoSat-2 SARIn altimetry in Norway. *ADVANCES IN SPACE RESEARCH*, **62**(6), 1344–1357.

Jiang, Yan, Dixon, Timothy H., & Wdowinski, Shimon. 2010. Accelerating uplift in the North Atlantic region as an indicator of ice loss. *NATURE GEOSCIENCE*, **3**(6), 404–407.

Katzberg, SJ, Torres, O, Grant, MS, & Masters, D. 2006. Utilizing calibrated GPS reflected signals to estimate soil reflectivity and dielectric constant: Results from SMEX02. *REMOTE SENSING OF ENVIRONMENT*, **100**(1), 17–28.

Khan, Shfaqat A., Wahr, John, Stearns, Leigh A., Hamilton, Gordon S., van Dam, Tonie, Larson, Kristine M., & Francis, Olivier. 2007. Elastic uplift in southeast Greenland due to rapid ice mass loss. *GEOPHYSICAL RESEARCH LETTERS*, **34**(21).

Khan, Shfaqat A., Sasgen, Ingo, Bevis, Michael, van Dam, Tonie, Bamber, Jonathan L., Wahr, John, Willis, Michael, Kjaer, Kurt H., Wouters, Bert, Helm, Veit, Csatho, Beata, Fleming, Kevin, Bjork, Anders A., Aschwanden, Andy, Knudsen, Per, & Munneke, Peter Kuipers. 2016. Geodetic measurements reveal similarities between post-Last Glacial Maximum and present-day mass loss from the Greenland ice sheet. *SCIENCE ADVANCES*, **2**(9).

Khan, Shfaqat Abbas, Wahr, John, Leuliette, Eric, van Dam, Tonie, Larson, Kristine M., & Francis, Olivier. 2008. Geodetic measurements of postglacial adjustments in Greenland. *JOURNAL OF GEOPHYSICAL RESEARCH-SOLID EARTH*, **113**(B2).

Khan, Shfaqat Abbas, Wahr, John, Bevis, Michael, Velicogna, Isabella, & Kendrick, Eric. 2010a. Spread of ice mass loss into northwest Greenland observed by GRACE and GPS. *GEOPHYSICAL RESEARCH LETTERS*, **37**(MAR 19).

Khan, Shfaqat Abbas, Liu, Lin, Wahr, John, Howat, Ian, Joughin, Ian, van Dam, Tonie, & Fleming, Kevin. 2010b. GPS measurements of crustal uplift near Jakobshavn Isbrae due to glacial ice mass loss. *JOURNAL OF GEOPHYSICAL RESEARCH-SOLID EARTH*, **115**(SEP 16).

Kim, Su-Kyung, & Park, Jihye. 2021. Monitoring a storm surge during Hurricane Harvey using multi-constellation GNSS-Reflectometry. *GPS SOLUTIONS*, **25**(2).

Kim, Su-Kyung, Lee, Eunju, Park, Jihye, & Shin, Sungwon. 2021. Feasibility Analysis of GNSS-Reflectometry for Monitoring Coastal Hazards. *REMOTE SENSING*, **13**(5).

King, Matt A., Keshin, Maxim, Whitehouse, Pippa L., Thomas, Ian D., Milne, Glenn, & Riva, Riccardo E. M. 2012. Regional biases in absolute sea-level estimates from tide gauge data due to residual unmodeled vertical land movement. *GEOPHYSICAL RESEARCH LETTERS*, **39**(JUL 27).

King, Michalea D., Howat, Ian M., Jeong, Seongsu, Noh, Myoung J., Wouters, Bert, Noel, Brice, & van den Broeke, Michiel R. 2018. Seasonal to decadal variability in ice discharge from the Greenland Ice Sheet. *CRYOSPHERE*, **12**(12), 3813–3825.

Kjeldsen, Kristian K., Khan, Shfaqat A., Bjork, Anders A., Nielsen, Karina, & Mouginot, Jeremie. 2017. Ice-dammed lake drainage in west Greenland: Drainage pattern and implications on ice flow and bedrock motion. *GEOPHYSICAL RESEARCH LETTERS*, **44**(14), 7320–7327.

Larson, Kristine M. 2016a. GPS interferometric reflectometry: applications to surface soil moisture, snow depth, and vegetation water content in the western United States. *WILEY INTERDISCIPLINARY REVIEWS-WATER*, **3**(6), 775–787.

Larson, Kristine M. 2021. GNSS Reflection Code. DOI: 10.5281/zenondo.5601495.

Larson, Kristine M., & Nievinski, Felipe G. 2013. GPS snow sensing: results from the EarthScope Plate Boundary Observatory. *GPS SOLUTIONS*, **17**(1), 41–52.

Larson, Kristine M., & Small, Eric E. 2016b. Estimation of Snow Depth Using L1 GPS Signal-to-Noise Ratio Data. *IEEE JOURNAL OF SELECTED TOPICS IN APPLIED EARTH OBSERVATIONS AND REMOTE SENSING*, **9**(10, SI), 4802–4808.

Larson, Kristine M., Small, Eric E., Gutmann, Ethan, Bilich, Andria, Axelrad, Penina, & Braun, John. 2008. Using GPS multipath to measure soil moisture fluctuations: initial results. *GPS SOLUTIONS*, **12**(3), 173–177.

Larson, Kristine M., Gutmann, Ethan D., Zavorotny, Valery U., Braun, John J., Williams, Mark W., & Nievinski, Felipe G. 2009. Can we measure snow depth with GPS receivers? *GEOPHYSICAL RESEARCH LETTERS*, **36**(SEP 11).

Larson, Kristine M., Braun, John J., Small, Eric E., Zavorotny, Valery U., Gutmann, Ethan D., & Bilich, Andria L. 2010. GPS Multipath and Its Relation to Near-Surface Soil Moisture Content. *IEEE JOURNAL OF SELECTED TOPICS IN APPLIED EARTH OBSERVATIONS AND REMOTE SENSING*, **3**(1), 91–99.

Larson, Kristine M., Lofgren, Johan S., & Haas, Rudiger. 2013a. Coastal sea level measurements using a single geodetic GPS receiver. *ADVANCES IN SPACE RESEARCH*, **51**(8), 1301–1310.

Larson, Kristine M., Ray, Richard D., Nievinski, Felipe G., & Freymueller, Jeffrey T. 2013b. The Accidental Tide Gauge: A GPS Reflection Case Study From Kachemak Bay, Alaska. *IEEE GEOSCIENCE AND REMOTE SENSING LETTERS*, **10**(5), 1200–1204.

Larson, Kristine M., Wahr, John, & Munneke, Peter Kuipers. 2015. Constraints on snow accumulation and firn density in Greenland using GPS receivers. *JOURNAL OF GLACIOLOGY*, **61**(225), 101–114.

Larson, Kristine M., Ray, Richard D., & Williams, Simon D. P. 2017. A 10-Year Comparison of Water Levels Measured with a Geodetic GPS Receiver versus a Conventional Tide Gauge. *JOURNAL OF ATMOSPHERIC AND OCEANIC TECHNOLOGY*, **34**(2), 295–307.

Larson, Kristine M., Macferrin, Michael, & Nylen, Thomas. 2020. Brief Communication: Update on the GPS reflection technique for measuring snow accumulation in Greenland. *CRYOSPHERE*, **14**(6), 1985–1988.

Larson, Kristine M., Lay, Thorne, Yamazaki, Yoshiki, Cheung, Kwok Fai, Ye, Lingling, Williams, Simon D. P., & Davis, James L. 2021a. Dynamic Sea Level Variation From GNSS: 2020 Shumagin Earthquake Tsunami Resonance and Hurricane Laura. *GEOPHYSICAL RESEARCH LETTERS*, **48**(4).

Liu, Lin, & Larson, Kristine M. 2018. Decadal changes of surface elevation over permafrost area estimated using reflected GPS signals. *CRYOSPHERE*, **12**(2), 477–489.

Liu, Lin, Khan, Shfaqat Abbas, van Dam, Tonie, Ma, Joseph Ho Yin, & Bevis, Michael. 2017. Annual variations in GPS-measured vertical displacements near Upernavik Isstrom (Greenland) and contributions from surface mass loading. *JOURNAL OF GEOPHYSICAL RESEARCH-SOLID EARTH*, **122**(1), 677–691.

Liu, Zhihao, Du, Lan, Zhou, Peiyuan, Liu, Zejun, Zhang, Zhongkai, & Xu, Zheyu. 2022. Performance assessment of GNSS-IR altimetry using signal-to-noise ratio data from a Huawei P30 smartphone. *GPS SOLUTIONS*, **26**(2).

Lomb, N. R. 1976. Least-squares frequency-analysis of unequally spaced data. *Astrophys Space Sci 39(2):447-462*.

Ludwigsen, Carsten Ankjaer, Khan, Shfaqat Abbas, Andersen, Ole Baltazar, & Marzeion, Ben. 2020. Vertical Land Motion From Present-Day Deglaciation in the Wider Arctic. *GEOPHYSICAL RESEARCH LETTERS*, **47**(19).

Luthcke, Scott B., Sabaka, T. J., Loomis, B. D., Arendt, A. A., McCarthy, J. J., & Camp, J. 2013. Antarctica, Greenland and Gulf of Alaska land-ice evolution from an iterated GRACE global mascon solution. *JOURNAL OF GLACIOLOGY*, **59**(216), 613–631.

Löfgren, J. S., Haas, R., Scherneck, H. G., & Bos, M. S. 2011. Three months of local sea level derived from reflected GNSS signals. *RADIO SCIENCE*, **46**(NOV 8).

Löfgren, Johan S., Haas, Rudiger, & Scherneck, Hans-Georg. 2014. Sea level time series and ocean tide analysis from multipath signals at five GPS sites in different parts of the world. *JOURNAL OF GEODYNAMICS*, **80**(SI), 66–80.

MacGregor, Joseph A., Boisvert, Linette N., Medley, Brooke, Petty, Alek A., Harbeck, Jeremy P., Bell, Robin E., Blair, J. Bryan, Blanchard-Wrigglesworth, Edward, Buckley, Ellen M., Christoffersen, Michael S., Cochran, James R., Csatho, Beata M., De Marco, Eugenia L., Dominguez, RoseAnne T., Fahnestock, Mark A., Farrell, Sinead L., Gogineni, S. Prasad, Greenbaum, Jamin S., Hansen, Christy M., Hofton, Michelle A., Holt, John W., Jezek, Kenneth C., Koenig, Lora S., Kurtz, Nathan T., Kwok, Ronald, Larsen, Christopher F., Leuschen, Carlton J., Locke, Caitlin D., Manizade, Serdar S., Martin, Seelye, Neumann, Thomas A., Nowicki, Sophie M. J., Paden, John D., Richter-Menge, Jacqueline A., Rignot, Eric J., Rodriguez-Morales, Fernando, Siegfried, Matthew R., Smith, Benjamin E., Sonntag, John G., Studinger, Michael, Tinto, Kirsty J., Truffer, Martin, Wagner, Thomas P., Woods, John E., Young, Duncan A., & Yungel, James K. 2021. The Scientific Legacy of NASA's Operation IceBridge. *REVIEWS OF GEOPHYSICS*, **59**(2).

Mankoff, Kenneth D., Solgaard, Anne, Colgan, William, Ahlstrom, Andreas P., Khan, Shfaqat Abbas, & Fausto, Robert S. 2020. Greenland Ice Sheet solid ice discharge from 1986 through March 2020. *EARTH SYSTEM SCIENCE DATA*, **12**(2), 1367–1383.

McCreight, James L., Small, Eric E., & Larson, Kristine M. 2014. Snow depth, density, and SWE estimates derived from GPS reflection data: Validation in the western U.S. *WATER RESOURCES RESEARCH*, **50**(8), 6892–6909.

Meredith, M., Sommerkorn, M., Cassotta, S., Derksen, C., Ekaykin, A., Hollowed, A., Kofinas, G., Mackintosh, A., Melbourne-Thomas, J., Muelbert, M.M.C., Ottersen, G., Pritchard, H., & Schuur, E.A.G. 2019. Polar regions. In: IPCC Special Report on the Oceans and Cryosphere in a Changing Climate. [Pörtner, H.-O., Roberts, D.C., Masson-Delmotte, V., Zhai, P., Tignor, M., Poloczanska, E., Mintenbeck, K., Alegría, A., Nicolai, M., Okem, A.,. Petzold, J., Rama, B. and Weyer, N.M. (eds.)]. In press.

Meyssignac, B., Piecuch, C. G., Merchant, C. J., Racault, M. F., Palanisamy, H., MacIntosh, C., Sathyendranath, S., & Brewin, R. 2017. Causes of the Regional Variability in Observed Sea Level, Sea Surface Temperature and Ocean Colour Over the Period 1993-2011. *SURVEYS IN GEOPHYSICS*, **38**(1, SI), 187–215.

Moon, T. A., Druckenmiller, M. L., & Thoman, R. L. Eds. 2021. Arctic Report Card 2021. https://doi.org/10.25923/5s0f-5163.

Mouginot, Jeremie, Rignot, Eric, Bjork, Anders A., van den Broeke, Michiel, Millan, Romain, Morlighem, Mathieu, Noel, Brice, Scheuchl, Bernd, & Wood, Michael. 2019. Forty-six years of Greenland Ice Sheet mass balance from 1972 to 2018. *PROCEEDINGS OF THE NATIONAL ACADEMY OF SCIENCES OF THE UNITED STATES OF AMERICA*, **116**(19), 9239–9244.

Nick, Faezeh M., Vieli, Andreas, Andersen, Morten Langer, Joughin, Ian, Payne, Antony, Edwards, Tamsin L., Pattyn, Frank, & van de Wal, Roderik S. W. 2013. Future sea-level rise from Greenland's main outlet glaciers in a warming climate. *NATURE*, **497**(7448), 235–238.

Nielsen, Karina, Khan, Shfaqat Abbas, Korsgaard, Niels J., Kjaer, Kurt H., Wahr, John, Bevis, Michael, Stearns, Leigh A., & Timm, Lars H. 2012. Crustal uplift due to ice mass variability on Upernavik Isstrom, west Greenland. *EARTH AND PLANETARY SCIENCE LETTERS*, **353**(NOV 1), 182–189.

Nilsson, Johan, Vallelonga, Paul, Simonsen, Sebastian B., Sorensen, Louise Sandberg, Forsberg, Rene, Dahl-Jensen, Dorthe, Hirabayashi, Motohiro, Goto-Azuma, Kumiko, Hvidberg, Christine S., Kjaer, Helle A., & Satow, Kazuhide. 2015. Greenland 2012 melt event effects on CryoSat-2 radar altimetry. *GEOPHYSICAL RESEARCH LETTERS*, **42**(10), 3919–3926.

Oppenheimer, M., Glavovic, B.C., Hinkel, J., van de Wal, R., Magnan, A.K., Abd-Elgawad, A., Cai, R., Cifuentes-Jara, M., DeConto, R.M., Ghosh, T., Hay, J., Isla, F., Marzeion, B., Meyssignac, B., & Sebesvari, Z. 2019. Sea Level Rise and Implications for Low-Lying Islands, Coasts and Communities. In: IPCC Special Report on the Oceans and

Cryosphere in a Changing Climate. [Pörtner, H.-O., Roberts, D.C., Masson-Delmotte, V., Zhai, P., Tignor, M., Poloczanska, E., Mintenbeck, K., Alegría, A., Nicolai, M., Okem, A.,. Petzold, J., Rama, B. and Weyer, N.M. (eds.)]. In press.

Ozeki, Masaru, & Heki, Kosuke. 2012. GPS snow depth meter with geometry-free linear combinations of carrier phases. *JOURNAL OF GEODESY*, **86**(3), 209–219.

Palmer, M. D., Domingues, C. M., Slangen, A. B. A., & Boeira Dias, F. 2021. An ensemble approach to quantify global mean sea-level rise over the 20th century from tide gauge reconstructions. *ENVIRONMENTAL RESEARCH LETTERS*, **16**(4).

Peng, Dongju, Hill, Emma M., Li, Linlin, Switzer, Adam D., & Larson, Kristine M. 2019. Application of GNSS interferometric reflectometry for detecting storm surges. *GPS SOLUTIONS*, **23**(2).

Pinat, Elisa, Defraigne, Pascale, Bergeot, Nicolas, Chevalier, Jean-Marie, & Bertrand, Bruno. 2021. Long-Term Snow Height Variations in Antarctica from GNSS Interferometric Reflectometry. *REMOTE SENSING*, **13**(6).

Previdi, Michael, Smith, Karen L., & Polvani, Lorenzo M. 2021. Arctic amplification of climate change: a review of underlying mechanisms. *ENVIRONMENTAL RESEARCH LETTERS*, **16**(9).

Quartly, Graham D., Rinne, Eero, Passaro, Marcello, Andersen, Ole B., Dinardo, Salvatore, Fleury, Sara, Guillot, Amandine, Hendricks, Stefan, Kurekin, Andrey A., Mueller, Felix L., Ricker, Robert, Skourup, Henriette, & Tsamados, Michel. 2019. Retrieving Sea Level and Freeboard in the Arctic: A Review of Current Radar Altimetry Methodologies and Future Perspectives. *REMOTE SENSING*, **11**(7).

Rayner, NA, Parker, DE, Horton, EB, Folland, CK, Alexander, LV, Rowell, DP, Kent, EC, & Kaplan, A. 2003. Global analyses of sea surface temperature, sea ice, and night marine air temperature since the late nineteenth century. *JOURNAL OF GEOPHYSICAL RESEARCH-ATMOSPHERES*, **108**(D14).

Roesler, Carolyn, & Larson, Kristine M. 2018. Software tools for GNSS interferometric reflectometry (GNSS-IR). *GPS SOLUTIONS*, **22**(3).

Roquet, F., Madec, G., McDougall, Trevor J., & Barker, Paul M. 2015. Accurate polynomial expressions for the density and specific volume of seawater using the TEOS-10 standard. *OCEAN MODELLING*, **90**(JUN), 29–43.

Rose, Stine Kildegaard, Andersen, Ole Baltazar, Passaro, Marcello, Ludwigsen, Carsten Ankjaer, & Schwatke, Christian. 2019. Arctic Ocean Sea Level Record from the Complete Radar Altimetry Era: 1991-2018. *REMOTE SENSING*, **11**(14).

Russell, Andrew J., Carrivick, Jonathan L., Ingeman-Nielsen, Thomas, Yde, Jacob C., & Williams, Meredith. 2011. A new cycle of jökulhlaups at Russell Glacier, Kangerlussuaq, West Greenland. *JOURNAL OF GLACIOLOGY*, **57**(202), 238–246.

Sasgen, Ingo, Wouters, Bert, Gardner, Alex S., King, Michalea D., Tedesco, Marco, Landerer, Felix W., Dahle, Christoph, Save, Himanshu, & Fettweis, Xavier. 2020. Return to rapid ice loss in Greenland and record loss in 2019 detected by the GRACE-FO satellites. *COMMUNICATIONS EARTH & ENVIRONMENT*, **1**(1).

Schumacher, M., King, M. A., Rougier, J., Sha, Z., Khan, S. A., & Bamber, J. L. 2018. A new global GPS data set for testing and improving modelled GIA uplift rates. *GEOPHYSICAL JOURNAL INTERNATIONAL*, **214**(3), 2164–2176.

Shean, David E., Christianson, Knut, Larson, Kristine M., Ligtenberg, Stefan R. M., Joughin, Ian R., Smith, Ben E., Stevens, C. Max, Bushuk, Mitchell, & Holland, David M. 2017. GPS-derived estimates of surface mass balance and ocean-induced basal melt for Pine Island Glacier ice shelf, Antarctica. *CRYOSPHERE*, **11**(6), 2655–2674.

Siegfried, M. R., Medley, B., Larson, K. M., Fricker, H. A., & Tulaczyk, S. 2017. Snow accumulation variability on a West Antarctic ice stream observed with GPS reflectometry, 2007-2017. *GEOPHYSICAL RESEARCH LETTERS*, **44**(15), 7808–7816.

Simonsen, Sebastian B., Barletta, Valentina R., Colgan, William T., & Sorensen, Louise Sandberg. 2021. Greenland Ice Sheet Mass Balance (1992-2020) From Calibrated Radar Altimetry. *GEOPHYSICAL RESEARCH LETTERS*, **48**(3).

Smith, Ben, Fricker, Helen A., Gardner, Alex S., Medley, Brooke, Nilsson, Johan, Paolo, Fernando S., Holschuh, Nicholas, Adusumilli, Susheel, Brunt, Kelly, Csatho, Bea, Harbeck, Kaitlin, Markus, Thorsten, Neumann, Thomas, Siegfried, Matthew R., & Zwally, H. Jay. 2020. Pervasive ice sheet mass loss reflects competing ocean and atmosphere processes. *SCIENCE*, **368**(6496), 1239+.

Spada, Giorgio, & Galassi, Gaia. 2012. New estimates of secular sea level rise from tide gauge data and GIA modelling. *GEOPHYSICAL JOURNAL INTERNATIONAL*, **191**(3), 1067–1094.

Stammer, D. 1997. Steric and wind-induced changes in TOPEX/POSEIDON large-scale sea surface topography observations. *JOURNAL OF GEOPHYSICAL RESEARCH-OCEANS*, **102**(C9), 20987–21009.

Strandberg, Joakim, & Haas, Rudiger. 2020. Can We Measure Sea Level With a Tablet Computer? *IEEE GEOSCIENCE AND REMOTE SENSING LETTERS*, **17**(11), 1876–1878.

Strandberg, Joakim, Hobiger, Thomas, & Haas, Rudiger. 2016. Improving GNSS-R sea level determination through inverse modeling of SNR data. *RADIO SCIENCE*, **51**(8), 1286–1296.

Strandberg, Joakim, Hobiger, Thomas, & Haas, Rudiger. 2017. Coastal Sea Ice Detection Using Ground-Based GNSS-R. *IEEE GEOSCIENCE AND REMOTE SENSING LETTERS*, **14**(9), 1552–1556.

Stuecker, Malte F., Bitz, Cecilia M., Armour, Kyle C., Proistosescu, Cristian, Kang, Sarah M., Xie, Shang-Ping, Kim, Doyeon, McGregor, Shayne, Zhang, Wenjun, Zhao, Sen, Cai, Wenju, Dong, Yue, & Jin, Fei-Fei. 2018. Polar amplification dominated by local forcing and feedbacks. *NATURE CLIMATE CHANGE*, **8**(12), 1076+.

Sørensen, L. S., Simonsen, S. B., Nielsen, K., Lucas-Picher, P., Spada, G., Adalgeirsdottir, G., Forsberg, R., & Hvidberg, C. S. 2011. Mass balance of the Greenland ice sheet (2003-2008) from ICESat data - the impact of interpolation, sampling and firn density. *CRYOSPHERE*, **5**(1), 173–186.

Sørensen, Louise Sandberg, Simonsen, Sebastian B., Meister, Rakia, Forsberg, Rene, Levinsen, Joanna F., & Flament, Thomas. 2015. Envisat-derived elevation changes of the Greenland ice sheet, and a comparison with ICESat results in the accumulation area. *REMOTE SENSING OF ENVIRONMENT*, **160**(APR), 56–62.

Sørensen, Louise Sandberg, Simonsen, Sebastian B., Forsberg, Rene, Khvorostovsky, Kirill, Meister, Rakia, & Engdahl, Marcus E. 2018. 25 years of elevation changes of the

Greenland Ice Sheet from ERS, Envisat, and CryoSat-2 radar altimetry. *EARTH AND PLANETARY SCIENCE LETTERS*, **495**(AUG 1), 234–241.

Tabibi, Sajad, & Francis, Olivier. 2020. Can GNSS-R Detect Abrupt Water Level Changes? *REMOTE SENSING*, **12**(21).

Tabibi, Sajad, Geremia-Nievinski, Felipe, Francis, Olivier, & van Dam, Tonie. 2020. Tidal analysis of GNSS reflectometry applied for coastal sea level sensing in Antarctica and Greenland. *REMOTE SENSING OF ENVIRONMENT*, **248**(OCT).

The IMBIE Team. 2020. Mass balance of the Greenland Ice Sheet from 1992 to 2018. *NATURE*, **579**(7798), 233+.

van As, Dirk, Fausto, Robert S., & Team, PROMICE Project. 2011. Programme for Monitoring of the Greenland Ice Sheet (PROMICE): first temperature and ablation records. *GEOLOGICAL SURVEY OF DENMARK AND GREENLAND BULLETIN*, 73–76.

van den Broeke, Michiel, Box, Jason, Fettweis, Xavier, Hanna, Edward, Noel, Brice, Tedesco, Marco, van As, Dirk, van de Berg, Willem Jan, & van Kampenhout, Leo. 2017. Greenland Ice Sheet Surface Mass Loss: Recent Developments in Observation and Modeling. *CURRENT CLIMATE CHANGE REPORTS*, **3**(4), 345–356.

VanderPlas, Jacob T. 2018. Understanding the Lomb-Scargle Periodogram. *ASTROPHYSICAL JOURNAL SUPPLEMENT SERIES*, **236**(1).

Vaughan, D.G., Comiso, J.C., Allison, I., Carrasco, J., Kaser, G., Kwok, R., Mote, P., Murray, T., Paul, F., Ren, J., Rignot, E., Solomina, O., Steffen, K., & Zhang, T. 2013. Cryosphere. In: Climate Change 2013: The Physical Science Basis. Contribution of Working Group I to the Fifth Assessment Report of the Intergovernmental Panel on Climate Change [Stocker, T.F., D. Qin, G.-K. Plattner, M. Tignor, S.K. Allen, J. Boschung, A. Nauels, Y. Xia, V. Bex and P.M. Midgley (eds.)]. Cambridge University Press, Cambridge, United Kingdom and New York, NY, USA.

Wake, Leanne M., Lecavalier, Benoit S., & Bevis, Michael. 2016. Glacial Isostatic Adjustment (GIA) in Greenland: a Review. *CURRENT CLIMATE CHANGE REPORTS*, **2**(3), 101–111.

Wan, Wei, Larson, Kristine M., Small, Eric E., Chew, Clara C., & Braun, John J. 2015. Using geodetic GPS receivers to measure vegetation water content. *GPS SOLUTIONS*, **19**(2), 237–248.

Wang, Hansheng, Xiang, Longwei, Jia, Lulu, Jiang, Liming, Wang, Zhiyong, Hu, Bo, & Gao, Peng. 2012. Load Love numbers and Green's functions for elastic Earth models PREM, iasp91, ak135, and modified models with refined crustal structure from Crust 2.0. *COMPUTERS & GEOSCIENCES*, **49**(DEC), 190–199.

WCRP, Global Sea Level Budget Group. 2018. Global sea-level budget 1993-present. *EARTH SYSTEM SCIENCE DATA*, **10**(3), 1551–1590.

Williams, S. D. P., & Nievinski, F. G. 2017. Tropospheric delays in ground-based GNSS Multipath Reflectometry – Experimental evidence from coastal sites. *Journal of Geophysical Research: Solid Earth*, n/a–n/a.

Williams, Simon D. P., Bell, Paul S., McCann, David L., Cooke, Richard, & Sams, Christine. 2020. Demonstrating the Potential of Low-Cost GPS Units for the Remote Measurement of Tides and Water Levels Using Interferometric Reflectometry. *JOURNAL OF ATMOSPHERIC AND OCEANIC TECHNOLOGY*, **37**(10), 1925–1935.

Woeppelmann, G., Letetrel, C., Santamaria, A., Bouin, M. N., Collilieux, X. Altamimi, Z., Williams, S. D. P., & Miguez, B. Martin. 2009. Rates of sea-level change over the past century in a geocentric reference frame. *GEOPHYSICAL RESEARCH LETTERS*, **36**(JUN 24).

Wouters, Bert, Gardner, Alex S., & Moholdt, Gait. 2019. Global Glacier Mass Loss During the GRACE Satellite Mission (2002-2016). *FRONTIERS IN EARTH SCIENCE*, **7**(MAY 21).

Wöppelmann, Guy, & Marcos, Marta. 2016. Vertical land motion as a key to understanding sea level change and variability. *REVIEWS OF GEOPHYSICS*, **54**(1), 64–92.

A Paper 1

remote sensing

MDPI

Technical Note

GNSS-IR Measurements of Inter Annual Sea Level Variations in Thule, Greenland from 2008–2019

Trine S. Dahl-Jensen [1,*], Ole B. Andersen [1], Simon D. P. Williams [2], Veit Helm [3] and Shfaqat A. Khan [1]

[1] Danish National Space Centre, Technical University of Denmark, 2800 Lyngby, Denmark; oa@space.dtu.dk (O.B.A.); abbas@space.dtu.dk (S.A.K.)
[2] National Oceanography Center, Liverpool L3 5DA, UK; sdwil@noc.ac.uk
[3] Alfred Wegener Institute, Helmholtz Centre for Polar and Marine Research, 27570 Bremerhaven, Germany; veit.helm@awi.de
* Correspondence: trdhj@space.dtu.dk

Abstract: Studies of global sea level often exclude Tide Gauges (TGs) in glaciated regions due to vertical land movement. Recent studies show that geodetic GNSS stations can be used to estimate sea level by taking advantage of the reflections from the ocean surface using GNSS Interferometric Reflectometry (GNSS-IR). This method has the immediate benefit that one can directly correct for bedrock movements as measured by the GNSS station. Here we test whether GNSS-IR can be used for measurements of inter annual sea level variations in Thule, Greenland, which is affected by sea ice and icebergs during much of the year. We do this by comparing annual average sea level variations using the two methods from 2008–2019. Comparing the individual sea level measurements over short timescales we find a root mean square deviation (RMSD) of 13 cm, which is similar to other studies using spectral methods. The RMSD for the annual average sea level variations between TG and GNSS-IR is large (18 mm) compared to the estimated uncertainties concerning the measurements. We expect that this is in part due to the TG not being datum controlled. We find sea level trends from GNSS-IR and TG of −4and −7 mm/year, respectively. The negative trend can be partly explained by a gravimetric decrease in sea level as a result of ice mass changes. We model the gravimetric sea level from 2008–2017 and find a trend of −3 mm/year.

Keywords: sea level; GPS; GNSS-IR; reflectometry; Greenland

check for updates

Citation: Dahl-Jensen, T.S.; Andersen, O.B.; Williams, S.D.P.; Helm, V.; Khan, S.A. GNSS-IR Measurements of Inter Annual Sea Level Variations in Thule, Greenland from 2008–2019. *Remote Sens.* **2021**, *13*, 5077. https://doi.org/10.3390/rs13245077

Academic Editor: Ferdinando Nunziata

Received: 5 November 2021
Accepted: 9 December 2021
Published: 14 December 2021

1. Introduction

Global sea level is currently rising at a rate of 3 mm/year as a result of ongoing climate change [1,2]. The distribution of local sea level rise is not uniform and thus some areas experience significantly higher than average sea level rise while other areas experience decreasing sea level [2,3].

Local relative sea level change is traditionally measured using Tide Gauges (TGs) while global sea level studies are often based on a combination with satellite altimetry. In general there are not many TGs in the arctic regions, which reduces the possibility of studying the local sea level change. Furthermore, in order to use TGs for studies of global eustatic sea level change, the TG measurements need to be corrected for bedrock movements of the solid earth. In glaciated regions, such as Greenland, the bedrock movement is large and complicated to model and is a combination of elastic movement caused by ongoing ice mass variability and a viscoelastic component caused by past ice variability over thousands of years (also known as the glacial isostatic adjustment). There is a large uncertainty on the modeled uplift, and therefore TG data from these areas are typically omitted from studies of global eustatic sea level [1,4].

Recent studies show that, under the right conditions, relative sea level change can be measured using GNSS Interferometric Reflectometry (GNSS-IR) [5,6]. Usage of GNSS stations to measure sea level has the immediate benefit that the bedrock movement is simultaneously measured with a high precision at the site allowing the local eustatic sea level to be calculated directly. The uncertainty on individual measurements of sea level is considerably higher using GNSS-IR compared to TGs. However, averages taken over a day are almost directly comparable and correlate very well [6]. A higher accuracy on the individual measurements can potentially be found using inverse modelling methods when necessary [7].

Larson et al. [6] studied sea level variations using GNSS-IR from a GNSS station installed at Friday Harbour, Washington. Though the GNSS station was installed with the purpose of studying tectonic movement, they found good agreement with a nearby TG for monthly averages over a 10 year period. The area is in some ways ideal for reflectometry studies as it experiences little vertical land movement and is not affected by sea ice. Kim and Park [8] use GNSS-IR to study sea level in St. Michael, Alaska using a GNSS station installed in 2018 and compare with nearby TGs. The results are promising, however, the closest TG with actual sea level data is in Unalakleet, 74 km from St. Michael.

In this study we will test whether GNSS-IR can be used for measurements of inter annual sea level variations in a complicated glaciated region affected by large vertical land movement, sea ice and icebergs.

In Greenland, an extensive network of 58 permanent geodetic GNSS stations, called GNET, have been installed on bedrock between 2007 and 2009 [9,10]. The main purpose of GNET is to investigate changes in the Greenland ice sheet by continuously measuring bedrock uplift. Tabibi et al. [11] used four GNET stations as well as four Antarctic stations to study tidal constituents in Arctic regions from GNSS-IR. Unfortunately the four used GNET stations (KULL, QAAR, PLPK and KULU) are not co-located with a TG for direct comparison.

Here, we compare sea level variations measured by GNSS-IR from a GNET GNSS station located at Thule Airbase with results from a nearby TG station together with satellite altimetry data. The three methods are illustrated in Figure 1. GNSS-IR and TG both measure the local sea level variations while altimetry measures the absolute sea level. In order to compare the GNSS-IR and TG measurements with altimetry we will have to correct for vertical bedrock movement, as measured by the GNSS station.

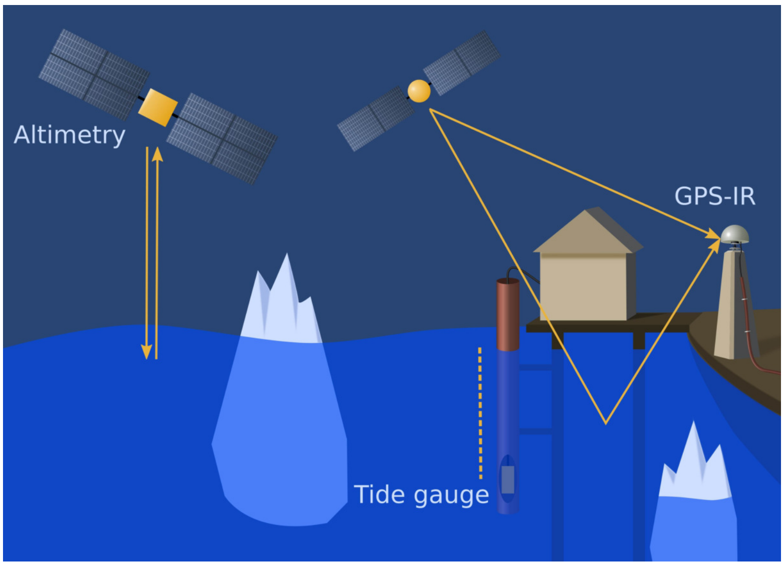

Figure 1. Illustration of the three methods used for measuring sea level in Thule in this study.

2. Materials and Methods

2.1. Sea Level Measurements

The TG in Thule is maintained by DTU Space and measures sea level every 5 min. It is not datum controlled, thus, there may be gross errors that are unidentified in the data set. It was installed in 2006, however, the data from the TG was of poor quality until late 2007 when it was maintained and moved to a new location. Therefore, only data from 2008 and onwards are used in this study. The station was returned to the original position in September 2015 (Figure 2c). We include the data after this date in this study as the data quality is similar to the 2008–2015 period and otherwise the usable time period will be short.

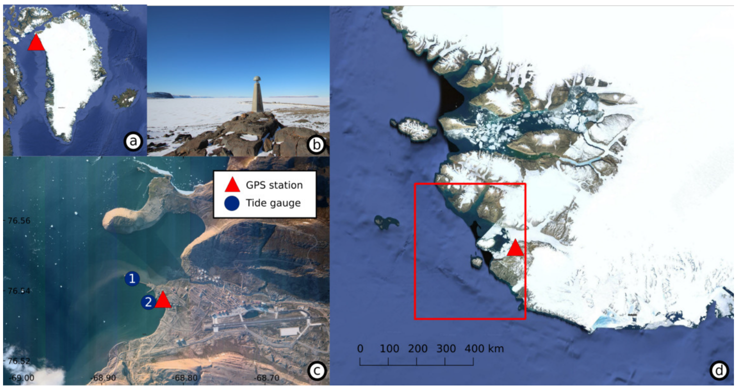

Figure 2. Maps illustrating the study area. (**a**) Map of Greenland. Thule is marked by the red triangle. (**b**) Picture of the GNSS station in Thule with the view over the ocean. (**c**) Map of Thule with GNSS- and TG station locations. 1 marks the position of the TG until September 2015 and 2 marks the position since then. (**d**) The red rectangle illustrates the area used for sea level extraction from altimetry.

The GNSS station in Thule is located approximately 60 m from the coast in a bay close to the harbor (Figure 2). The distance between the TG and the GNSS station is less than 2 km from 2008–2015 and shorter after the move. From GNSS-IR we have sub daily estimates of sea surface height from 2002 to early 2020. However, only data from the period covered by the TG is used in this study.

We used the same methodology to measure sea level using GNSS Signal to Noise Ratio (SNR) measurements as described in Larson et al. [6] and Williams et al. [12]. Individual satellite passes are split into ascending and descending nodes and masked using a pre-selected elevation and azimuth mask to select satellite passes where the main reflector should be the water surface. The measured SNR data are translated to a linear scale from decibels-hertz and a low-order polynomial is used to remove the direct signal effect. Spectral analysis of the residual SNR as a function of the wavelength of the carrier signal and the elevation angle of the satellite should produce a peak at a frequency that is related to the height of the antenna above the horizontal reflecting surface, the primary observation in GNSS-IR water level studies. We include corrections for non-stationary reflector height (the $\dot{H}$ effect) [13] and tropospheric delay [14]. We use an initial elevation mask of between 2° and 20° and an azimuth range of between 160° and 290°. During the initial Quality Control (QC) process passes with an average azimuth lower than 170°, higher than 270° or an estimated reflector height lower than 17 m were removed. The final, iterative, QC process is described in Williams et al. [12]. Maps illustrating the reflection zones (fresnel zones) are included in the supplementary material.

The altimetry data used in this study are the ESA CCI DTU/TUM sea level anomaly [15]. It is based on data from ERS-1, ERS-2, Envisat and Cryosat-2. The data used here is from the period covered by Envisat and Cryosat-2 and an average is calculated over the area between 68.5 and 72 degrees west and 76 and 77 north (Figure 2d).

Both TG and GNSS-IR observations were analyzed using the response method extended with the orthotide formalism [16] in order to remove the tidal signal. The advantage of using this method is as follows: by assuming a smooth admittance function described by a relatively low number of parameters within each tidal band (orthotide parameters) a solution for any constituent can be inferred and hence corrected for. For 2016, removing the ocean tides reduces the RMS of the observed sea level from the TG from 72 cm to 15 cm.

After removing the tides, all sea level data are filtered in order to enhance the inter annual signal. The annual and semi-annual signal is removed using a least squares fit of the two harmonics [17]. By removing the annual and semi-annual signal, the influence of potential gaps in the data on annual average sea level will be smaller. The error in the annual average sea levels from GNSS-IR and TG as well as the annual measured uplift are estimated by calculating the standard deviation of the daily measurement over all periods of 60 daily values. After that the average value of this standard deviation for each year is calculated and from that the standard deviation of the mean is calculated using the number of daily measurements from that year.

The uncertainty of the annual altimetry results are estimated as the standard deviation of the mean from the monthly sea levels after filtering out the annual and bi-annual signal.

In order to be able to compare GNSS-IR and TG results with the altimetry, we need to correct for vertical land movement. For this we use daily positions of the same GNSS station [9,10]. The GNSS station in Thule covers a period from 1999 to present and daily positions are available throughout 2019 with minor gaps.

In order to avoid differences in the annual averages of the TG and GNSS-IR sea level measurements due to gaps in the data series, only data from days where there is data from both methods are used to calculate the annual values.

2.2. Sea Level Change Due to Reduced Gravity

As ice mass is lost in e.g., Greenland and Antarctica, the local gravity attraction drops, resulting in decreasing sea levels. To estimate this gravitational effect, we convolve ice mass change with the Green's functions for geoid anomaly derived by Wang et al. [18] for elastic Earth model iasp91 with refined crustal structure from Crust 2.0. We use ice mass changes from both Greenland, Antarctica and other glaciers as these may all influence sea levels in Thule.

For the ice mass changes in Antarctica we use the gridded mass balance product from Groh and Horwath [19] which is available until mid 2016. The annual mean sea level change due to reduced gravitational effect from Antarctica is 0.05 mm which is at least an order of magnitude smaller than for Greenland or other glaciers due to the long distance from Thule. The uncertainty on the gravitational results in 2016-2018 is altered to account for this added uncertainty.

For Greenland we interpolate a 2×2 km grid of annual ice height changes from 2007–2015 and a 2.5×2.5 km grid from 2016–2017 using altimeter data from NASA's ATM flights [20] supplemented with high resolution ICESat laser altimetry data from 2003 to 2009 [21] and Cryosat-2 data (2011–2017) [22], complemented with ENVISAT data from 2009 to 2012 [23]. The method used to create the height change grid is described in detail by Khan et al. [23].

Mass changes from other glaciers are extracted from an update of the model by Marzeion et al. [24] and available until 2017. They model mass changes of all glaciers in the Randolph Glacier Inventory [25] from temperature and precipitation. They use measurements of the mass balance of 255 glaciers to estimate model parameters and carry out a leave-one-out validation as well as a validation using geodetic data.

The errors in the sea level variations from the reduced gravity are estimated by calculating the sea level change as a result of the estimated error of the Greenland ice height changes [26] and adding the uncertainty from the other glaciers and the Earth model. In the calculations we assume that the error on the ice height data from 2016–2017 is the same as for the previous years. The uncertainty related to the mass loss from other glaciers is calculated in a similar manner by calculating the uplift resulting from the estimated errors of the glacier mass changes. For the Earth model we use an uncertainty in gravity related sea level change of 2% of the annual signal as suggested by Wang et al. [18]. Data from Antarctica is available from 2008–2015 and errors from ice mass changes in Antarctica are not included during this period since the gravity related sea level change resulting from these changes are at least an order of magnitude smaller than from Greenland and other glaciers. For 2016 to 2018, where the data set from Antarctica is not available, we add an error corresponding to the average gravity related sea level change contribution from Antarctica during the period by propagation of errors.

3. Results

We compare the sea level change in Thule measured using three different methods: GNSS-IR, TG and satellite altimetry.

The annual average sea level anomaly using each method is shown in Figure 3. Monthly sea level results from TG, GNSS-IR and altimetry can be found in the supplementary material. Since the TG is not datum controlled, it is not possible to compare the absolute sea level using the three methods. Instead, we compare inter annual changes in the sea level. To directly compare sea level measured using GNSS and TG with altimetry, GNSS-IR and TG results are corrected for vertical land movement as measured by the GNSS station. Since the estimated error on the measured uplift is an order of magnitude smaller than on the sea level and the same vertical uplift correction is done for GNSS-IR and TG sea levels, the error of the uplift measurement is not included in the error bars.

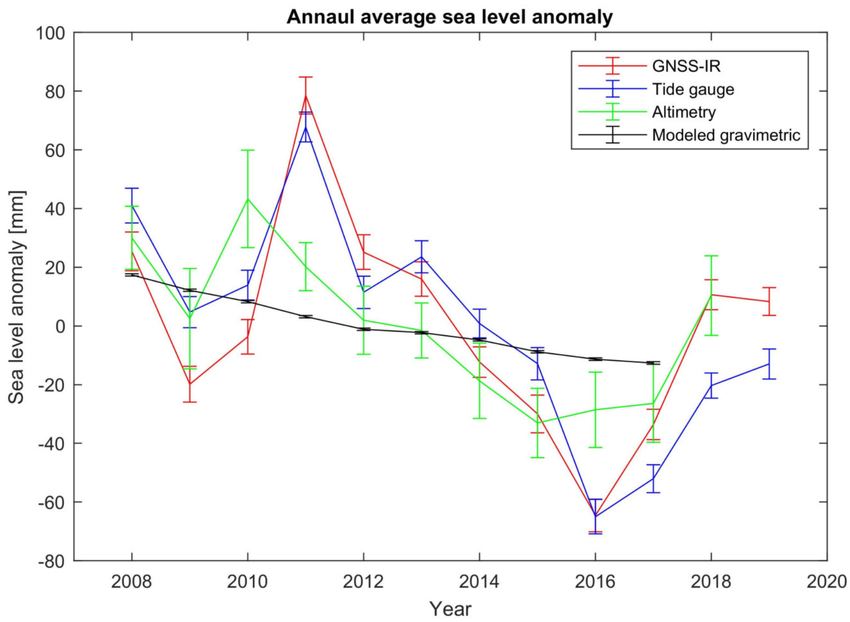

Figure 3. Annual average sea level change at Thule using GNSS-IR, TG and altimetry. The error bars illustrate the annual standard deviation of the mean as described in Section 2. The figure also includes variations in the modeled gravity related sea level.

We estimate a linear correlation between annual sea level from GNSS-IR and TG of 0.87. The linear trend in sea level is -4 ± 7 mm/year and -7 ± 5 mm/year for GNSS-IR and TG, respectively. The linear trend in annual sea level measured by altimetry is -5 ± 4 mm/year.

The estimated uncertainty of the annual average sea level measurements using TG and GNSS varies between 4 and 6 mm. The estimated uncertainty of the annual Altimetry results is between 2 and 8 mm and depends strongly on the satellite altimeter used, with considerably larger error estimates for Envisat than for Cryosat-2. It can be seen that though the three timeseries show similar variations they still differ more than would be expected from the estimated measurement errors. The RMSD between annual GNSS-IR and TG sea level changes is 18 mm which is considerably higher than the estimated errors. For the altimetry results, the RMSD with TG and GNSS-IR is 31 and 24 mm, respectively. Deviations larger that the uncertainty is not unexpected between altimetry and the other methods as the TG and GNSS-IR are local measurements, while the sea level from altimetry is calculated over an area off the coast (Figure 2).

Figure 4 shows one week of sea level variation from August 2018 using GNSS-IR and TG. Note that the TG in Thule is not datum controlled and therefore the mean sea level is subtracted from both time series and the sea level variations compared. The Root Mean Square Deviation (RMSD) of individual measurements of sea level variation is 13 cm for August 2018 which compares well with other spectral SNR studies [5,6]. Figures of individual GNSS-IR measurements for the full year 2018 can be found in the supplementary material. If we instead compare daily values of sea level from GNSS-IR and TG for the whole study period the correlation between the two is 0.84 and the RMS deviation is 65 mm.

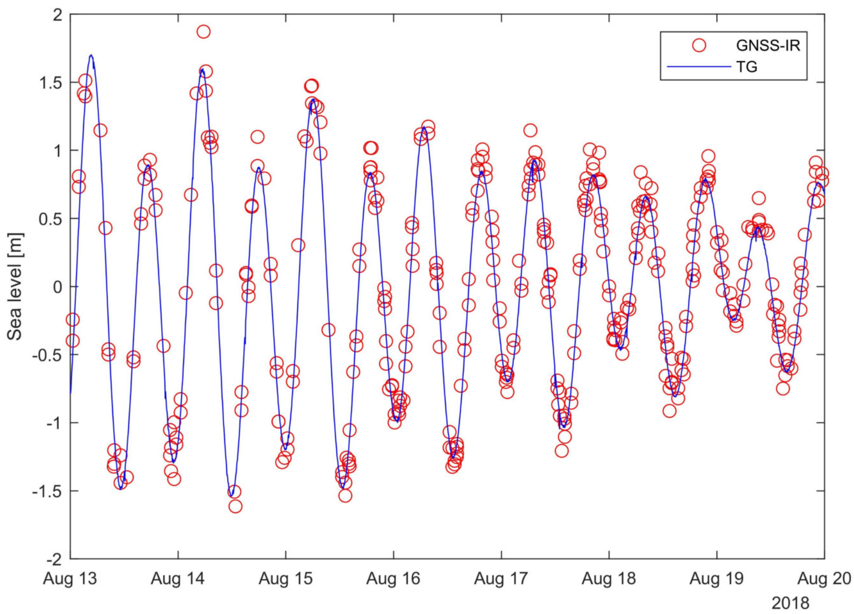

Figure 4. Individual measurements of sea level variation using GNSS Interferometric Reflectometry (GNSS-IR) and Tide Gauge (TG) from one week in August 2018 (13 to 19 of August).

Figure 3 also includes the modeled gravity related sea level change. The average gravity related sea level has been altered such that the average is the same as the average of GNSS-IR and TG sea levels over the covered period. The trend in the modeled gravitational sea level is -3 ± 0.4 mm/year while it is -8 ± 9 mm/year and -10 ± 7 mm/year for GNSS-IR and TG, respectively, for this period. The inter annual variations in the gravity related sea level are very small compared to the measured sea level and therefore it is unlikely that the large year-to-year variations are related to gravitational effects. The large year-to-year variations combined with the relatively short timescale also result in large uncertainties on the trends. Thus one should be careful when comparing the trends as the large year-to-year variations will strongly affect the calculated trend.

4. Discussion

We have compared inter annual sea level variations in Thule measured by GNSS-IR, TG and satellite altimetry. We find that the annual variations from GNSS-IR are comparable with those from TG, but that the differences are larger than the estimated errors.

The sea level trends also differ between the three methods but due to high uncertainties on the trends they are within the estimated errors. We expect that the high uncertainties on the trends are a result of the large inter annual variations in the sea level compared to the trend, combined with a relatively short time series when it comes to long term studies.

The standard deviation of the daily GNSS-IR and TG measurements, used to estimate the error, is 110 and 94 mm respectively. For comparison, the RMSD between the two is 65 mm. This indicates that our estimated errors on the two measurements may be too large. This is especially true since the two methods are expected to deviate in winter due to sea ice formation, which introduces a difference that is not a measurement error in traditional terms. If we instead look at the annual averages, the RMSD between TG and GNSS-IR is 18 mm, which is about 4 times the estimated error of the mean. This may seem strange as the RMSD was smaller than the standard deviation for the daily measurements, used to estimate the errors. We expect that this is related to the fact that a considerable part of the difference between the two data sets is not random errors on the individual measurements. These differences will be passed to the means and are not captured by the estimated errors.

The ocean around Thule is covered by sea ice during much of the year and only consistently ice free a couple of months each year. Strandberg et al. [27] show that there are significant changes in the SNR from the GNSS station when sea ice is present. Furthermore, TGs estimate sea level by measuring the pressure at a certain position in the water column while GNSS-IR estimates the distance from GNSS antenna and to the sea surface. Therefore, one source of such non-random deviations could be differences in sea ice cover from year to year, as this would affect the two measurements differently. However, if a similar comparison is done using only data from August and September, where the water is assumed to be ice free, the correlation is 0.69 and the RMSD 37 mm. Thus, the correlation decreases and the RMSD is larger than for the full year average. The increase in RMSD and decrease in correlation is likely due to the use of much less data in total when we limit the mean to this period. However, the RMSD is still large compared to what we would expect from the daily and individual measurements and thus we do not believe that inter annual variations in sea ice alone can explain the differences that we observe.

Other studies comparing sea levels extracted from GNSS-IR with TGs, generally find lower RMSD than we do here. Larson et al. [13] compares GNSS-IR from Kachemak Bay, Alaska, with tide gauge data over one year. They find a RMSD of 23 mm for the daily means. In another study, Larson et al. [6] analyse 10 years of sea level data at Friday Harbor, Washington, and find an RMSD between daily sea levels from GNSS-IR and TG of 21 mm. Both mentioned studies were conducted using one-antenna geodetic GNSS stations, which were installed with the purpose of measuring land motion. Thus, the GNSS equipment used is comparable to the station installed in Thule.

The significant deviations between TG and GNSS-IR may be partly due to the TG not being datum controlled and thus there may be small unknown shifts or drifts in the data series. These could happen at the time of maintenance or be related to changes in the equipment. There have been no changes in the GNSS antenna during the period of interest, but there has been a couple of changes to the TG. The TG sensor was exchanged in 2008, 2015 and 2017. In 2015 the TG was also moved to a different location (Figure 2). On top of this there is an unknown amount of other maintenance jobs which could also disturb the time series as the TG is not datum controlled.

If we compare the sea level from GNSS-IR and TG until 2015 where the TG was moved the RMSD is 13 mm. Though the RMSD on the annual averages are smaller than for the full period it is still large compared to the estimated errors and though the move may explain some of the difference it does not explain all.

The sea level estimates from altimetry differs significantly from both GNSS-IR and TG results. Thus the altimetry does not indicate the source of the discrepancy between the two. The large discrepancies in sea level variations between the local measurements and altimetry in 2010–2011 is likely related to the transition from Envisat to Cryosat-2 measurements during the first half of 2011. Cryosat-2 uses a new Synthetic Aperture Radar altimetric technology, which greatly reduces footprint. This result in an increased amount of data from leads in the sea-ice compared to its pre-decessor, Envisat. As sea level is generally low during the winter season, this causes the altimeter to miss the 2011 peak in sea level.

The modeled gravity related sea level shows a negative trend that is smaller than measured by GNSS-IR and TG but within the uncertainties on these trends. Thus, changes in the gravity field as a result of ice mass changes in the region can explain why we observe a negative sea level trend in Thule. The inter-annual variations, however, are much smaller than what we observe and must be a result of other effects.

Figure 5 shows a map of all GNET GNSS stations in Greenland as well as TGs with a temporal overlap with the nearest GPS station. There are currently 4 TGs in operation in Greenland: Thule (close to THU2), Scoresbysund (close to SCOR), Godthaab (close to NUUK) and Qaqortoq (close to QAQ1). Unfortunately, neither the Scoresbysund, Nuuk or Qaqortoq GNSS station have a view of the open ocean which is suitable for GNSS-IR purposes. The TG station near KELY was located in Sisimiut but it has not been in operation since 1999. Furthermore, the nearest GNSS station in KELY does not see the open water. Thus, Thule is currently the only place in Greenland where we can directly compare inter annual changes in sea level measured by TG and GNSS-IR.

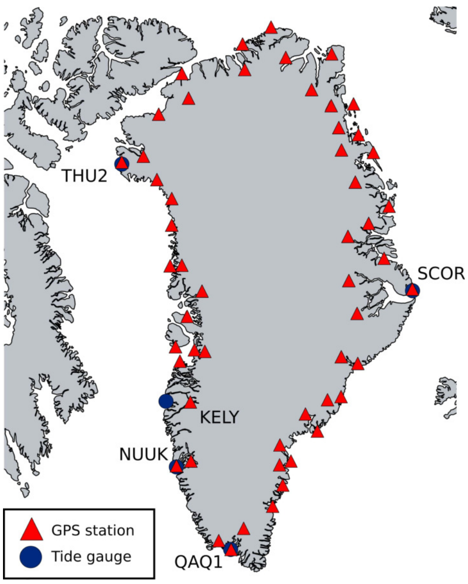

Figure 5. Map of Greenland with indication of GNET GNSS stations and tide gauges with data overlapping the nearest GPS station.

5. Conclusions

Our results show that the sea level variations measured by GNSS-IR and TG match well on short timescales (Figure 4) and are comparable to other studies. However, there are considerable differences in the inter annual variation that cannot be explained by differences in sea ice cover. We suspect that this difference is related to maintenance on the non-datum controlled TG station. The TG is corrected for uplift using position data from the GNSS station but there may be changes e.g., during maintenance not captured by this. The altimetry differs significantly from both the two local measurements and thus cannot be used to indicate whether one or the other is most representative of the sea level in Thule. Modeled gravity related sea level has a negative trend of -3 ± 0.4 mm/year with only small inter annual variations. We suggest that the GNSS-IR method should be further tested in glaciated areas, preferably against a datum controlled TG.

Since the uncertainty on individual measurements is high [5,28] and the measurement frequency is controlled by the passing of satellites, GNSS-IR cannot replace tide gauges, and should instead be seen as a potential supplement. The technique has the immediate benefit that we have an on-site measurement of vertical land movement and the results can be used directly for studies of eustatic sea level change. This is especially useful in places with large vertical land movements such as glaciated regions and in tectonically active areas.

We suggest that the option of using GNSS stations for sea level monitoring is taken into consideration when installing new GNSS stations in coastal areas and that the stations are installed with an open view of the ocean when feasible.

Supplementary Materials: The following are available at https://www.mdpi.com/article/10.3390/rs13245077/s1.

Author Contributions: Methodology, T.S.D.-J.; Formal analysis, T.S.D.-J.; data processing, S.D.P.W. (reflectometry) and V.H. (ice heights); writing—original draft preparation, T.S.D.-J.; writing—review and editing, All; visualization, T.S.D.-J.; supervision, S.A.K. and O.B.A. All authors have read and agreed to the published version of the manuscript.

Funding: S.A. Khan, O.B. Andersen and T.S. Dahl-Jensen was funded by the INTAROS GA No. 727890 funded by European Union's Horizon 2020 Research and Innovation Programme.

Institutional Review Board Statement: Not applicable.

Informed Consent Statement: Not Applicable.

Data Availability Statement: Data sources are referenced in the text. The GNSS data from the station in Thule (THU2) is publicly available from the UNAVCO website (https://www.unavco.org/data/gps-gnss/gps-gnss.html, accessed on 1 December 2021). The mass change data from Antarctica can be downloaded from the Technical University of Dresden (https://data1.geo.tu-dresden.de/ais_gmb/, accessed on 1 December 2021). The ESA CCI DTU/TUM altimetry product is available at https://ftp.space.dtu.dk/pub/ARCTIC_SEALEVEL/DTU_TUM_V3_2019/, accessed on 1 December 2021. The data from the tide gauge in Thule is available at https://ftp.space.dtu.dk/pub/Sealevel/, accessed on 1 December 2021.

Conflicts of Interest: The authors declare no conflict of interest.

References

1. Spada, G.; Galassi, G. New estimates of secular sea level rise from tide gauge data and GIA modelling. *Geophys. J. Int.* **2012**, *191*, 1067–1094. [CrossRef]
2. Church, J.; White, N.; Coleman, R.; Lambeck, K.; Mitrovica, J. Estimates of the regional distribution of sea level rise over the 1950–2000 period. *J. Clim.* **2004**, *17*, 2609–2625. [CrossRef]
3. Hsu, C.W.; Velicogna, I. Detection of sea level fingerprints derived from GRACE gravity data. *Geophys. Res. Lett.* **2017**, *44*, 8953–8961. [CrossRef]
4. Woeppelmann, G.; Letetrel, C.; Santamaria, A.; Bouin, M.N.; Collilieux, X. Altamimi, Z.; Williams, S.D.P.; Miguez, B.M. Rates of sea-level change over the past century in a geocentric reference frame. *Geophys. Res. Lett.* **2009**, *36*. [CrossRef]
5. Lofgren, J.S.; Haas, R.; Scherneck, H.G. Sea level time series and ocean tide analysis from multipath signals at five GPS sites in different parts of the world. *J. Geodyn.* **2014**, *80*, 66–80. [CrossRef]
6. Larson, K.M.; Ray, R.D.; Williams, S.D.P. A 10-Year Comparison of Water Levels Measured with a Geodetic GPS Receiver versus a Conventional Tide Gauge. *J. Atmos. Ocean. Technol.* **2017**, *34*, 295–307. [CrossRef]
7. Strandberg, J.; Hobiger, T.; Haas, R. Improving GNSS-R sea level determination through inverse modeling of SNR data. *Radio Sci.* **2016**, *51*, 1286–1296. [CrossRef]
8. Kim, S.K.; Park, J. Monitoring Sea Level Change in Arctic using GNSS-Reflectometry. In Proceedings of the 2019 International Technical Meeting of the Institute of Navigation, Reston, VA, USA, 28–31 January 2019; pp. 665–675. [CrossRef]

9. Khan, S.A.; Sasgen, I.; Bevis, M.; van Dam, T.; Bamber, J.L.; Wahr, J.; Willis, M.; Kjaer, K.H.; Wouters, B.; Helm, V.; et al. Geodetic measurements reveal similarities between post-Last Glacial Maximum and present-day mass loss from the Greenland ice sheet. *Sci. Adv.* **2016**, *2*, e1600931. [CrossRef] [PubMed]
10. Bevis, M.; Wahr, J.; Khan, S.A.; Madsen, F.B.; Brown, A.; Willis, M.; Kendrick, E.; Knudsen, P.; Box, J.E.; van Dam, T.; et al. Bedrock displacements in Greenland manifest ice mass variations, climate cycles and climate change. *Proc. Natl. Acad. Sci. USA* **2012**, *109*, 11944–11948. [CrossRef]
11. Tabibi, S.; Geremia-Nievinski, F.; Francis, O.; van Dam, T. Tidal analysis of GNSS reflectometry applied for coastal sea level sensing in Antarctica and Greenland. *Remote Sens. Environ.* **2020**, *248*, 111959. [CrossRef]
12. Williams, S.D.P.; Bell, P.S.; McCann, D.L.; Cooke, R.; Sams, C. Demonstrating the Potential of Low-Cost GPS Units for the Remote Measurement of Tides and Water Levels Using Interferometric Reflectometry. *J. Atmos. Ocean. Technol.* **2020**, *37*, 1925–1935. Available online: https://journals.ametsoc.org/jtech/article-pdf/37/10/1925/5010618/jtechd200063.pdf (accessed on 1 December 2021). [CrossRef]
13. Larson, K.M.; Ray, R.D.; Nievinski, F.G.; Freymueller, J.T. The Accidental Tide Gauge: A GPS Reflection Case Study From Kachemak Bay, Alaska. *IEEE Geosci. Remote Sens. Lett.* **2013**, *10*, 1200–1204. [CrossRef]
14. Williams, S.D.P.; Nievinski, F.G. Tropospheric delays in ground-based GNSS Multipath Reflectometry— Experimental evidence from coastal sites. *J. Geophys. Res. Solid Earth* **2017**, *122*, 2310–2327. [CrossRef]
15. Rose, S.K.; Andersen, O.B.; Passaro, M.; Ludwigsen, C.A.; Schwatke, C. Arctic Ocean Sea Level Record from the Complete Radar Altimetry Era: 1991–2018. *Remote Sens.* **2019**, *11*, 1672. [CrossRef]
16. Andersen, O. Shallow water tides in the northwest European shelf region from TOPEX/POSEIDON altimetry. *J. Geophys. Res.-Ocean.* **1999**, *104*, 7729–7741. [CrossRef]
17. Khan, S.A.; Wahr, J.; Leuliette, E.; van Dam, T.; Larson, K.M.; Francis, O. Geodetic measurements of postglacial adjustments in Greenland. *J. Geophys. Res.-Solid Earth* **2008**, *113*. [CrossRef]
18. Wang, H.; Xiang, L.; Jia, L.; Jiang, L.; Wang, Z.; Hu, B.; Gao, P. Load Love numbers and Green's functions for elastic Earth models PREM, iasp91, ak135, and modified models with refined crustal structure from Crust 2.0. *Comput. Geosci.* **2012**, *49*, 190–199. [CrossRef]
19. Groh, A.; Horwath, M. The method of tailored sensitivity kernels for GRACE mass change estimates. *Geophys. Res. Abstr.* **2016**, *18*, EGU2016-12065.
20. Krabill, W. *IceBridge ATM L2 Icessn Elevation, Slope, and Roughness, [1994–2010]*; National Snow and Ice Data Center: Boulder, CO, USA, 2011.
21. Zwally, H.J.; Schutz, R.; Bentley, C.; Bufton, J.; Herring, T.; Minster, J.; Spinhirne, J.; Thomas, R. *GLAS/ICESat L2 Antarctic and Greenland Ice Sheet Altimetry Data, Version 34*; Indicate Subset Used; NASA National Snow and Ice Data Center: Boulder, CO, USA, 2014. [CrossRef]
22. Helm, V.; Humbert, A.; Miller, H. Elevation and elevation change of Greenland and Antarctica derived from CryoSat-2. *Cryosphere* **2014**, *8*, 1539–1559. Available online: https://tc.copernicus.org/articles/8/1539/2014/tc-8-1539-2014.pdf (accessed on 1 December 2021). [CrossRef]
23. Khan, S.A.; Kjaer, K.H.; Korsgaard, N.J.; Wahr, J.; Joughin, I.R.; Timm, L.H.; Bamber, J.L.; van den Broeke, M.R.; Stearns, L.A.; Hamilton, G.S.; et al. Recurring dynamically induced thinning during 1985 to 2010 on Upernavik Isstrom, West Greenland. *J. Geophys. Res.-Earth Surf.* **2013**, *118*, 111–121. [CrossRef]
24. Marzeion, B.; Jarosch, A.H.; Hofer, M. Past and future sea-level change from the surface mass balance of glaciers. *Cryosphere* **2012**, *6*, 1295–1322. [CrossRef]
25. RGI Consortium. Randolph Glacier Inventory—A Dataset of Global Glacier Outlines: Version 6.0. In *Global Land Ice Measurements from Space*; Technical Report; Digital Media: Denver, CO, USA, 2017. [CrossRef]
26. Khan, S.A.; Kjaer, K.H.; Bevis, M.; Bamber, J.L.; Wahr, J.; Kjeldsen, K.K.; Bjork, A.A.; Korsgaard, N.J.; Stearns, L.A.; van den Broeke, M.R.; et al. Sustained mass loss of the northeast Greenland ice sheet triggered by regional warming. *Nat. Clim. Chang.* **2014**, *4*, 292–299. [CrossRef]
27. Strandberg, J.; Hobiger, T.; Haas, R. Coastal Sea Ice Detection Using Ground-Based GNSS-R. *IEEE Geosci. Remote. Sens. Lett.* **2017**, *14*, 1552–1556. [CrossRef]
28. Larson, K.M.; Lofgren, J.S.; Haas, R. Coastal sea level measurements using a single geodetic GPS receiver. *Adv. Space Res.* **2013**, *51*, 1301–1310. [CrossRef]

B Supplementary material for paper 1

This supplementary information is comprised of multiple plots of the sea level data discussed in the paper. While the paper focus on annual average sea levels, here monthly averages and individual measurements is plotted.

B.1 Monthly sea level anomalies

Figure B.1 illustrates the monthly sea level estimated by tide gauge (TG), GNSS Interferometric Reflectometry (GNSS-IR) and altimetry. The data used is the same as for figure 3 in the paper. The only difference is that averages are taken over a month in stead of a year. The gravimetry is not shown here since the data used to estimate this is annual. There are considerable differences between TG and GNSS-IR results but no clear seasonal pattern.

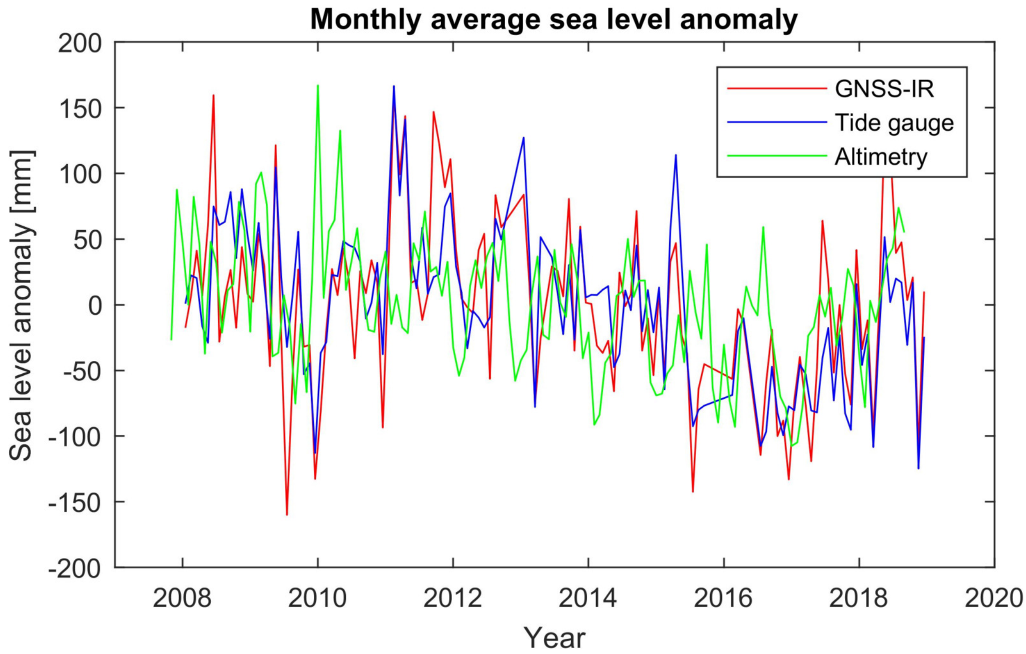

Figure B.1: Monthly sea level from GNSS-IR, tide gauge and altimetry

B.2 Individual sea level measurements

Figure B.2 compares individual measurements of sea level by GNSS-IR and TG before filtering tides and annual and biannual variations. Note that the figure compares variations not absolute values (mean has been subtracted from both time series). There is a tendency that GNSS-IR is higher than TG during late winter and spring and lower during summer. This is an expected result of sea ice in the fjord. The RMSE between the two calculated over all of 2018 is 20 cm which is higher than the RMSE for August of 13 cm used the estimate errors in the paper, but not high enough to explain the differences in the annual sea level measurements.

Figures B.3 to B.14 show the monthly comparisons of individual measurements of sea level by GNSS-IR and TG before filtering tides and annual and biannual variations. A for

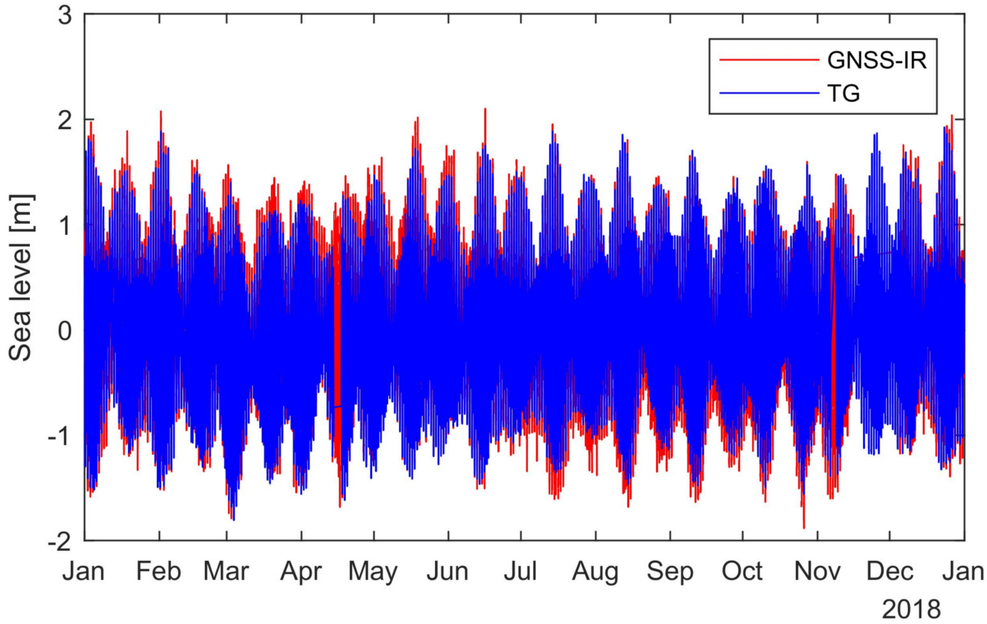

Figure B.2: Comparison of individual sea level measurements by tide gauge and GNSS-IR for 2018

S2 the figures compare variations not absolute values.

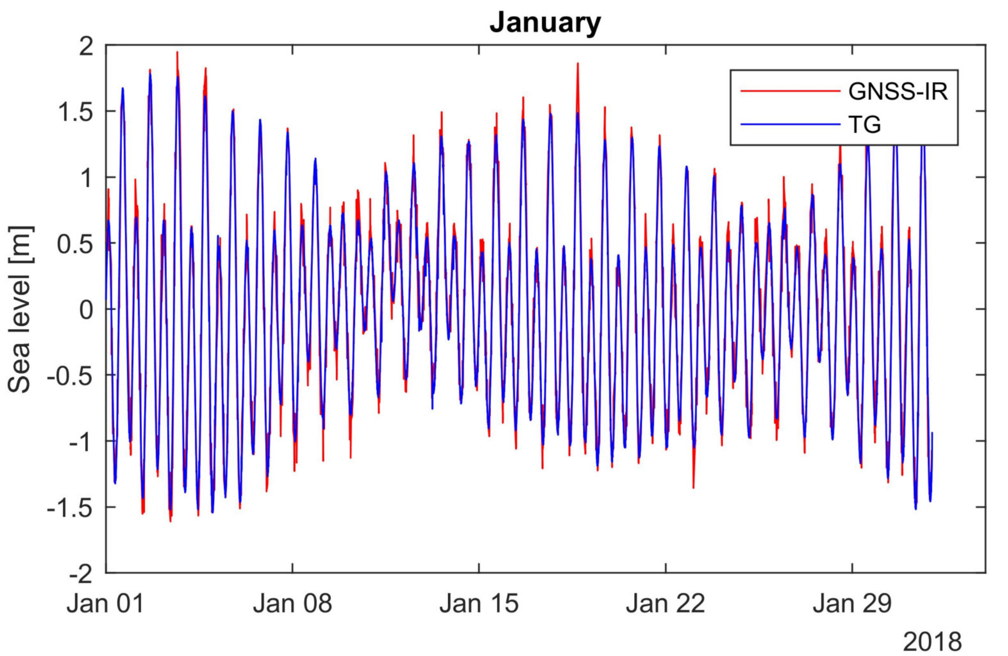

Figure B.3: Comparison of individual sea level measurements by tide gauge and GNSS-IR for Janunary 2018

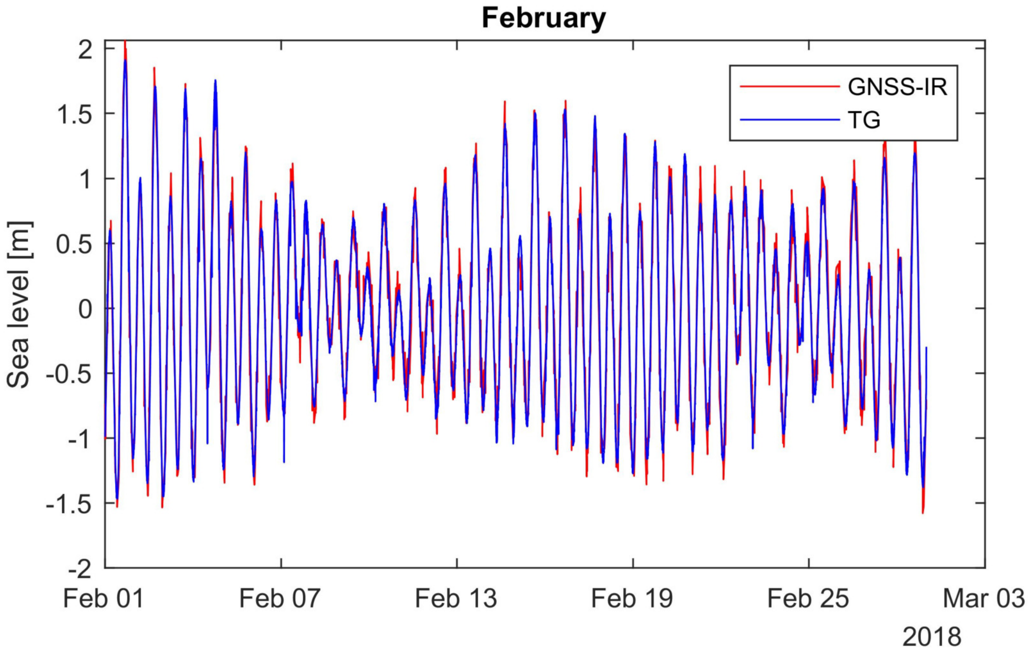

Figure B.4: Comparison of individual sea level measurements by tide gauge and GNSS-IR for February 2018

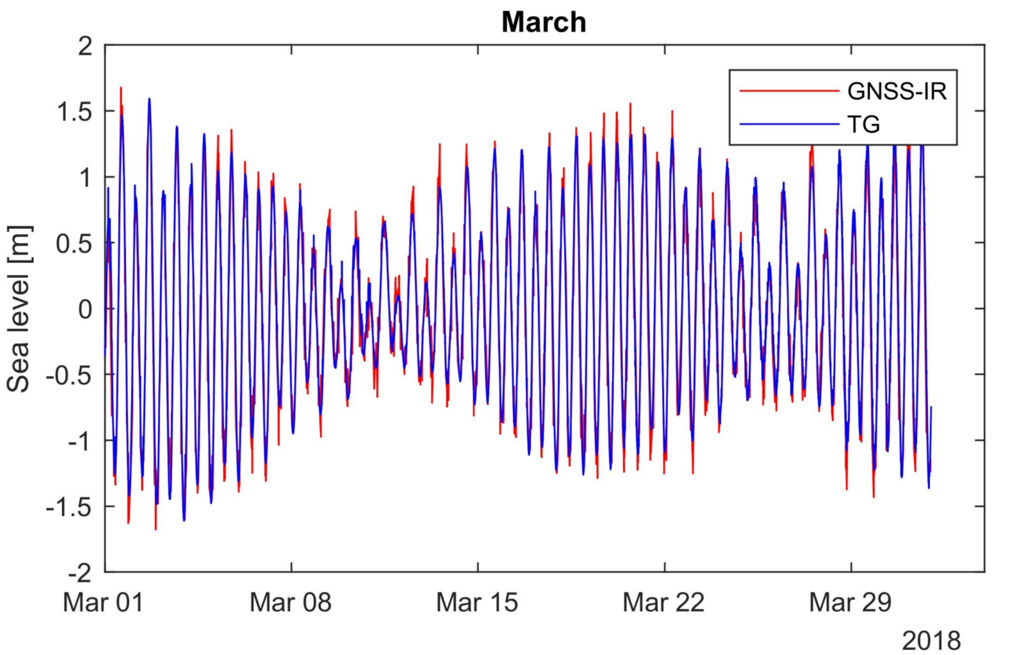

Figure B.5: Comparison of individual sea level measurements by tide gauge and GNSS-IR for March 2018

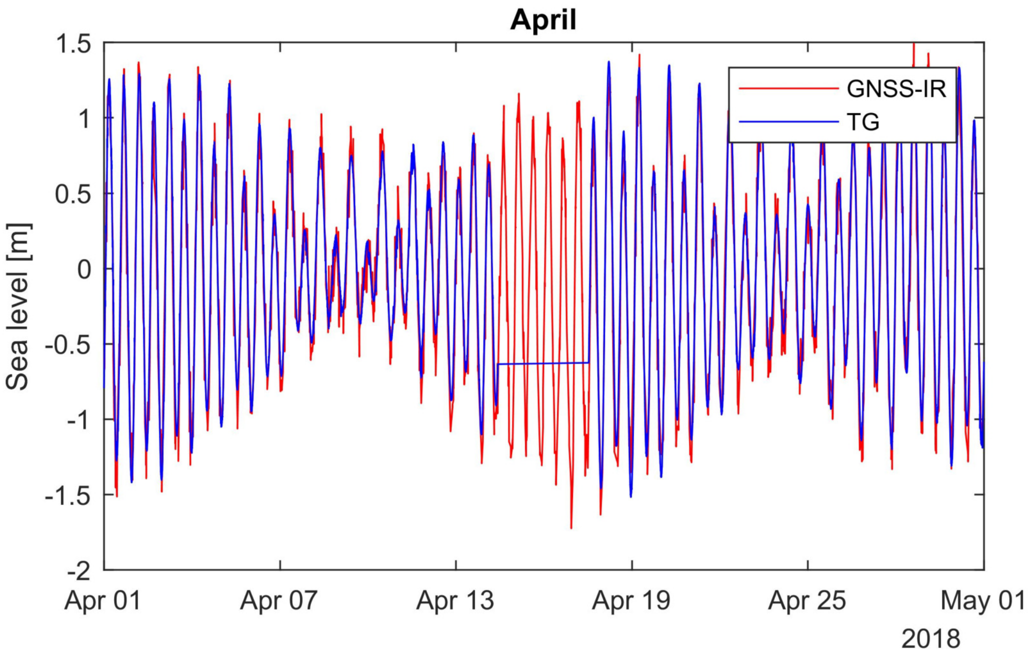

Figure B.6: Comparison of individual sea level measurements by tide gauge and GNSS-IR for April 2018

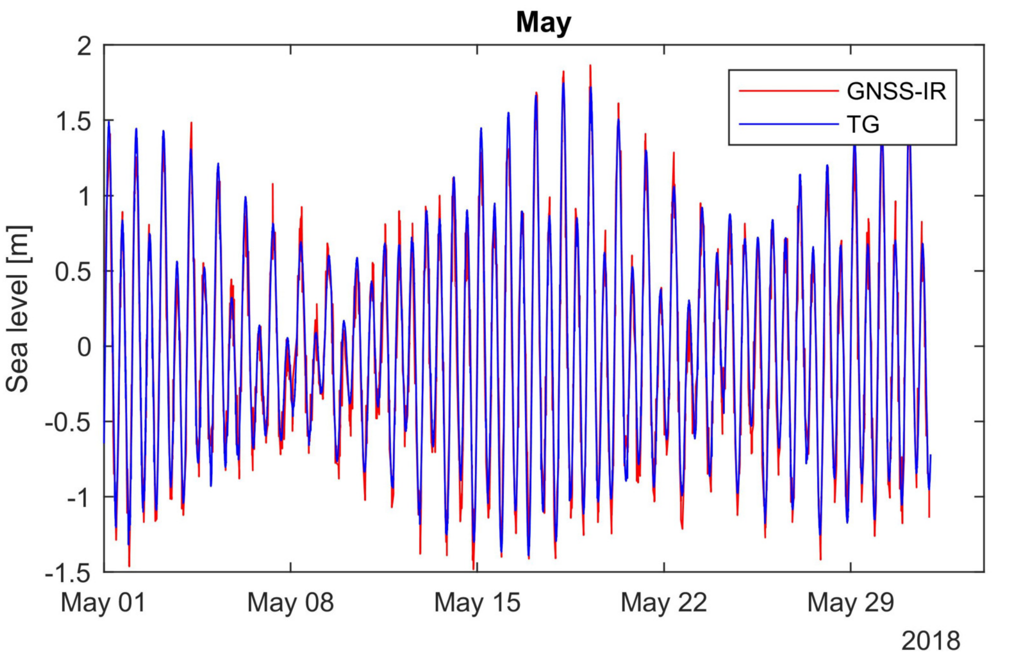

Figure B.7: Comparison of individual sea level measurements by tide gauge and GNSS-IR for May 2018

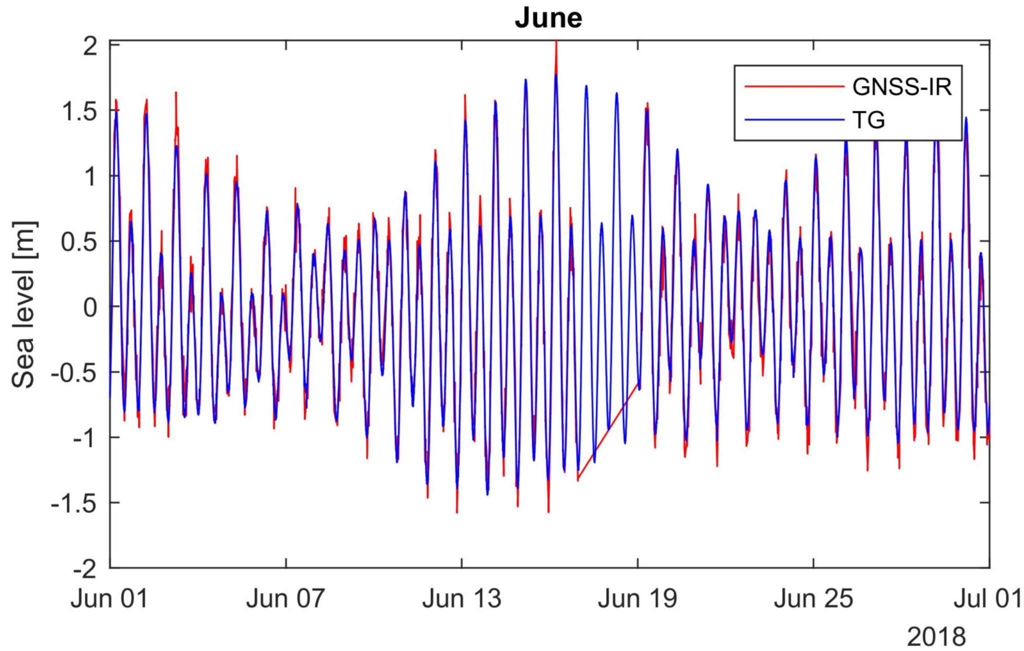

Figure B.8: Comparison of individual sea level measurements by tide gauge and GNSS-IR for June 2018

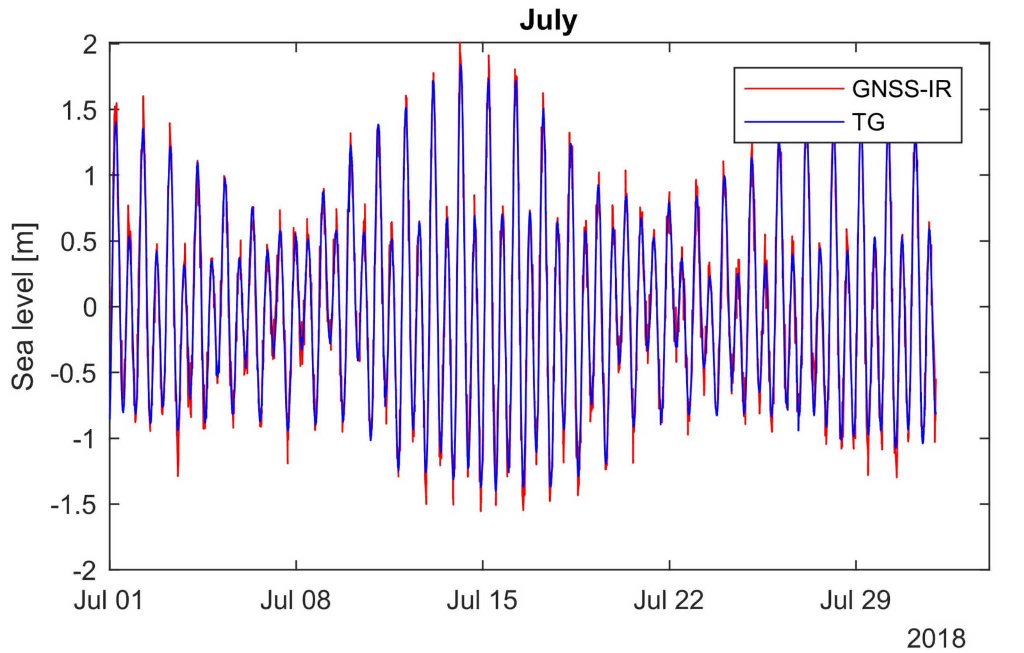

Figure B.9: Comparison of individual sea level measurements by tide gauge and GNSS-IR for July 2018

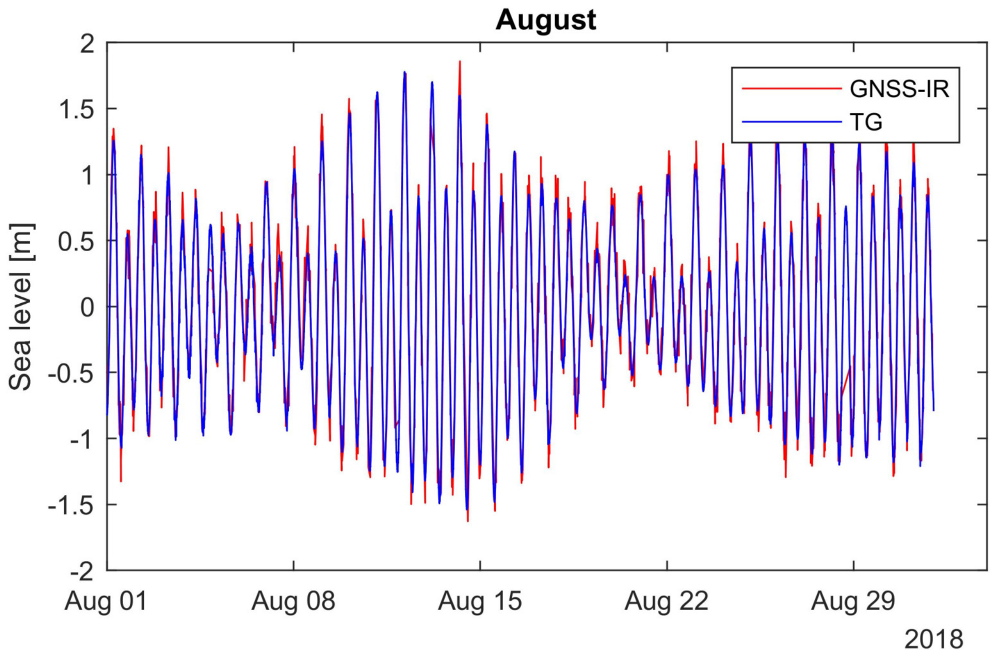

Figure B.10: Comparison of individual sea level measurements by tide gauge and GNSS-IR for August 2018

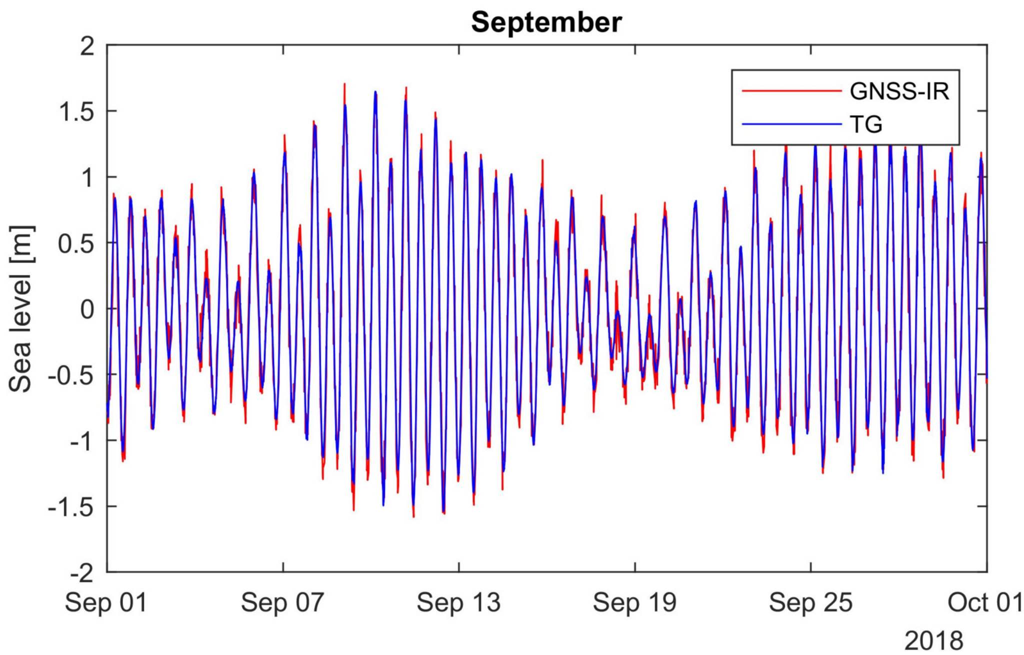

Figure B.11: Comparison of individual sea level measurements by tide gauge and GNSS-IR for September 2018

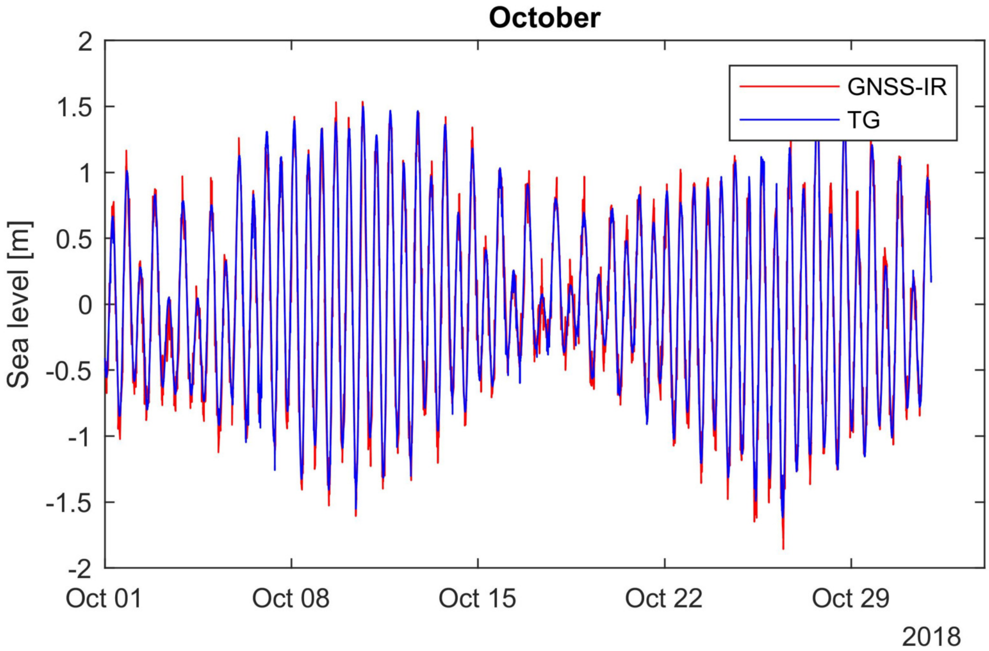

Figure B.12: Comparison of individual sea level measurements by tide gauge and GNSS-IR for October 2018

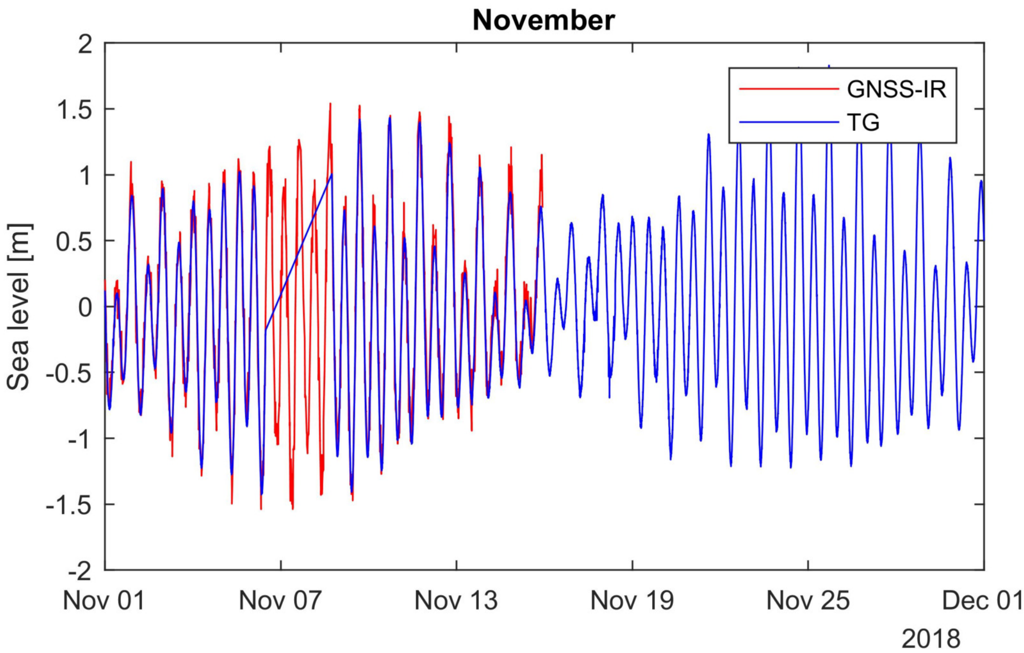

Figure B.13: Comparison of individual sea level measurements by tide gauge and GNSS-IR for November 2018

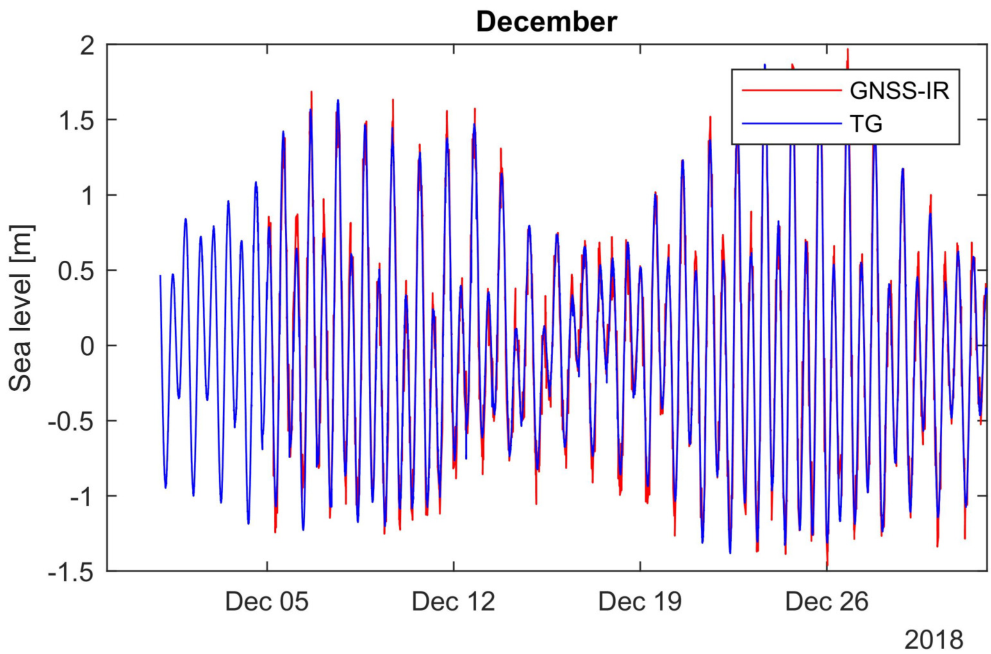

Figure B.14: Comparison of individual sea level measurements by tide gauge and GNSS-IR for December 2018

B.3 Uplift at THU2

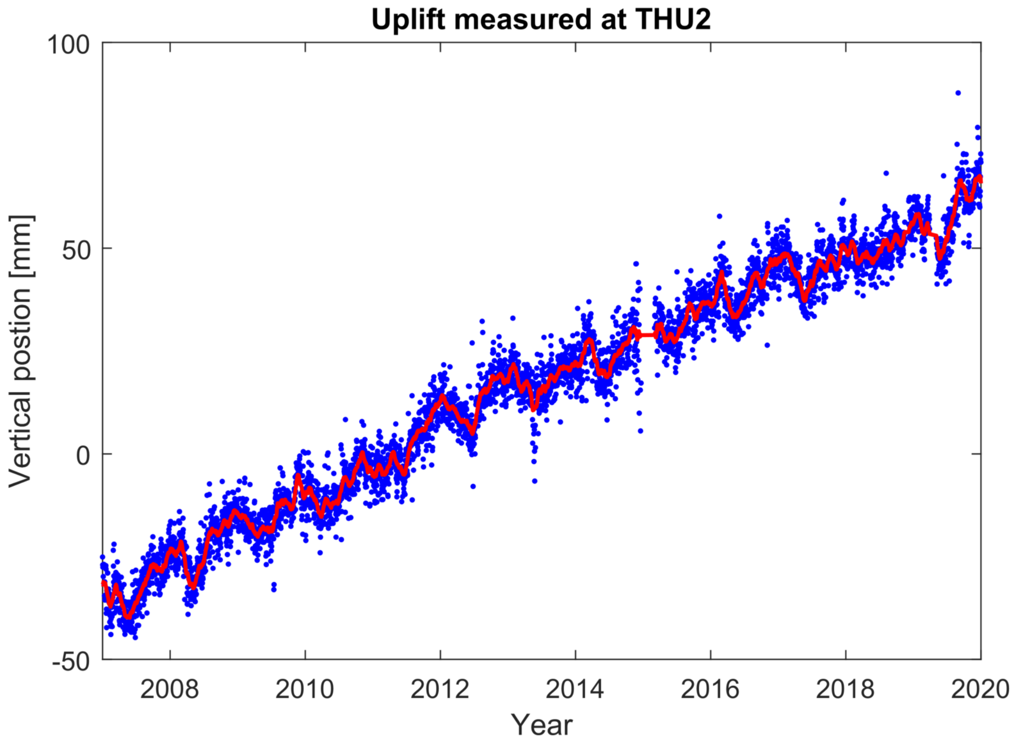

Figure B.15: Variations in measured vertical position at THU2 during the study period. Blue dots are daily values and the red line is a 30 day running average of the daily values.

B.4 Fresnelzones

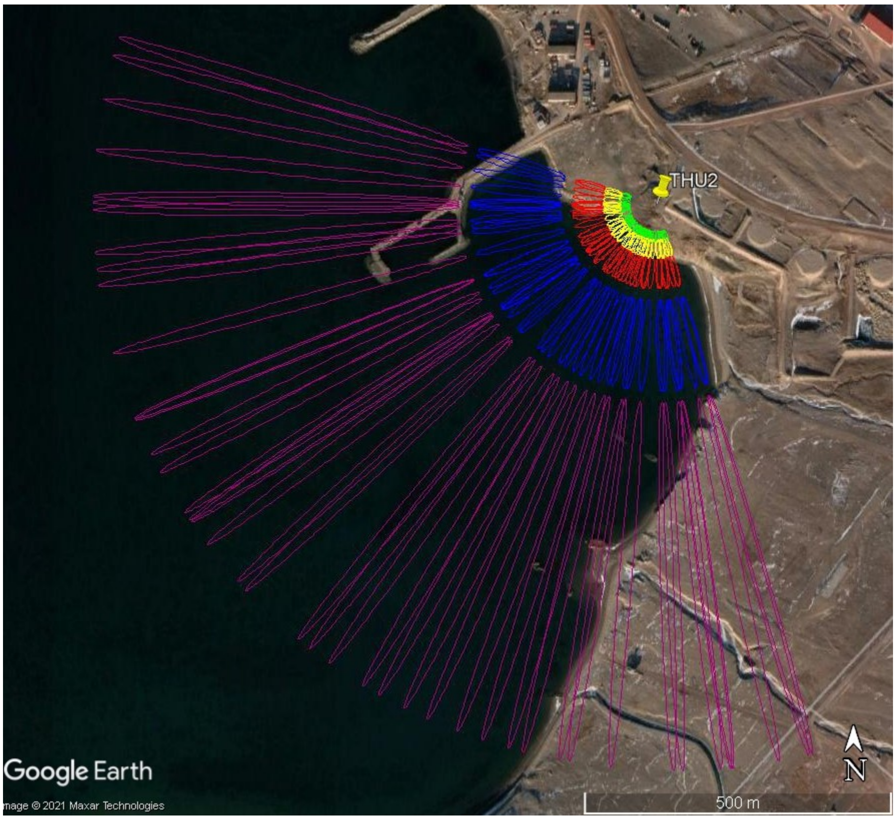

Figure B.16: Fresnel-zones for azimuth 160-290 for elevation angles: 2, 5, 10, 15, 20.

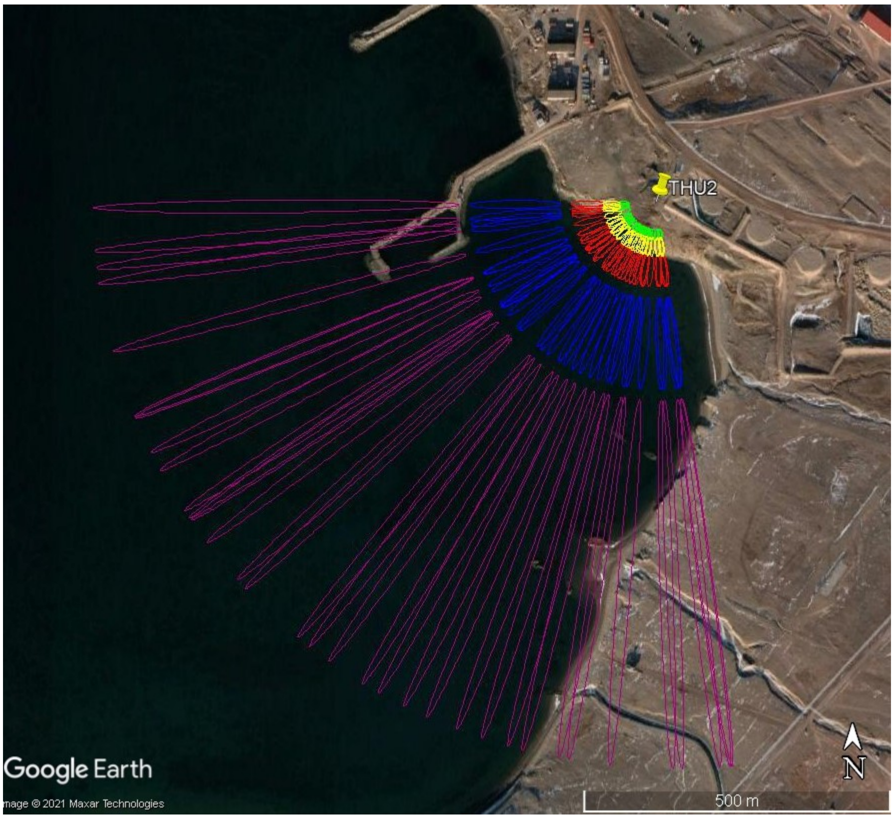

Figure B.17: Fresnel-zones for azimuth 170-270 for elevation angles: 2, 5, 10, 15, 20.

C Paper 2

remote sensing MDPI

Technical Note

Snow Depth Measurements by GNSS-IR at an Automatic Weather Station, NUK-K

Trine S. Dahl-Jensen [1,*], Michele Citterio [2], Jakob Jakobsen [2], Andreas P. Ahlstrøm [2], Kristine M. Larson [3] and Shfaqat A. Khan [1]

1 Danish National Space Centre, Technical University of Denmark, 2800 Lyngby, Denmark; abbas@space.dtu.dk
2 Department of Glaciology and Climate, The Geological Survey of Denmark and Greenland, GEUS, 1350 Copenhagen, Denmark; mcit@geus.dk (M.C.); jj@geus.dk (J.J.); apa@geus.dk (A.P.A.)
3 Institute of Geodesy and Geoinformation, University of Bonn, 53115 Bonn, Germany; klarson@uni-bonn.de
* Correspondence: trdhj@space.dtu.dk

Abstract: Studies have shown that geodetic Global Navigation Satellite System (GNSS) stations can be used to measure snow depths using GNSS interferometric reflectometry (GNSS-IR). Here, we study the results from a customized GNSS setup installed in March through August 2020 at the Programme for Monitoring of the Greenland Ice Sheet (PROMICE) automatic weather station NUK-K located on a small glacier outside Nuuk, Greenland. The setup is not optimized for reflectometry purposes. The site is obstructed between 85 and 215 degrees, and as the power supply is limited due to the remote location, the logging time is limited to 3 h per day. We estimate reflector heights using GNSS-IR and compare the results to a sonic ranger also placed on the weather station. We find that the snow melt measured by GNSS-IR is comparable to the melt measured by the sonic ranger. We expect that a period of up to 45 cm difference between the two is likely related to the much larger footprint GNSS-IR and the topography of the area. The uncertainty on the GNSS-IR reflector heights increase from approximately 2 cm for a snow surface to approximately 5 cm for an ice surface. If reflector height during snow free periods are part of the objective of a similar setup, we suggest increasing the logging time to reduce the uncertainty on the daily estimates.

Keywords: automatic weather stations; GNSS-IR; reflectometry; snow depth; Greenland

Citation: Dahl-Jensen, T.S.; Citterio, M.; Jakobsen, J.; Ahlstrøm, A.P.; Larson, K.M.; Khan, S.A. Snow Depth Measurements by GNSS-IR at an Automatic Weather Station, NUK-K. *Remote Sens.* **2022**, *14*, 2563. https://doi.org/10.3390/rs14112563

Academic Editors: Dariusz Ignatiuk and Shridhar Jawak

Received: 7 April 2022
Accepted: 23 May 2022
Published: 27 May 2022

1. Introduction

The Greenland ice sheet has recently become the largest individual ice mass contributor to global eustatic sea level rise [1]. In recent years, the Surface Mass Balance (SMB) has come to dominate the mass loss from the Greenland ice sheet and, consequently, its contribution to global sea level rise [2,3]. In situ observations of snow depth are important for constraining or verifying models of surface mass balance and improving SMB estimates [4–6].

In the last decade, Global Navigation Satellite System Interferometric Reflectometry (GNSS-IR) has been introduced as a method to estimate snow depth using existing geodetic GNSS stations (e.g., [7–9]). The method is highly suitable for remote regions, as the stations are simple to run and often deployed for other purposes. The footprint of the daily snow depth estimates depend on the height of the antenna above the surface and is typically on the order 1000–10,000 m^2 (e.g., [10,11]). In comparison, sonic rangers, traditionally installed for in situ measurements of snow depth, have a footprint of just around 1 m^2. The result is a measurement which is very sensitive to local snow conditions [12]. Furthermore, it has a delicate membrane that degrades over time due to the thaw-freeze cycles and needs to be replaced regularly, preferably each year [13]. In remote locations such as the Greenland ice sheet, yearly visits are expensive and time consuming, and compared to sonic rangers, a GNSS station requires little maintenance. Another advantage of using GNSS-IR to measure snow depth is that the position of the antenna can be determined with a high precision using GNSS positioning, and thus, the snow surface elevation can be determined in a geocentric reference frame. This snow surface estimate can be useful as reference points for altimetry products.

The Programme for Monitoring of the Greenland Ice Sheet (PROMICE) runs 27 automatic weather stations in Greenland. Most of these are located in the ablation zone of the Greenland ice sheet. The weather stations measure multiple meteorological parameters as well as snow depth (using sonic rangers) and ablation [14]. In order to locate the weather stations on flowing glaciers, they are currently equipped with a simple GPS, logging and transmitting only the position and time.

In an effort to measure precise ice flow velocities, a dual-frequency carrier phase GNSS station was installed at NUK-K to test if a suitable setup could be made at the weather stations. Even though this experiment was sub-optimally designed for GNSS reflections, we will use this dataset to compute snow accumulation and compare the results with data collected with a sonic ranger.

2. Materials and Methods

2.1. Automatic Weather Station

On 6 March 2020, a GNSS station was installed at the PROMICE weather station NUK-K, situated on a small local glacier outside Nuuk, Greenland (Figure 1). The setup consists of a Novatel pinwheel 704 antenna and a Septentrio AsteRx-m receiver. The GNSS station was equipped with its own power supply consisting of a 2 watt solar panel and a small internal battery. The glacier is approximately 1100 m (north–south) by 600 m (east–west). The purpose was to test the setup for high precision positioning with the goal of installing a similar setup on other PROMICE weather stations to measure ice velocities. As it was a test setup, it was removed when the data were collected on August 31st of the same year. The GNSS station tracks GPS, Galileo and Glonass signals at 5 s intervals. Due to the remote location of the weather station, the power supply is very limited, and therefore, the GNSS data logging is limited to three hours each day. The GNSS antenna is placed at the top of the central mast of the weather station with the antenna phase center approximately 2.95 m above the ice surface (Figure 2).

Figure 1. Map of the area including Nuuk and the weather station. The red triangle marks the position of the weather station (NUK-K). Map data ©2015 Google.

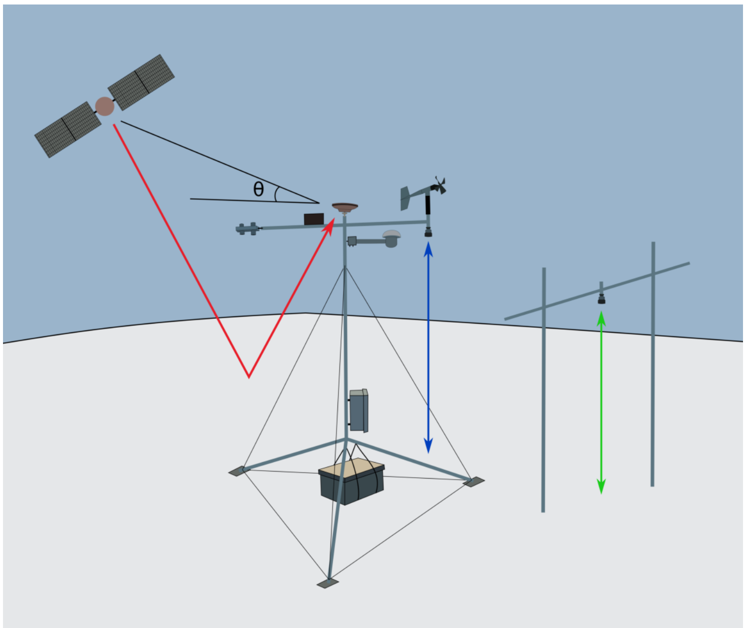

Figure 2. Illustration of PROMICE weather station NUK-K. The red arrow illustrates reflected signal used for Global Navigation Satellite System Interferometric Reflectometry (GNSS-IR) reflector heights. The blue arrow illustrates reflector height measured by the sonic ranger on the boom. The green arrow illustrates the distance to the snow surface as measured by the sonic ranger on stakes.

The weather station, NUK-K, has been running since July 2014 and continuously measures a number of climate variables such as radiation (in and out), temperature, pressure, wind speed and direction, humidity and snow height [14,15]. Currently, snow height is measured using sonic rangers. A sonic ranger measures the distance to the surface by transmitting a ultrasonic pulse and measuring the time it takes for the pulse to return. The pulse is sent out in a cone of 22 degrees resulting in a footprint of less than one m^2 for a distance up to 2.6 m [12]. The station is equipped with two sonic rangers. One is placed on the sensor boom (blue arrow on Figure 2) and located approximately 2.6 m above the ice surface. As the station is standing on the ice, it will follow any ice melt, and therefore, the sonic ranger on the boom is unable to measure ice melt. The other sonic ranger is installed on stakes drilled into the ice and, thus, also measures the ice melt (green arrow in Figure 2).

Albedo estimates are used to confirm the transition from a snow surface to an ice surface. They are distributed with the data from the weather station and based on measured incoming and outgoing shortwave radiation, as described in Fausto et al. [14].

2.2. GNSS-IR

It has long been known that reflected signals cause error in GNSS positioning because the modeled direct signal path is different than the observed reflected signal path. The impact of reflected signals on Signal to Noise Ratio (SNR) data is less appreciated because SNR data are rarely used in positioning applications. The direct GNSS signal observed in SNR data smoothly increases as a satellite rises and then smoothly decreases as the satellite sets. Without the multipath effect, this effect can be modeled as a low-order polynomial. When a GNSS site is impacted by reflected signals, the observed SNR data include the direct signal and the interference between the direct signal and the reflected signal. In the GNSS-IR method, the direct signal is removed by fitting a low-order polynomial to SNR data for either the rising or setting satellite arc. What remains in the satellite arc is only the interferometric data. For convenience, in the figures, we call this SNR data, but it should be understood that this is the interferometric effect retrieved from the SNR data. If the contribution from the direct signal is removed, the SNR can be modeled as a function of the satellite elevation angle, θ (e.g., [16–18]):

$$\mathrm{SNR}(\theta) = A(\theta)sin\left(\frac{4\pi H_R}{\lambda}sin(\theta) + \phi\right) \quad (1)$$

where A is the amplitude, which depends on the transmitted GNSS signal power, the elevation angle, the antenna gain pattern and the dielectric constant and roughness of the reflecting surface, H_R is the reflector height, λ is the wavelength of the transmitted signal and ϕ is a phase constant. Changing the variable from elevation angle to the sine of the elevation angle, the SNR has a constant frequency of:

$$f = \frac{2H_R}{\lambda} \quad (2)$$

thus, the reflector height can be determined from the dominant frequency in the SNR data. In order to be able to estimate the reflector height, it has to be at least two times the wavelength, which, depending on the GNSS signal, corresponds to between 0.4 and 0.5 m.

The footprint of GNSS-IR estimates of snow depth is determined by the first Fresnel zones and depends on the elevation angle of the satellite and the height of the reflector [19]. For elevation angles down to 5 degrees, as used here, the daily reflector heights are sensitive to snow height in an area between approximately 4000 m^2 (for a reflector height of 0.5 m) and 20,000 m^2 (for a reflector height of 3 m). However, at NUK-K a hill on the south-eastern side of the weather station is blocking the view at low elevation angles, and thus, we have no reflector height extractions between 85 and 215 degrees and the area of sensitivity is reduced to between approximately 2500 m^2 and 13,000 m^2 (see Figure 3).

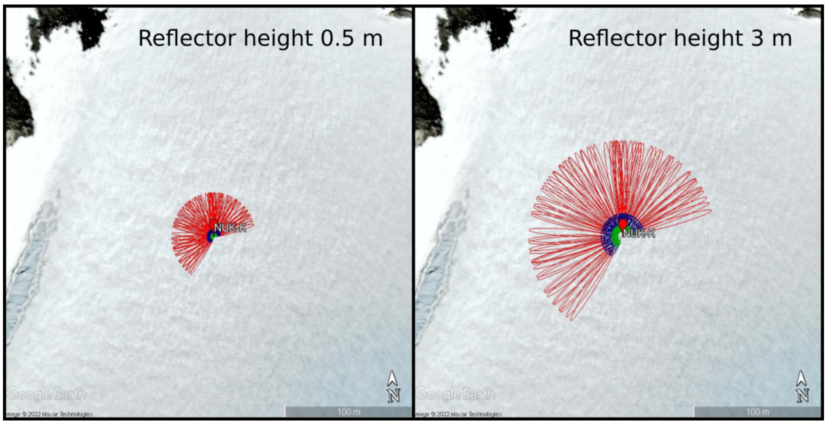

Figure 3. Reflection zones at NUK-K for a reflector height of 0.5 and 3 m at three satellite elevation angles. Red: 5 degree elevation, blue: 15 degree elevation and green: 25 degree elevation.

The software used to estimate reflector heights from the GNSS data is available on GitHub [20] and the method described in Roesler and Larson [21]. First, SNR data are extracted from the Rinex files. The direct signal is removed by fitting and subtracting a fourth-order polynomial. The reflector height is then estimated from each satellite track and frequency using a Lomb-Scargle periodogram [22]. For each estimate, a set of requirements are set in order to accept the estimated reflector height and include it in the daily estimates: the track has to cover the elevation angles from 10 to 20 degrees, the peak to noise ratio over estimated heights between 0.5 and 5 m has to be 3 or higher and the peak amplitude has to be at least 5. There is one exception from these general Quality Control (QC) parameters, namely the minimum peak amplitude for GPS L2C, which is set to 2 since the signal is considerably weaker than for the other frequencies. These QC parameters were determined from inspection of periodograms for a number of days evenly spread over the measuring period and at all tracked frequencies. We find useful reflections from GPS L1 and L2C, Glonass L1 and L2 and Galileo E1, E5a and E5b. Unfortunately, GPS L5 was not tracked at this station.

After estimating the reflector heights from the satellite tracks, daily solutions are obtained from the average of the accepted tracks.

3. Results

Figure 4a shows the distance to the snow surface measured by GNSS-IR and the sonic ranger on the sensor boom. There is a period of missing data from day 154 to 183 due to issues with the power supply limiting the logging to a degree where it was not possible to extract reflector heights. The uncertainty for the daily GNSS-IR reflector heights are estimated as the standard deviation of mean and has an average of 3 cm. There is also a sonic ranger on stakes next to the weather station. However, it did not function during most of the measurement time for the GNSS station, and as it also measures the ice melt, and is, therefore, not directly comparable to the GNSS-IR reflector height, it was not included in the plot.

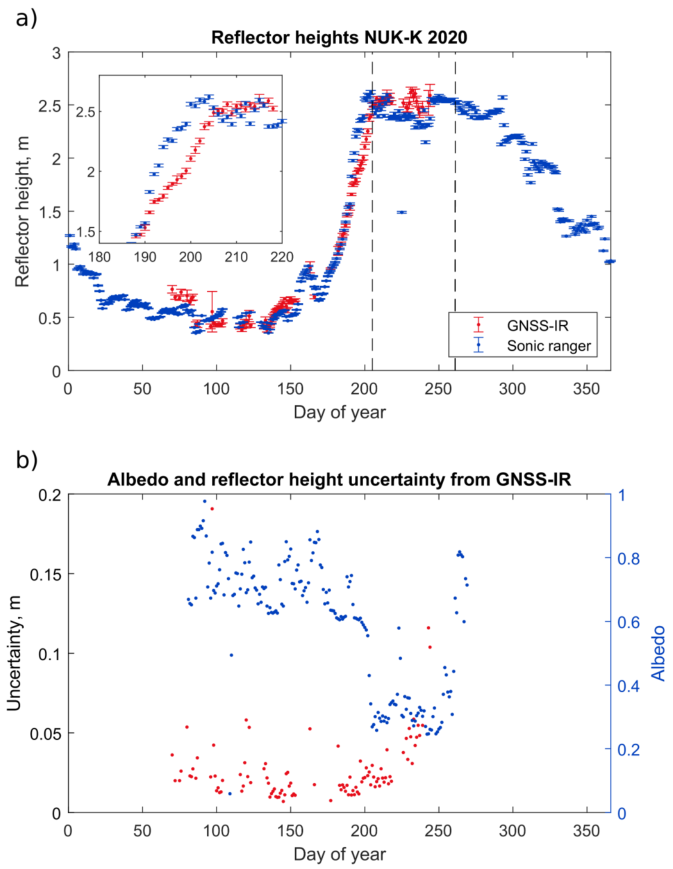

Figure 4. (**a**) Daily average reflector heights measured by GNSS-IR and the sonic ranger on the boom. The GNSS-IR reflector height has been corrected for a bias as compared to the sonic ranger. The bars are the uncertainty estimated as the daily standard deviation of mean. The dashed lines indicate when the snow cover is effectively lost in the summer and when the first snow returns in the autumn as indicated by the albedo. (**b**) Albedo estimated from in- and outgoing shortwave radiation together with the uncertainty on the estimated daily reflector heights from GNSS-IR.

Before comparison, we correct the GNSS-IR data for a bias of 26.5 cm to align the two data series as the GNSS antenna and the sonic ranger is not located at the same height above surface and the GNSS setup measures snow height over a much larger area. The GNSS-IR reflector height clearly captures the snow melt as measured by the sonic ranger. However, in some periods there are significant differences between the two, most clearly from day 190 to 210, where the sonic ranger shows faster melt than the GNSS station, reaching a difference between the two reflector heights of 45 cm on day 200. The linear correlation between the results from the sonic ranger and the GNSS station is 0.98 and the RMSD is 17 cm.

The estimated uncertainty on the daily GNSS-IR reflector heights vary over the measurement period. It is generally small (average of 2 cm) during most of the melt period and increasing towards the end of the data series (average of 5 cm). Figure 5 shows the periodograms for all tracked signals from day 140, where the uncertainty is low, and day 229, where it is high. The two days are chosen as they are representative of the two states of the measurement. On both days there are multiple successful extractions (red curves). However, while the peaks of all accepted tracks are close together on day 140, there is considerable noise on day 229.

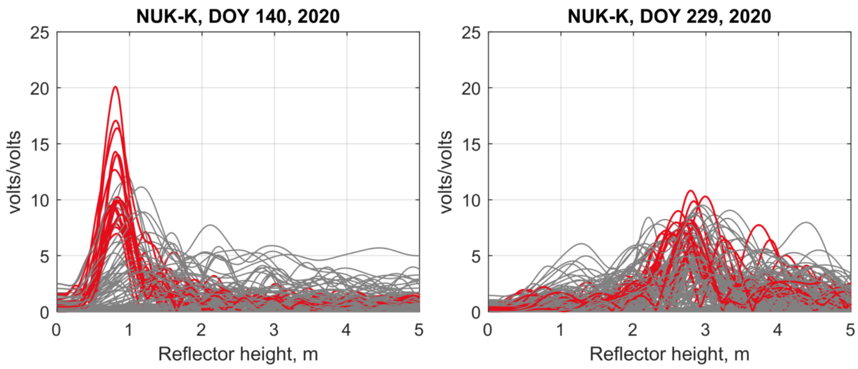

Figure 5. Periodograms from the GNSS-IR extractions of all tracked frequencies on day 140 (**left**) and 229 (**right**). The grey lines are satellite tracks that are discarded in the QC process and the red lines are tracks that are accepted.

We expect that the reason for the increased noise in the periodograms and resulting uncertainty is a change in the reflecting surface. When the snow melts, the smooth snow surface is exchanged for a potentially much rougher ice surface, which is not as good a reflector. Figure 4b shows the estimated albedo together with the uncertainty on the daily reflector heights from GNSS-IR. Around the time where the albedo drop to ice levels, the uncertainty starts to increase and continues to do so. Thus, changes in surface properties and in particularly smoothness after the snow has melted is a likely reason for the increased uncertainty.

4. Discussion

The reflector height from the GNSS-IR shows a snow melt similar to what is measured by the sonic ranger on the weather station. However, the RMSE is considerably larger than the estimated uncertainty on the measurements. The difference between the two measurements is not evenly distributed over the year; while it is small in the first part of the melt season, it is large towards the second half of the melt season (approximately day 190–210), reaching up to 0.5 m. As the glacier is not completely horizontal, a possible reason for this change could be that the azimuths of the accepted reflections changed, resulting in a different area of sensitivity and a different reflector height. However, comparing the number of accepted tracks in three azimuth quadrants over the measurement period, no clear change is seen around this time (Figure 6). The quadrant from 90 to 180 degrees is not included in the figure, as it is completely obstructed by the hill, and thus, there are no extractions. We also observe larger differences between the GNSS-IR and sonic ranger results from before the melt season. In this case, there is a difference in the azimuths compared to later with a significantly larger part of the measurements coming from the 180–270 degree bin. This can be explained by that part of the glacier being uphill from the station resulting in lower reflector heights.

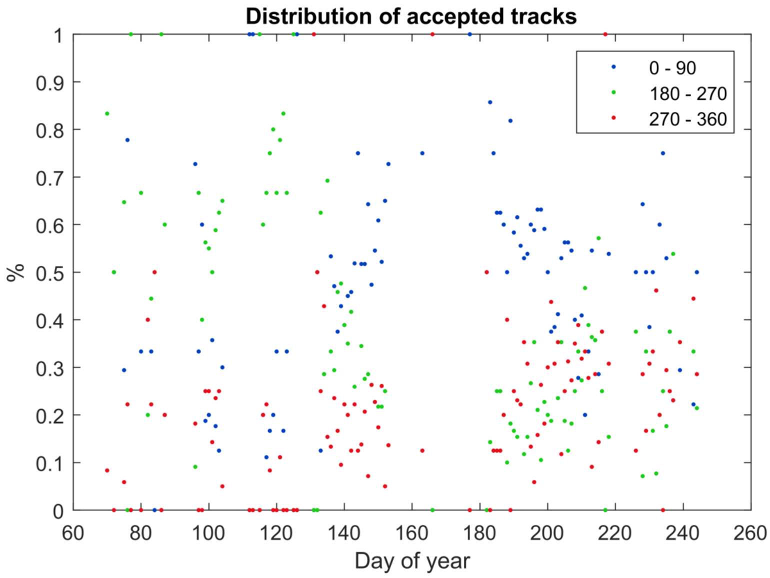

Figure 6. Azimuthal distribution of accepted satellite tracks for GNSS-IR.

Larson and Nievinski [11] ran simulations of the error resulting from slopes up to 8 degrees for a reflector height between 1 and 2 m and found that the error as a result of the slope was within 10 cm. Thus, though slope in some parts of the sensing area may be just slightly larger than 8 degrees, the slope in itself cannot explain the large differences from day 190 to 210.

The snow density also affects the reflections. However, Gutmann et al. [23] modeled the effect of snow density, and though it has significant influence on the amplitude of the SNR oscillations, it did not affect the frequency (and thereby reflector height) significantly.

Larson et al. [10] calculated reflector height at the old radar station DYE-2 and compared the result with in situ measurements of snow accumulation. They found a standard deviation of difference between 9.4 and 9.5 cm, which is about half of what we find here. However, there are several reasons we should not expect results at NUK-K to be equally good. DYE-2 is located at the interior of the ice sheet with no obstructions and logging every 15 s all day. In comparison, the GNSS station at NUK-K is logging 3 h a day at best (often less due to lack of power) and is obstructed over an angle of 130 degrees, corresponding to a data loss of 36%. Furthermore, the topography of the area likely results in an uneven snow distribution, and since the GNSS-IR and sonic ranger have different areas of sensitivity, a considerable part of the difference may also be an actual difference in the surface height changes at the point right below the sonic ranger and over the area covered by the GNSS-IR measurement.

The increased uncertainty after the snow has melted is not an issue as long as the goal is measuring changes in snow depths. Since the GNSS-IR is mounted on the weather station, GNSS-IR reflector heights will not directly capture any melt of the ice after the snow is gone. However, the ice melt could be estimated from the change in the vertical position of the GNSS antenna and the surface could be estimated in a geocentric reference frame by combining position and reflector height (e.g., [9,10]). In this case, one should take into account that the uncertainty of the measurement might increase significantly for an ice surface. This ability to measure ice melt and absolute surface heights is an advantage compared to the sonic rangers. A second sonic ranger on stakes is needed in order to measure ice melt, and this setup is relatively unstable, as it needs regular re-drilling in order to keep it from melting out or collapsing [13].

If more GNSS stations are installed at PROMICE stations in the future, the power consumption could be decreased by setting the logging rate to once each 30 s. This would decrease both the power consumption of the GNSS station and the needed disk space while being safely within the pseudo-Nyquist limit for the antenna height of this setup [21]. If it is possible to increase the logging time by decreasing the sampling rate, this would be highly beneficial, as it would increase the number of daily extractions and, thereby, decrease uncertainty. This is particularly important if there is interest in the absolute height of the ice surface, as we have seen that the uncertainty of the measurement increases significantly after the transition from a snow to an ice surface. Currently, this setup is not stable enough to replace the sonic rangers on the PROMICE weather stations as the power issues result in some gaps in the data set (e.g., day 154 to 183). Furthermore, as these weather stations are already visited regularly for other forms of maintenance, the membranes can be exchanged without additional travel cost. However, it is valuable as it estimates the melt over a larger area of the glacier and adds the possibility of measuring ice melt and the position of the ice surface in a geocentric reference frame.

In studies where high precision positioning is not needed, an option could be to install a simple GPS for GPS-IR. Williams et al. [18] installed a consumer-type GPS unit for measurements of sea level from reflectometry. They found that reflectometry results were at least as good as for a geodetic station, though positioning accuracy is a couple of orders of magnitude worse than a geodetic station.

It should be noted that the method may not be suitable at all PROMICE locations, as the surface may be too rough and fractured or there may be too much topography or obstruction by mountains.

5. Conclusions

A dual-frequency carrier phase GNSS unit was installed to measure velocity changes at the NUK-K site from early March to end of August 2020. The deployment was poorly designed for GNSS reflections because of local obstructions and the need to restrict tracking to three hours to save power. These restrictions resulted in only 1/20 of a typical polar deployment dataset being available. This degraded the results compared to previous studies (e.g., [5,10]). Even so, we were able to successfully extract snow accumulation from the three constellations being tracked which compared reasonably well with a sensor that is nearby but not in a coincident footprint.

We find that the uncertainty on the measurement is low when the surface is snow covered, while it increases when the snow has melted, leaving a rougher ice surface. We compare the results to data from a sonic ranger on the instrument boom. We find that the two measurements generally capture similar snow melt, but that in the second half of the melt season, the total snow melt as measured by the sonic ranger is higher than measured by GNSS-IR. We expect that this is because the footprint of GNSS-IR ($\sim$10,000 m^2) is much larger than for the sonic ranger ($\sim$1 m^2), thus capturing snow melt over a larger area.

If a similar setup is made with the purpose of doing both positioning and reflectometry, several changes to this setup could be made to improve it for GNSS-IR:

- A measurement frequency of 5 s is much higher than needed. A 30 s sampling would be sufficient.
- The reflectometry is severely obstructed by the landscape. If possible, this should be considered when placing the station.
- GPS L5 was not tracked here. It is more suited for reflectometry than L1 and should be tracked if possible.

Author Contributions: Methodology, T.S.D.-J.; Formal analysis, T.S.D.-J.; Hardware and Fieldwork: M.C.; Software, K.M.L.; Resources, J.J., A.P.A. and M.C.; Writing—original draft preparation, T.S.D.-J.; Writing—review and editing, All; Visualization, T.S.D.-J.; Supervision, S.A.K. and K.M.L. All authors have read and agreed to the published version of the manuscript.

Funding: Design and construction of the GNSS receiver was supported by the EU Horizon 2020 Integrated Arctic Observation System (INSTAROS) Project GA No. 727890. Field deployment and the AWS were supported by the Danish Energy Agency through the Programme for the Monitoring of the Greenland Ice Sheet (PROMICE) and the Greenland Ecosystem Monitoring (GEM) GlacioBasis Programme. The field visits were carried out in coordination with Asiaq Greenland Survey.

Data Availability Statement: Weather station data from NUK-K can be downloaded from the PROMICE database [15]. The GNSS data from NUK-K are available upon request.

Conflicts of Interest: The authors declare no conflict of interest.

References

1. Oppenheimer, M.; Glavovic, B.; Hinkel, J.; van de Wal, R.; Magnan, A.; Abd-Elgawad, A.; Cai, R.; Cifuentes-Jara, M.; DeConto, R.; Ghosh, T.; et al. Sea level rise and implications for low-lying islands, coasts and communities. In *IPCC Special Report on the Oceans and Cryosphere in a Changing Climate*; Pörtner, H.-O., Roberts, D.C., Masson-Delmotte, V., Zhai, P., Tignor, M., Poloczanska, E., Mintenbeck, K., Alegría, A., Nicolai, M., Okem, A., et al., Eds.; Cambridge University Press: Cambridge, UK; New York, NY, USA, 2019; pp. 321–445. [CrossRef]
2. Mouginot, J.; Rignot, E.; Bjork, A.A.; van den Broeke, M.; Millan, R.; Morlighem, M.; Noel, B.; Scheuchl, B.; Wood, M. Forty-six years of Greenland Ice Sheet mass balance from 1972 to 2018. *Proc. Natl. Acad. Sci. USA* **2019**, *116*, 9239–9244. [CrossRef] [PubMed]
3. The IMBIE Team. Mass balance of the Greenland Ice Sheet from 1992 to 2018. *Nature* **2020**, *579*, 233–239. [CrossRef] [PubMed]
4. Marzeion, B.; Jarosch, A.H.; Hofer, M. Past and future sea-level change from the surface mass balance of glaciers. *Cryosphere* **2012**, *6*, 1295–1322. [CrossRef]
5. Siegfried, M.R.; Medley, B.; Larson, K.M.; Fricker, H.A.; Tulaczyk, S. Snow accumulation variability on a West Antarctic ice stream observed with GPS reflectometry, 2007–2017. *Geophys. Res. Lett.* **2017**, *44*, 7808–7816. [CrossRef] [PubMed]
6. van den Broeke, M.; Box, J.; Fettweis, X.; Hanna, E.; Noel, B.; Tedesco, M.; van As, D.; van de Berg, W.J.; van Kampenhout, L. Greenland Ice Sheet Surface Mass Loss: Recent Developments in Observation and Modeling. *Curr. Clim. Chang. Rep.* **2017**, *3*, 345–356. [CrossRef]
7. Larson, K.M.; Gutmann, E.D.; Zavorotny, V.U.; Braun, J.J.; Williams, M.W.; Nievinski, F.G. Can we measure snow depth with GPS receivers? *Geophys. Res. Lett.* **2009**, *36*, L17502 . [CrossRef]
8. McCreight, J.L.; Small, E.E.; Larson, K.M. Snow depth, density, and SWE estimates derived from GPS reflection data: Validation in the western U.S. *Water Resour. Res.* **2014**, *50*, 6892–6909. [CrossRef]
9. Shean, D.E.; Christianson, K.; Larson, K.M.; Ligtenberg, S.R.M.; Joughin, I.R.; Smith, B.E.; Stevens, C.M.; Bushuk, M.; Holland, D.M. GPS-derived estimates of surface mass balance and ocean-induced basal melt for Pine Island Glacier ice shelf, Antarctica. *Cryosphere* **2017**, *11*, 2655–2674. [CrossRef]
10. Larson, K.M.; Macferrin, M.; Nylen, T. Brief Communication: Update on the GPS reflection technique for measuring snow accumulation in Greenland. *Cryosphere* **2020**, *14*, 1985–1988. [CrossRef]
11. Larson, K.M.; Nievinski, F.G. GPS snow sensing: Results from the EarthScope Plate Boundary Observatory. *Gps Solut.* **2013**, *17*, 41–52. [CrossRef]
12. Ryan, W.A.; Doesken, N.J.; Fassnacht, S.R. Evaluation of ultrasonic snow depth sensors for U.S. snow measurements. *J. Atmos. Ocean. Technol.* **2008**, *25*, 667–684. [CrossRef]
13. Fausto, R.S.; Van As, D.; Ahlstrom, A.P.; Citterio, M. Assessing the accuracy of Greenland ice sheet ice ablation measurements by pressure transducer. *J. Glaciol.* **2012**, *58*, 1144–1150. [CrossRef]
14. Fausto, R.S.; van As, D.; Mankoff, K.D.; Vandecrux, B.; Citterio, M.; Ahlstrom, A.P.; Andersen, S.B.; Colgan, W.; Karlsson, N.B.; Kjeldsen, K.K.; et al. Programme for Monitoring of the Greenland Ice Sheet (PROMICE) automatic weather station data. *Earth Syst. Sci. Data* **2021**, *13*, 3819–3845. [CrossRef]
15. Fausto, R.; van As, D.; Mankoff, D. *Rogramme for Monitoring of the Greenland Ice Sheet (PROMICE): Automatic Weather Station Data*; Version: V03; Dataset Published via Geological Survey of Denmark and Greenland: Copenhagen, Denmark, 2019. [CrossRef]
16. Löfgren, J.S.; Haas, R.; Scherneck, H.G. Sea level time series and ocean tide analysis from multipath signals at five GPS sites in different parts of the world. *J. Geodyn.* **2014**, *80*, 66–80. [CrossRef]
17. Larson, K.M.; Wahr, J.; Munneke, P.K. Constraints on snow accumulation and firn density in Greenland using GPS receivers. *J. Glaciol.* **2015**, *61*, 101–114. [CrossRef]
18. Williams, S.D.P.; Bell, P.S.; McCann, D.L.; Cooke, R.; Sams, C. Demonstrating the Potential of Low-Cost GPS Units for the Remote Measurement of Tides and Water Levels Using Interferometric Reflectometry. *J. Atmos. Ocean. Technol.* **2020**, *37*, 1925–1935. [CrossRef]

19. Katzberg, S.; Torres, O.; Grant, M.; Masters, D. Utilizing calibrated GPS reflected signals to estimate soil reflectivity and dielectric constant: Results from SMEX02. *Remote Sens. Environ.* **2006**, *100*, 17–28. [CrossRef]
20. Larson, K.M. GNSS Reflection Code. 2021. Available online: https://github.com/kristinemlarson/gnssrefl (accessed on 24 April 2022). [CrossRef]
21. Roesler, C.; Larson, K.M. Software tools for GNSS interferometric reflectometry (GNSS-IR). *Gps Solut.* **2018**, *22*, 80. [CrossRef]
22. Lomb, N.R. Least-squares frequency-analysis of unequally spaced data. *Astrophys. Space Sci.* **1976**, *39*, 447–462. [CrossRef]
23. Gutmann, E.D.; Larson, K.M.; Williams, M.W.; Nievinski, F.G.; Zavorotny, V. Snow measurement by GPS interferometric reflectometry: An evaluation at Niwot Ridge, Colorado. *Hydrol. Process.* **2012**, *26*, 2951–2961. [CrossRef]

D Paper 3

The evolution of the drainage cycles of Lake Tininnilik

Trine S. Dahl-Jensen [1], Kristian Kjeldsen[2], William Colgan[2], Michael Bevis[3], Shfaqat Abbas Khan [1]

[1]National Space Institute, Technical University of Denmark, Kgs. Lyngby, Denmark.
[2]Department of Glaciology and Climate, Geological Survey of Denmark and Greenland, Copenhagen K, Denmark.
[3]Division of Geodetic Science, School of Earth Sciences, The Ohio State University, Columbus, OH, USA.

Abstract

Ice dammed lakes in Greenland act as a buffer between meltwater runoff from the ice sheet and sea level contribution. Several of these lakes are known to drain at nearly regular intervals when the ice dam is breached. Here we will study the drainage cycles of Lake Tininnilik in West Greenland using satellite data and measured uplift of a nearby GNSS station. The lake drained in the late autumn of 2020, 5 years after the previous drainage event. The draining occurred at a lower lake water level than previously, following an approximately linear trend since 2003. The inferred reduction in the volume of water lost in successive drainage events is supported by observed differential crustal uplift in 2020 amounting to about half of that observed in the 2010 event. The decreasing water level prior to drainage coincides with decreasing surface elevations of the ice dam, which supports the theory of a drainage trigger mechanism related to the balance between ice overburden pressure and hydrostatic pressure at the bottom of the lake. By estimating the infill rate and by extrapolating the linear trend in pre-event water level, we estimate that the next drainage event will likely take place in 2024. We suggest that if the linear trend in pre-event water level continues, the maximum lake water level will reach a level equivalent to a drained lake by year 2053, and the drainage events will then cease.

Keywords: Ice dammed lakes, GLOFs, Greenland, draining cycles

1 Introduction

Large drainage events of ice- or moraine-dammed lakes, often referred to as Glacial Lake Outburst Floods (GLOFs), have been recorded for centuries and are widely studied (e.g. Huss *et al.*, 2007; Anacona *et al.*, 2015; Carrivick & Tweed, 2019; Bazai *et al.*, 2021). In populated areas these floods pose a risk to local infrastructure and communities, including loss of life (Tomasson, 1996; Carrivick & Tweed, 2016; Dubey & Goyal, 2020; Zheng *et al.*, 2021). Recent studies found that, in response to global warming, ice marginal lakes are increasing in number and size, inflating GLOF-related risks in vulnerable regions (Carrivick *et al.*, 2017; How *et al.*, 2021; Zheng *et al.*, 2021). In Greenland drainage of ice marginal lakes are rarely a threat to infrastructure and people as the country is sparsely populated and the drainage routes of GLOFs rarely pass through permanent settlements (Larsen *et al.*, 2013). However, ice marginal lakes play an important role as a buffer zone between meltwater runoff and sea level contributions from the Greenland ice sheet, and moreover, have been studied in relation to hydropower installations (Braithwaite & Thomsen, 1984; Larsen *et al.*, 2013).

How *et al.* (2021) identified more than 3000 ice marginal lakes in Greenland that were larger than 0.05 km2 in 2017. In contrast to moraine-dammed lakes, ice-dammed lakes often drain at regular intervals (Kjeldsen *et al.*, 2014; Bazai *et al.*, 2021). Due to thinning of the glaciers, which results in a weakening of the damming ice, some lakes are now draining more frequently or have transitioned into regular draining behavior (Russell *et al.*, 2011; Weidick & Citterio, 2011; Kjeldsen *et al.*, 2017).

Here, we focus on the ice-dammed Lake Tininnilik, located in the Disco Bay region of West Greenland, which drains under the glacier Sarqardliup Sermia (Figure 1). In the early 1980s the area around Lake Tininnilik was studied in relation to the installation of a hydropower plant which could supply energy to nearby towns Christianshåb (Qasigiannguit) and Egedesminde (Aasiaat) (Braithwaite & Thomsen, 1984; Thomsen, 1984). The main focus of those studies was the lake just south of Tininnilik, Kuussuup Tasia, with the possibility of including Tininnilik as a secondary reservoir. At that time the lake was estimated to drain every 10 years and the draining seemed to take about 1 to 1.5 years before refilling. Furuya & Wahr (2005) studied the lake using InSAR measurements of bedrock movement from 1992 to 2004 covering the two drainage episodes in 1993 and 2003. They model the loading of the lake and estimate that the lake level decreases by a total of around 75 m at each draining episode. After 2003 the drainage behavior changed from the previous 10 years between events to 5-7 years between each draining, and at the same time the maximum water level decreased following a thinning of the damming glacier, Sarqardliup Sermia (Kjeldsen *et al.*, 2017).

We study the recent drainage events of Lake Tininnilik using satellite altimetry of the water level and the damming glacier as well as uplift measured by the nearby GNSS station TIN1. The GNSS station was re-installed in 2019 and thus captured the elastic response to the draining of the lake in the late autumn of 2020. Based on the water level record, we can estimate the timing of the next drainage event using previous infill rates and the temporal trend in pre-event water level.

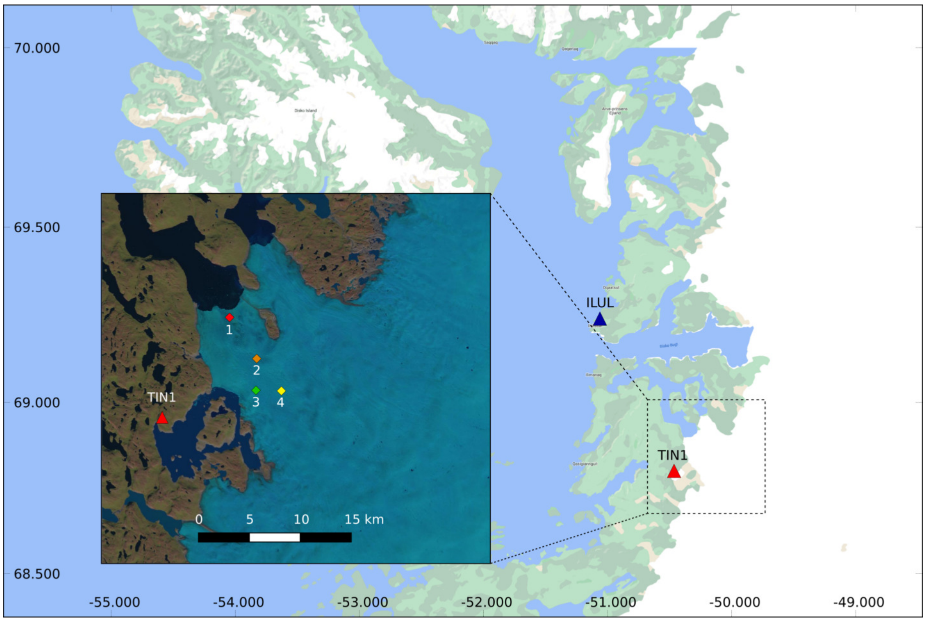

Figure 1: Map of the study region. Triangles mark the GNSS stations TIN1 and ILUL. Numbered diamonds mark the on-ice altimetry locations. The insert is a Landsat 8 image from the 8th of August 2020, courtesy of the U.S. Geological Survey. For the larger map, data is ©2015 Google.

2 Data and Methods

The lake water level and ice surface elevation records have been updated from Kjeldsen *et al.* (2017). These records were comprised of ICESat GLA12 Release 34 data (Zwally *et al.*, 2012), NASA's Airborne Topographic Mapper (ATM) and Land, Vegetation and Ice Sensor (LVIS) flight lines (Blair & Hofton, 2015; Krabill, 2015), CryoSat-2, AeroDEM (Korsgaard *et al.*, 2016), ArcticDEM (http://pgc.umn.edu/arcticdem; (Noh & Howat, 2015)), and additionally, Landsat, Sentinel-2, Advanced Spaceborne Thermal Emission and Reflection (ASTER), and Moderate Resolution Imaging Spectroradiometer (MODIS) archive satellite imagery (http://earthexplorer.usgs.gov). In this study we update the above-mentioned records and incorporate ICESat2 data. Moreover, to complete the historical part of the record we include the observations compiled by Thomsen (1984), and Furuya & Wahr (2005) after transforming their observations to the WGS84 ellipsoid. For a given time stamp, lake water level is determined as the mean of all elevation data that intersect the lake, though obvious outliers are excluded as these may reflect small icebergs. The adopted uncertainty is the standard deviation associated with the data or the reported uncertainty of each specific dataset, depending on which is larger. Locations on ice are defined as where the ATM-, LVIS-, and ICESat tracks overlap and can be seen on Figure 1. Around these locations we define a 100 m radius and extract all data to determine the mean elevation, including that of the DEMs, and use the standard deviation as uncertainty.

2.1 GNSS positions

We use GNSS position results from the Greenland GPS Network (GNET) stations TIN1 and ILUL. TIN1 is located next to the lake, while ILUL is located in Ilulissat about 50 km away (see Figure 1). The time series from TIN1 consists of less than one year of data obtained in 2010 and 2012, and a more complete time series since mid- 2019. ILUL has been in operation since 2006 with only minor data gaps. To estimate GNSS site coordinates, we use the Gipsy X software package version GipsyX-1.7 developed at the Jet Propulsion Laboratory (JPL) and released in 2021 (Bertiger *et al.*, 2020). We use JPL final orbit products, which include satellite orbits, satellite clock parameters, and Earth orientation parameters. The orbit products take the satellite antenna phase center offsets into account. The atmospheric delay parameters are modeled using the Vienna Mapping Function 1 (VMF1) with VMF1 grid nominals (Boehm *et al.*, 2006). Corrections are applied to remove the solid Earth tide and ocean tidal loading. The amplitudes and phases of the main ocean tidal loading terms are calculated using the Automatic Loading Provider (http://holt.oso.chalmers.se/loading/) applied to the FES2014b (Carrère *et al.*, 2016) ocean tide model, including correction for center of mass motion of the Earth due to the ocean tides. The site coordinates are computed in the IGS14 frame (Altamimi *et al.*, 2016). Our data processing strategy is identical to that of Hansen *et al.* (2021).

2.2 Temperature

The temperature record from the DMI weather station in Ilulissat (Cappelen, J. (ed), 2021) has been included to assess the general changes in the climatic. This time series began in 1807, but here we use data after 1940 to estimate climatic trends in the region.

2.3 Draining estimate

To estimate when the lake will drain again, we first estimate the infill rate using the last three cycles. We use a linear model of lake water level in time and use only the part of the infill period up until the water level at the onset of the next drainage event. This trend is estimated using an iterative process. First, the calculations are computed for water levels up to the level just before the last drainage event. Then, this resulting time and water level is used, and the calculations redone. We estimate the trend in water level at draining from the last four cycles as the 2003 draining is the last event to have approximately the same water level as previous events. Using this trend and the average calculated infill rate from the three last draining episodes, we estimate the timing of the next drainage event as the intersection between the two. The uncertainty is estimated from the standard deviation of the infill rates from the last three cycles.

3 Results

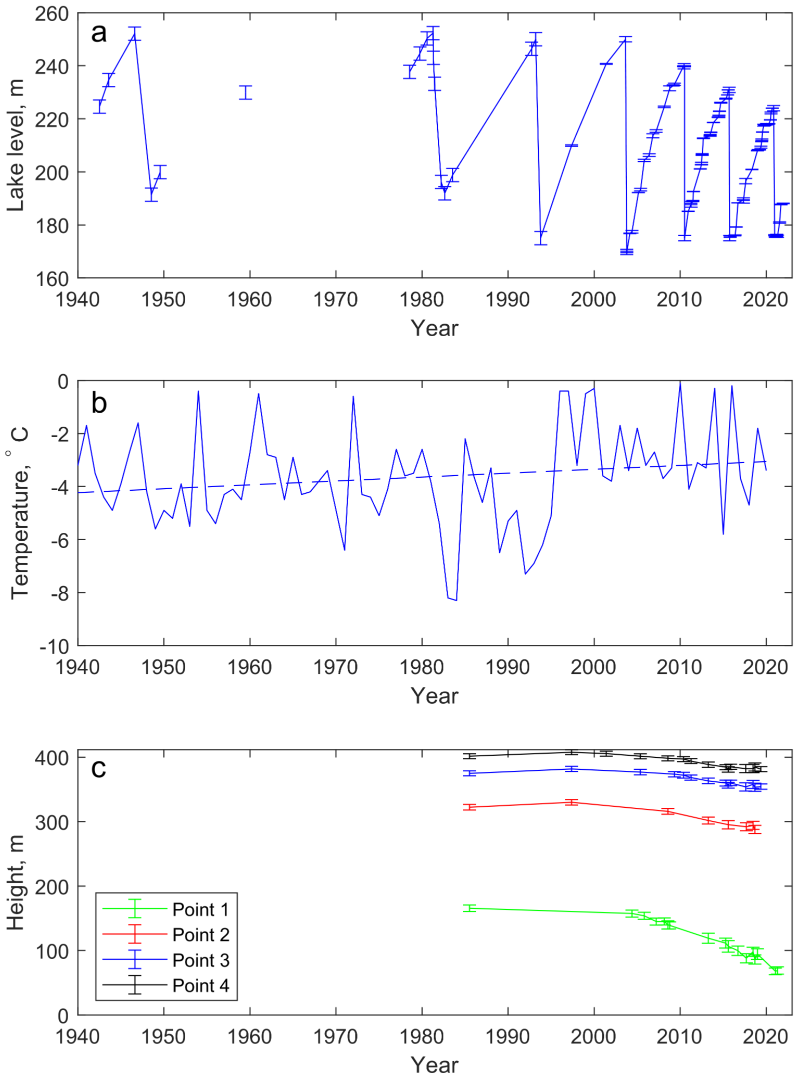

Figure 2: a: Lake water level from a combination of the observations from Thomsen (1984), Furuya & Wahr (2005) and an extension of the lake levels from Kjeldsen *et al.* (2017). b: Annual average temperature from weather station in Ilulissat. c: Ice surface heights at the four locations shown in figure 1

Figure 2a shows the compiled lake water level data since the 1940s. Before 1978 there is limited data, but we assume that the lake has drained approximately every ten years as described by Braithwaite & Thomsen (1984) and Thomsen (1984). The water level after sudden draining is approximately constant since 1993, while it appears to be higher during previous cycles, though this may be a result of limited data availability. The water level at the time of draining is more or less constant at approximately 250 m between the first observed draining in 1981-1982 and the draining in 2003. The next three drainage events occurred with a shorter time interval between events and at a progressively lower maximum water level. In 2020 the lake drained in early November at a record low water level of 224 m. The time series reveals that the lake did not start to refill until after April 2021.
Over the years the ice dam has thinned at all four study locations (Figure 2c). Thinning is most pronounced at the front of the glacier and appears to have started in the early 2000s.

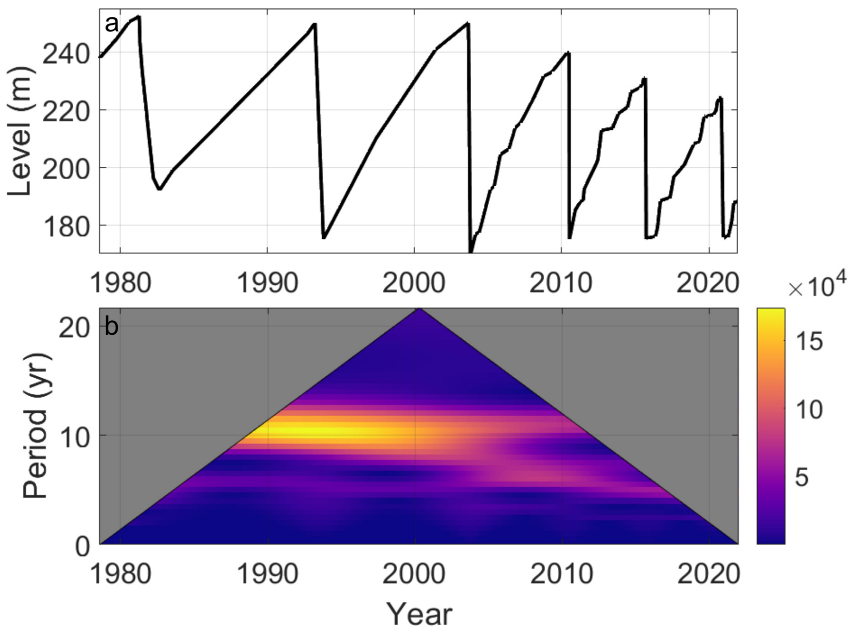

Figure 3: a: Lake water level for the time period with regular data used for the wavelet analysis. b: Power spectrum from the wavelet analysis. Unit is time squared.

The annual mean temperature record from Ilulissat reveals considerable variation from year to year, with an increase at a rate of 0.012 °C per year during 1940 to 2020 (Figure 2b). The record shows generally cooler annual temperatures during the 1980s and first half of the 1990s, before the warmest half decade in the last part of the 1990s and sustained, above average conditions after year 2000, coinciding with thinning of the damming ice.

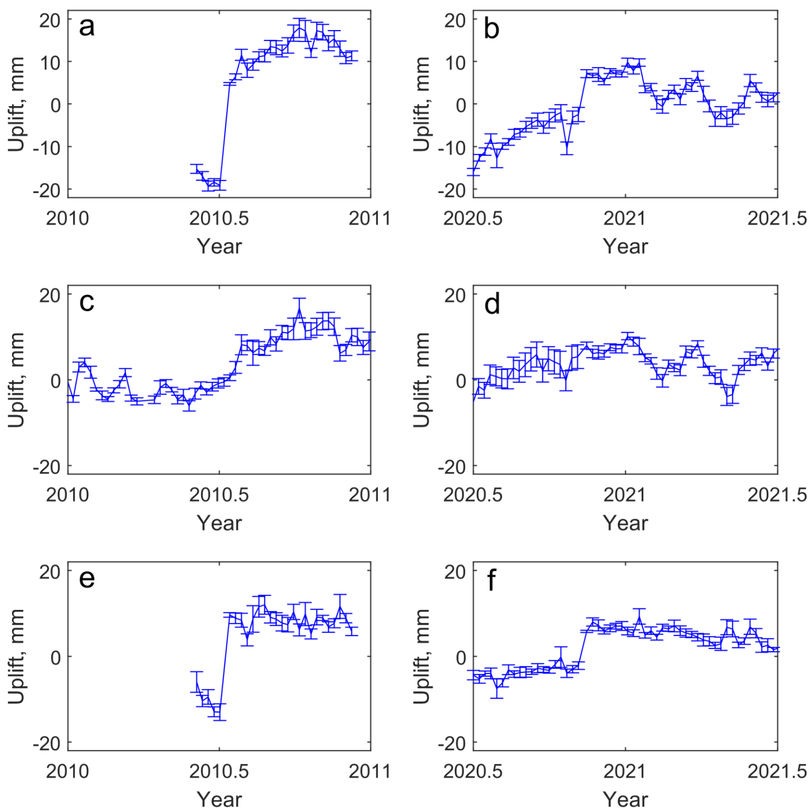

Figure 4: a, b: 7 day average uplift measured at TIN1; c, d: 7 day average uplift at ILUL; e, f: 7 day average uplift at TIN1 relative to ILUL.

To confirm the transition to a new draining frequency we conducted a wavelet analysis (Erickson, 2022) on the water level since 1978 when we start to have more continuous data. The resulting power spectrum is shown in figure 3b and highlights a clear 10-year period up until mid-2000s, at which point it becomes less clear as it transitions to a period of about 5 years during the later part of the record. We expect that the remaining peak at 10 years after the transition, is due to the new period being approximately half of the initial 10-year period and that the lack of clear patterns is

a result of the limited length of the record.
Figure 4a,b shows 7-day average vertical displacement of the GNSS station TIN1. The 7-day averages are calculated before and after the drainage events and the uncertainty is estimated as the standard deviation of mean. The drainage event in 2010 is clearly seen, while it is less obvious in 2020. The latter event is seen at approximately year 2020.8 but the uplift is of about the same size as other observed variations, which are due, for instance, to changes in ice mass. Assuming that the influence of the atmosphere and ice mass changes are similar at TIN1 and ILUL, we subtracted the vertical position of the GNSS station ILUL (Figure 4c,d) to obtain a clearer signal of the bedrock motion induced by abrupt lake drainage. The resulting differential uplift is plotted in Figure 4e,f. In the revised differential uplift record the uplift produced by drainage in 2020 is better defined and that the continuing upwards motion after drainage in 2010 seen in the original TIN1 record is largely removed.
We estimate the total differential uplift using 30-day averages before and after each of the two events, while the uncertainty is estimated using the standard deviation of the daily measurements. In 2010 the differential uplift at TIN1 was 19 ± 1 mm, while it was 9 ± 1 mm in 2020. The larger uplift in 2010, compared to 2020, confirms the reduced volume of drainage inferred from the water level record.

4 Discussion

The last drainage event for Lake Tininnilik was in November 2020, which was later in the year than is usual (Figure 2a). Following that event, the lake water level remained constant until April 2021 after which the lake started to re-fill. This could indicate two things; 1) that the drainage system under the glacier does not close before spring 2021 and/or 2) meltwater inflow to the lake ceased over the winter. We assume that there is little or no meltwater at this time of year, based on the step-like features on previous fillings, though we cannot exclude that some meltwater was produced and escaped through the drainage system before it was sealed later during the winter. A similar pattern, i.e. constant water level over winter, was observed following the event in 2015, also suggesting limited availability of meltwater during the winter.
The water level of Lake Tininnilik at the initiation of successive drainage events has decreased fairly steadily since 2003. At the same time the ice dam has thinned, coinciding with an increase in temperature in the region. There are multiple potential trigger mechanisms for GLOFs including breaching of dams, changes in the subsurface drainage system, volcanic activity, and ice flotation (Carrivick *et al.*, 2017). The thinning glacier combined with reduced water level at draining suggests that the trigger mechanism for lake drainage at Lake Tininnilik is ice flotation when the hydrostatic water pressure exceeds the ice overburden pressure.
As the lake drains, the underlying and surrounding bedrock instantaneously reacts to the change in surface loading. Comparing the revised uplift at TIN1 (Figure 4e,f) to the original (Figure 4a,b), the former better depicts the bedrock response to lake drainage. While the original TIN1 record (Figure 4a,b) shows a bedrock motion in relation to the 2010 event on June 30th/July 1st, it also shows continued uplift post event. Though Kjeldsen *et al.* (2017) mention that daily and seasonal variability atmospheric- and ice mass loads becomes more pronounced after drainage, the revised uplift record clearly shows the impact of these on bedrock motion and yields a clearer response to lake drainage. Although the vast majority of the drained volume exits the lake within 7 days, based on the water level record, the record also shows reduced ongoing drainage until 16th-25th July,

when the water level stabilizes, and by August 10th the water level was rising again. Post-event seepage is so small that it does not impact the bedrock motion, as seen in Figure 4e. The same clear pattern of bedrock motion in response to lake drainage is also evident in 2020 (Figure 4f), where the incorporation of the ILUL record cancels out a large part of the surface loading signal external to the lake, although minor variability still occurs.

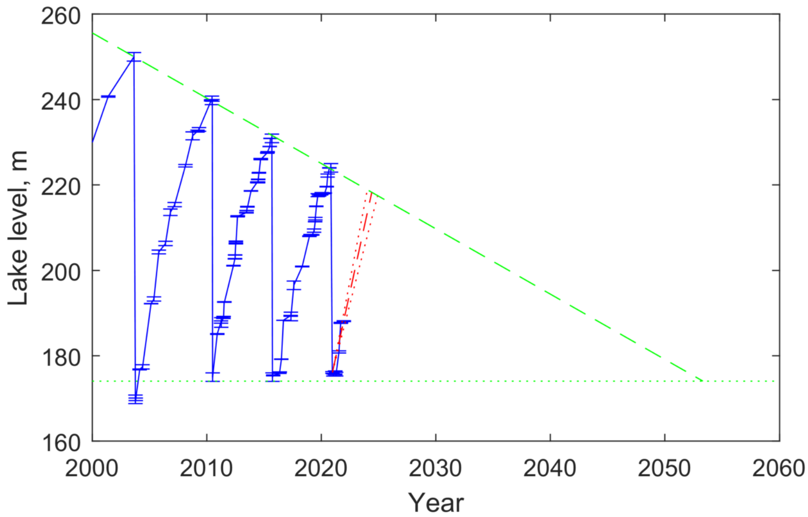

Figure 5: Measured water level in Lake Tininnilik with modelled maximum lake level (green dashed line), modelled minimum lake level (green dotted line) and infill (red lines).

As the climate continues to warm, it will likely sustain the ongoing thinning of the damming glacier, leading to further reduction of the draining water level. Based on the last four draining water levels, we estimate reduction in lake water level at draining of 1.5 ± 0.2 m/year. We estimate a future infill rate of 12 ± 2 m/year based on the last three cycles. The interception of the two trends suggests that the next drainage event should occur in 2024. The mean rate results in a draining in May, while the minimum and maximum estimated infill rates imply draining in the beginning or end of 2024 (Figure 5). If this holds true, this will further change the drainage frequency of the lake. At this stage, however, it is uncertain when/if the lake will enter a new phase of regular drainage events or if the current trend continues, leading to continuously decreasing intervals between events. Our simple model suggests that around year 2053 the pre-event water level will reach the level of the drained lake and the quasi-periodic draining cycles of the lake will cease entirely. Until now there has been no spillway, water has only escaped sub-glacially, yet this may change in the future, which will likely cause the quasi-cyclic drainage behavior to cease even before 2053.

5 Conclusion

The ice-dammed Lake Tininnilik drained in November 2020, 5 years after the previous drainage event. The 2020 event happened when the lake water level reached 224 m, consistent with the decreasing trend in maximum water level following the drainage event of 2003. This decreasing pre-event water level coincides with a thinning of the ice dam. In 2015 and 2020 the lake did not start to fill until about 6 months after the drainage event. However, due to the timing of the draining in September and November, respectively, and the resulting limited available melt water, we cannot conclude when the drainage path under the glacier closed.
Our reanalysis of the displacement time series at GNSS station TIN1 clarifies the bedrock response to lake drainage, and suggests that most of the volume lost by the lake drained in just a few days, both in 2010 and in 2020.
We estimate the timing of the next drainage event by comparing a simple linear model of the infill and the decreasing water level at drainage, and conclude that the lake will likely drain again during 2024. If this decreasing trend in water level continues, pre-event water level will eventually reach a level equivalent to a drained lake, implying that the quasi-cyclic, abrupt drainage behavior of the lake will cease entirely, probably by or before 2053.

Acknowledgements

S.A.K. acknowledges support from the Danish Council for Independent Research (grant no. 1026-00085B), Villum Experiment grant (grant no. 40718). K.K.K. acknowledges support from the Programme for monitoring of the Greenland ice sheet (PROMICE) at the Geological survey of Denmark and Greenland (GEUS).

Data availability

GNSS data from TIN1 and ILUL can be obtained from the UNAVCO file server
(https://data.unavco.org/archive/gnss/rinex/obs/).
Water level time series can be obtained from https://ftp.space.dtu.dk/pub/abbas/JoG2022/.

Author contributions

Water level time series, K.K.K.; GNSS processing, S.A.K.; Formal analysis, T.S.D.-J.; Establish GNSS station TIN1, M.B; Writing - original draft preparation, T.S.D.-J.; Writing - review and editing, All; Visualization, T.S.D.-J., W.C.

Conflict of interest

The authors declare no conflict of interest.

References

Altamimi, Zuheir, Rebischung, Paul, Metivier, Laurent, & Collilieux, Xavier. 2016. ITRF2014: A new release of the International Terrestrial Reference Frame modeling nonlinear station motions. *JOURNAL OF GEOPHYSICAL RESEARCH-SOLID EARTH*, **121**(8), 6109–6131.

Anacona, Pablo Iribarren, Mackintosh, Andrew, & Norton, Kevin Patrick. 2015. Hazardous processes and events from glacier and permafrost areas: lessons from the Chilean and Argentinean Andes. *EARTH SURFACE PROCESSES AND LANDFORMS*, **40**(1), 2–21.

Bazai, Nazir Ahmed, Cui, Peng, Carling, Paul A., Wang, Hao, Hassan, Javed, Liu, Dingzhu, Zhang, Guotao, & Jin, Wen. 2021. Increasing glacial lake outburst flood hazard in response to surge glaciers in the Karakoram. *EARTH-SCIENCE REVIEWS*, **212**(JAN).

Bertiger, Willy, Bar-Sever, Yoaz, Dorsey, Angie, Haines, Bruce, Harvey, Nate, Hemberger, Dan, Heflin, Michael, Lu, Wenwen, Miller, Mark, Moore, Angelyn W., Murphy, Dave, Ries, Paul, Romans, Larry, Sibois, Aurore, Sibthorpe, Ant, Szilagyi, Bela, Vallisneri, Michele, & Willis, Pascal. 2020. GipsyX/RTGx, a new tool set for space geodetic operations and research. *ADVANCES IN SPACE RESEARCH*, **66**(3), 469–489.

Blair, B., & Hofton, M. 2015. IceBridge LVIS L2 Geolocated Ground Elevation and Return Energy Quartiles, [2007-2013]. *National Snow and Ice Data Center, Boulder, CO, USA. Boulder, CO, USA: NASA Distributed Active, Archive Center at the National Snow and Ice Data Center. Retrieved from http://nsidc.org/data/ilvis2.html.*

Boehm, Johannes, Werl, Birgit, & Schuh, Harald. 2006. Troposphere mapping functions for GPS and very long baseline interferometry from European Centre for Medium-Range Weather Forecasts operational analysis data. *JOURNAL OF GEOPHYSICAL RESEARCH-SOLID EARTH*, **111**(B2).

Braithwaite, R. J., & Thomsen, H. H. 1984. Runoff conditions at Kuussuup Tasia, Christianshåb, estimated by modelling. *Grønlands geol. Undersøgelser, Gletscher-hydrologiske meddelser*, **2**, 1–23.

Cappelen, J. (ed). 2021. Greenland – DMI Historical Climate Data Collection 1784-2020. *DMI Report 21-04.*

Carrivick, Jonathan L., & Tweed, Fiona S. 2016. A global assessment of the societal impacts of glacier outburst floods. *GLOBAL AND PLANETARY CHANGE*, **144**(SEP), 1–16.

Carrivick, Jonathan L., & Tweed, Fiona S. 2019. A review of glacier outburst floods in Iceland and Greenland with a megafloods perspective. *EARTH-SCIENCE REVIEWS*, **196**(SEP).

Carrivick, Jonathan L., Tweed, Fiona S., Ng, Felix, Quincey, Duncan J., Mallalieu, Joseph, Ingeman-Nielsen, Thomas, Mikkelsen, Andreas B., Palmer, Steven J., Yde, Jacob C., Homer, Rachel, Russell, Andrew J., & Hubbard, Alun. 2017. Ice-Dammed Lake Drainage Evolution at Russell Glacier, West Greenland. *FRONTIERS IN EARTH SCIENCE*, **5**(NOV 28).

Carrère, L., Lyard, F., Cancet, M., Guillot, A., & Picot, N. 2016. FES 2014, a new tidal model—Validation results and perspectives for improvements. *In: Proceedings of the ESA living planet symposium*, 9–13.

Dubey, Saket, & Goyal, Manish Kumar. 2020. Glacial Lake Outburst Flood Hazard, Downstream Impact, and Risk Over the Indian Himalayas. *WATER RESOURCES RESEARCH*, **56**(4).

Erickson, J. 2022. Continuous wavelet transform and inverse (https://www.mathworks.com/matlabcentral/fileexchange/20821continuous-wavelet-transform-and-inverse). *MATLAB Central File Exchange.*

Furuya, M, & Wahr, JM. 2005. Water level changes at an ice-dammed lake in west Greenland inferred from InSAR data. *GEOPHYSICAL RESEARCH LETTERS*, **32**(14).

Hansen, Karina, Truffer, Martin, Aschwanden, Andy, Mankoff, Kenneth, Bevis, Michael, Humbert, Angelika, van den Broeke, Michiel R., Noel, Brice, Bjork, Anders, Colgan, William, Kjaer, Kurt H., Adhikari, Surendra, Barletta, Valentina, & Khan, Shfaqat A. 2021. Estimating Ice Discharge at Greenland's Three Largest Outlet Glaciers Using Local Bedrock Uplift. *GEOPHYSICAL RESEARCH LETTERS*, **48**(14).

How, Penelope, Messerli, Alexandra, Matzler, Eva, Santoro, Maurizio, Wiesmann, Andreas, Caduff, Rafael, Langley, Kirsty, Bojesen, Mikkel Hoegh, Paul, Frank, Kaab, Andreas, & Carrivick, Jonathan L. 2021. Greenland-wide inventory of ice marginal lakes using a multi-method approach. *SCIENTIFIC REPORTS*, **11**(1).

Huss, Matthias, Bauder, Andreas, Werder, Mauro, Funk, Martin, & Hock, Regine. 2007. Glacier-dammed lake outburst events of Gornersee, Switzerland. *JOURNAL OF GLACIOLOGY*, **53**(181), 189–200.

Kjeldsen, K. K., Mortensen, J., Bendtsen, J., Petersen, D., Lennert, K., & Rysgaard, S. 2014. Ice-dammed lake drainage cools and raises surface salinities in a tidewater outlet glacier fjord, west Greenland. *JOURNAL OF GEOPHYSICAL RESEARCH-EARTH SURFACE*, **119**(6), 1310–1321.

Kjeldsen, Kristian K., Khan, Shfaqat A., Bjork, Anders A., Nielsen, Karina, & Mouginot, Jeremie. 2017. Ice-dammed lake drainage in west Greenland: Drainage pattern and implications on ice flow and bedrock motion. *GEOPHYSICAL RESEARCH LETTERS*, **44**(14), 7320–7327.

Korsgaard, Niels J., Nuth, Christopher, Khan, Shfaqat A., Kjeldsen, Kristian K., Bjork, Anders A., Schomacker, Anders, & Kjaer, Kurt H. 2016. Digital elevation model and orthophotographs of Greenland based on aerial photographs from 1978-1987. *SCIENTIFIC DATA*, **3**(MAY 10).

Krabill, W.B. 2015. IceBridge ATM L2 Icessn Elevation, Slope, and Roughness, [1993-2015]. *National Snow and Ice Data Center, Boulder, CO, USA. Boulder, CO, USA: NASA Distributed Active Archive Center at National Snow and Ice Data Center. Retrieved from http://nsidc.org/data/ilatm2.html.*

Larsen, Morten, Tottrup, Christian, Matzler, Eva, Naamansen, Bo, Petersen, Dorthe, & Thorsoe, Kisser. 2013. A satellite perspective on jokulhlaups in Greenland. *HYDROLOGY RESEARCH*, **44**(1), 68–77.

Noh, Myoung-Jong, & Howat, Ian M. 2015. Automated stereo-photogrammetric DEM generation at high latitudes: Surface Extraction with TIN-based Search-space Minimization (SETSM) validation and demonstration over glaciated regions. *GISCIENCE & REMOTE SENSING*, **52**(2), 198–217.

Russell, Andrew J., Carrivick, Jonathan L., Ingeman-Nielsen, Thomas, Yde, Jacob C., & Williams, Meredith. 2011. A new cycle of jökulhlaups at Russell Glacier, Kangerlussuaq, West Greenland. *JOURNAL OF GLACIOLOGY*, **57**(202), 238–246.

Thomsen, H. H. 1984. Glaciologiske undersøgelser i disko bugt området 1983. *Grønlands geol. Undersøgelser, Gletscher-hydrologiske meddelser*, **84/1**.

Tomasson, H. 1996. The jokulhlaup from Katla in 1918. *Pages 249–254 of:* Collins, D (ed), *ANNALS OF GLACIOLOGY, VOL. 22, 1996: PROCEEDINGS OF THE INTERNATIONAL SYMPOSIUM ON GLACIAL EROSION AND SEDIMENTATION*. ANNALS OF GLACIOLOGY, vol. 22. Int Glaciol Soc. International Symposium on Glacial Erosion and Sedimentation, REYKJAVIK, ICELAND, AUG 20-25, 1995.

Weidick, Anker, & Citterio, Michele. 2011. The ice-dammed lake Isvand, West Greenland, has lost its water. *JOURNAL OF GLACIOLOGY*, **57**(201), 186–188.

Zheng, Guoxiong, Allen, Simon Keith, Bao, Anming, Ballesteros-Canovas, Juan Antonio, Huss, Matthias, Zhang, Guoqing, Li, Junli, Yuan, Ye, Jiang, Liangliang, Yu, Tao, Chen, Wenfeng, & Stoffel, Markus. 2021. Increasing risk of glacial lake outburst floods from future Third Pole deglaciation. *NATURE CLIMATE CHANGE*, **11**(5), 411+.

Zwally, H. J., Schutz, R., Bentley, J., Herring, T., Minster, J., Spinhirne, J., & Thomas, R. 2012. GLAS/ICESat L2 Antarctic and Greenland Ice Sheet Altimetry Data, V031. *National Snow and Ice Data Center, Boulder, CO, USA. Boulder, CO, USA: NASA Distributed Active Archive Center at the National Snow and Ice Data Center.*

E Thermosteric sea level from SST

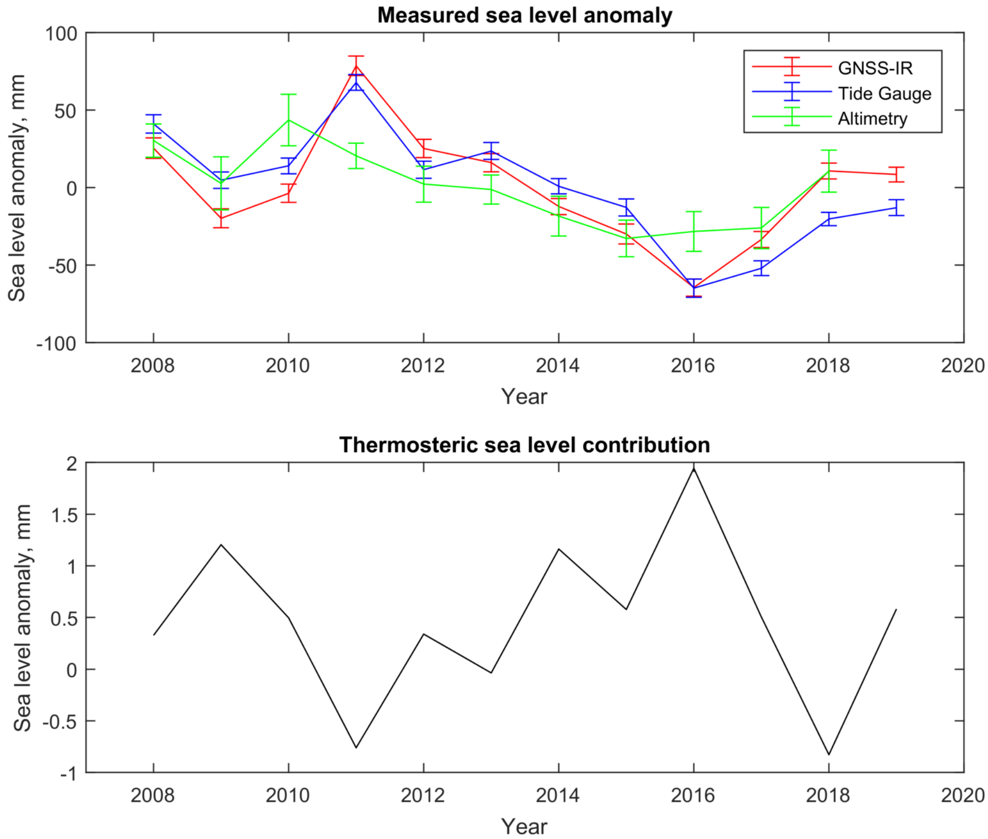

Figure E.1: Thermosteric sea level contribution calculated using SST with a salinity of 30 and a water depth of 50 m.

Technical
University of
Denmark

Elektrovej, Building 328
2800 Kgs. Lyngby
Tlf. 4525 1700

www.space.dtu.dk